Development of Imine-based pH-responsive Polymeric Drug Delivery Systems

Xiaolei Hu

A Thesis

in

The Department

of

Chemistry and Biochemistry

Presented in Partial Fulfillment of the Requirements

for the Degree of

Master of Science (Chemistry) at

Concordia University

Montreal, Quebec, Canada

June 2021

CONCORDIA UNIVERSITY

School of Graduate Studies

This is to certify that the thesis prepared

By: Xiaolei Hu

Entitled: Development of Imine-based pH-responsive Polymeric Drug Delivery Systems

and submitted in partial fulfillment of the requirements for the degree of

Master of Science (Chemistry)

complies with the regulations of the University and meets the accepted standards with respect to originality and quality.

Signed by the final Examining Committee:

Dr. Marek Majewsk Chair

Dr. Ingo Salzmann Examiner

Dr. Zhibin Ye Examiner

Dr. Jung Kwon Oh Supervisor

Approved by: Dr. Yves Gélinas Graduate Program Director

Dr. Pascale Sicotte Dean of Faculty of Arts and Science.

June/2021

Abstract

Development of Imine-based pH-responsive Polymeric Drug Delivery Systems

Xiaolei Hu

Block copolymer-based nanoassemblies that can disassemble in response to endogenous stimuli found in tumor tissues and cancer cells are promising candidates for intracellular drug delivery exhibiting enhanced release of encapsulated drugs. Owning to excellent colloidal stability during blood circulation (pH = 7.4) and accelerated drug release ability in tumoral and endo/lysosomal acidic environments (pH = 4.0-6.8), acid-responsive degradable nanoassemblies have emerged as promising nanocarriers for advanced drug delivery with precisely controlled drug release. Benzoic imine bond, which is cleavable at acidic pH while stable under physiological pH, has been widely explored for the design of novel acid-degradable block copolymers. A general method to synthesize imine-containing block copolymers involves the post-polymerization modification. Functional copolymer precursors bearing primary amine or carbonyl groups are conjugated with hydrophobic moieties, drug molecules, and hydrophilic species through *in situ* imine formation reaction.

My master research explores a new approach to synthesize acid-degradable block copolymers bearing pendant imine groups (ImPs). The approach explores direct polymerization of a novel imine-containing methacrylate utilizing controlled radical polymerization techniques, enabling the synthesis of well-controlled ImPs with tunable functionalities. The resultant ImPs undergo self-assembly to form nanometer-sized micelles, composed of hydrophilic poly(ethylene glycol) (PEG) corona and acid-degradable hydrophobic core bearing imine linkages. In response to tumoral and endo/lysosomal acidic environments, they disassemble through a change in hydrophilic/hydrophobic balance upon the cleavage of imine linkages to the corresponding aldehyde and primary amine. As a consequence, such acid-catalyzed hydrolysis of imine linkages in hydrophobic cores leads to the enhanced release of encapsulated doxorubicin (Dox, a clinically used anticancer drug).

The proof-of-concept results suggest that this robust approach is versatile to further design advanced nanoassemblies responding to dual/multiple stimuli, thus being more effective to intracellular drug delivery.

Acknowledgements

I first would like to give my sincere thanks to my supervisor Dr. Jung Kwon Oh for providing me the great opportunity to work in his research lab. Throughout my master study, he gives me lots of support and guidance on my experiments, scientific writing, and presentations. His vast knowledge and passion for research set a great example for me, which will continuously motivate me in my future research career.

I also would like to take this opportunity to express my appreciation to Dr. Ingo Salzmann, Dr. Zhibin Ye, and Dr. Xiaolei Wang for their time and effort to serve as the committee members for my master studies. Their insight questions and helpful discussion during committee meetings provide me great feedback and inspiration for my research.

I also would like to thank all lab mates in Oh's group who accompany me during this fantastic journey. Especially, I would like to thank Arman, Dr. Gandhi, Newsha, Kay, Yuqing, Hourieh, Twinkle, Bakr, and Kamal for their generous assistance and helpful discussion.

Finally, I would express my greatest love and appreciation to my parents Xiuqian and Jinshuang, and sister Lingli for their unwavering love, support, and encouragement at every stage of my life. Only with their countless support, I am able and will continue to chase my dream in science.

Contribution of Authors

The majority of the research described in this thesis was conducted independently by the author of this thesis under the supervision of Dr. John Oh.

Chapter 2: Parts of the submitted review manuscript as **Xiaolei Hu**, Arman Moini Jazani, Jung Kwon Oh. Recent Advances in Development of Imine-Based Acid-Degradable Polymeric Nanoassemblies for Intracellular Drug Delivery. **2021**.

Contribution: Arman Moini Jazani summarized Section 2.6. Dual stimuli-responsive imine-based nanoassemblies in Chapter 2.

Chapter 3 and 4: Parts of the published paper as **Xiaolei Hu**, Jung Kwon Oh. Direct polymerization approach to synthesize acidic pH-degradable block copolymers bearing imine pendants for tunable pH-sensitivity and enhanced release. Macromolecular Rapid Communication, **2020**, *41*, 2000394.

Table of Contents

List of Figures

List of Tables

List of Abbreviations

ABP	Amphiphilic block copolymer
AMBN	2,2′-azodi(2-methylbutyronitrile)
ATRP	Atom transfer radical polymerization
BA	Benzaldehyde
Br-iBuBr	Bromoisobutyryl bromide
CDI	1,1′-Carbonyldiimidazole
CL	Caprolactone
CLSM	Confocal laser scanning microscopy
CMC	Critical micelle concentration
CTA	4-Cyano-4-(phenylcarbonothioylthio) pentanoic acid
CuAAc	Copper-catalyzed alkyne-azide cycloaddition
CUR	Curcumin
DBU	1,8-Diazabicyclo[5.4.0]undec-7-ene
DMAP	4-(methylamino)pyridine
DMAEMA	Dimethylaminoethyl methacrylate
Dox	Doxorubicin
DDS	Drug delivery systems
EDC	1-ethyl-3-(3 dimethylaminopropyl) carbodiimide•HCl
EPR	Enhanced permeability and retention
Et_3N	Triethylamine
GPC	Gel permeation chromatography
GSH	Glutathione
HEMA	2-Hydroxylethyl methacrylate
HNK	Honokiol
I.V.	Intravenous
LCST	Lower critical solution temperature
MW	Molecular weight
MWCO	Molecular weight cutoff
M_n	Number average molecular weight
NMR	Nuclear magnetic resonance
NPs	Nanoparticles

NR	Nile red
OEGMA	Oligo (ethylene glycol) methyl ether methacrylate
PDDS	Polymeric drug delivery systems
PEI	Polyethylenimine
PTX	Paclitaxel
PEG	Poly(ethylene glycol)
PLA	Polylactide
RES	Reticuloendothelial system
RAFT	Reversible addition−fragmentation chain-transfer
ROP	Ring opening polymerization
SRD	Stimuli-responsive degradation
siRNA	Small interfering ribonucleic acid
TPMA	Tris(2-pyridylmethyl)amine

Chapter 1. Introduction and background

1.1 Brief overview of my research and goals

My research aims to explore a new approach to synthesize acid-degradable block copolymers bearing pendant imine groups (PEG-b-PBzImMA or ImP) for the development of a promising drug delivery platform for the treatment of cancers. This approach explores direct polymerization of a novel imine-containing methacrylate utilizing controlled radical polymerization techniques for the synthesis of well-controlled ImPs. The Dox-loaded micelles through self-assembly of resultant ImP exhibit greatly enhanced drug release in tumoral and endo/lysosomal acidic environments (pH = 4.0-6.9) by acid-catalyzed hydrolysis of incorporated imine linkages.

1.2 General concept for nanoparticles-based drug delivery systems

Chemotherapy has been wildly used in clinics for the treatment of cancers. Therapeutic drug molecules are administrated into patients by intravenous injection (I.V.) and transported to disease sites to exert their cancer killing function.[1] However, the therapeutic efficacy of administrated drugs is intrinsically limited by poor water solubility, non-specific biodistribution, short circulation time, and rapid clearance from blood by reticuloendothelial system (RES) during blood circulation. Meanwhile, these drawbacks cause serious side-effects during treatment.

Nanomedicine that employs nanometer-sized particles from tens to a few hundred nanometer (named nanoparticles or NPs) as drug delivery carriers, has attracted great attention owning to its capacity to effectively resolve above-mentioned biological obstacles during *in vivo* drug delivery.[2] Various nanocarriers with different physicochemical properties have been developed, typically including liposomes, polymeric NPs, inorganic NPs (typically, metal NPs and carbon nanotubes), hybrid NPs, and dentrimers (see Figure 1.1).[3] Among these, polymeric NPs have been extensively explored as promising candidates for advanced drug delivery applications. The broad chemical design space to molecularly engineer polymer chemical structure, architecture and functionality allows for the facile modulation of physicochemical properties of the formed nanocarriers.[4] Through the physical encapsulation or covalent

conjugation, polymer nanotherapeutics are able to significantly improve water solubility, enhance colloidal stability, prolong circulation time, and prevent the premature release of drugs.

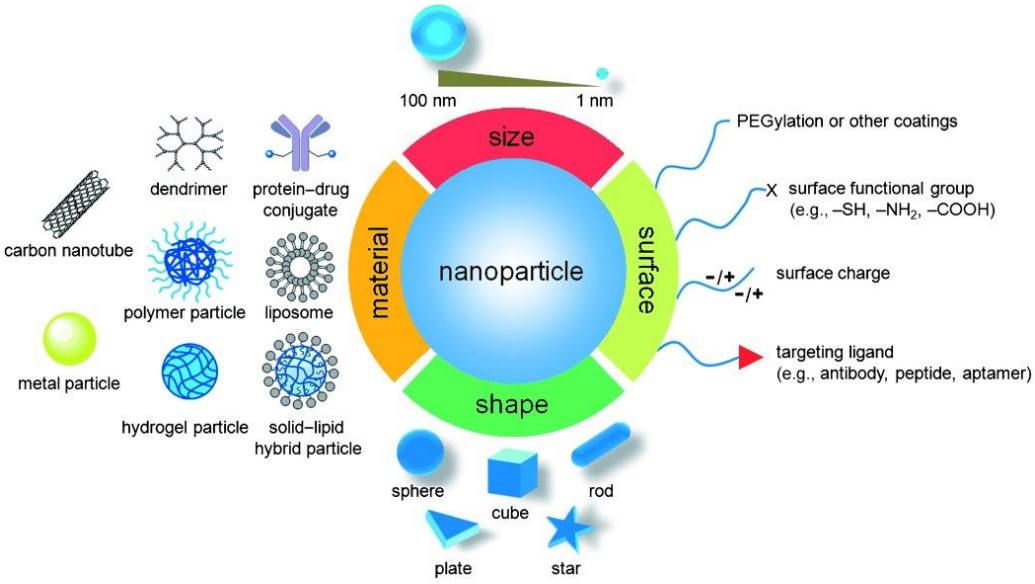

Figure 1.1. A summary of nanoparticles explored as carriers for drug delivery in cancer therapy, together with illustrations of physicochemical properties.[3] Copyright 2014 Royal Society of Chemistry.

Meanwhile, the size of polymer nanocarriers could be readily tailored with relatively narrow size distribution, which is one of the critical parameters for the successful *in vivo* intracellular drug delivery for cancer treatment. After I.V. injection into the body, they are able to specifically extravasate and accumulate at tumor tissues during blood circulation through enhanced permeability and retention (EPR) effects by taking advantage of combined leaky vasculature and poor lymphatic drainage in solid tumor sites (Figure 1.2).[5-6] Moreover, surface functionalization with specific targeting agents could further enhanced the tumor targeting and cellular uptake of NPs, commonly known as active targeting.[7]

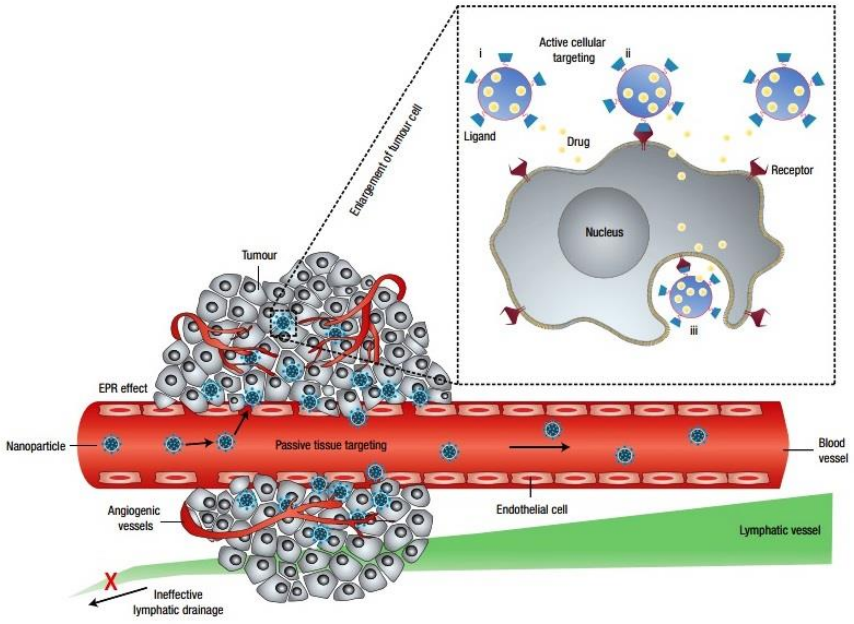

Figure 1.2. Schematic illustration of different mechanisms by which nanocarriers can specifically deliver drugs to tumor by ERP effects and active targeting strategy.[6] Copyright 2007 Springer Nature.

1.3 Polymer micelles for enhanced drug delivery

A great number of polymer-based drug delivery systems have been extensively explored. Typical examples include polymer-drug conjugates (prodrug),[8] micelles,[9] polymersomes,[10] and nanogels.[11] Among these, micelles are fabricated by self-assembly of amphiphilic block copolymers in aqueous solution.[9] They possess a variety of promising characteristics for effective intracellular drug delivery. These features include (1) tunable sizes with narrow size distribution; (2) great colloidal stability with a low critical micelle concentration (CMC); (3) protection of drugs from degradation or clearance during circulation; (4) prolonged circulation time; (5) tumor-targeting capacity through EPR effects or active targeting strategies; and (6) encapsulation of single or multiple anti-cancer drugs and other therapeutics in high loading content and efficiency. Genexol-PM is the first example of commercialized polymer nanotherapeutics for clinical treatment of cancers, based on poly(ethylene glycol)-b-poly(ε-carprolactone) (PEG-b-PCL) block copolymer with anticancer drug paclitaxel.[12] Currently, several other polymer micelle-based nanomedicines such as SP1049C,[13] NK911,[14] CRLX-101,[15]

and BIND-014[16] are in clinical studies for commercialization. These successful examples validate the versatility of polymeric micelles as effective drug delivery systems.[17]

1.4 Acid-responsive degradable polymer micelles for drug delivery

Despite of tremendous progress in the development of polymer-based drug delivery systems, uncontrolled and slow drug release from non-responsive polymeric micelles through diffusion mechanism still limits the further improvement of their therapeutic efficacy in clinical cancer treatment. To maximize therapeutic efficacy of administrated drugs, it is crucial to maintain drug concentration in optimal range at tumor sites and thus effectively induce the apoptosis of cancerous cells. The development of advanced polymeric drug delivery systems that allow for precise control over drug release profile with excellent spatial and temporal control at tumor sites is highly desired. Such advanced delivery systems can offer numerous advantages compared to conventional dosage forms, including improved efficacy, reduced toxicity, and improved patient compliance and convenience by reducing the number of required drug administration.

Amphiphilic block copolymers exhibiting stimuli-responsive degradation (SRD) through the cleavage of covalent bonds in response to stimuli have emerged as a promising choice of means in construction of advanced delivery nanocarriers with programmable release profile.[18-19] These SRD-exhibiting block copolymers have been synthesized by the incorporation of stimuli-responsive linkages into the design of block copolymers. In response to stimuli, self-assembled SRD micelles can undergo dissociation through the change in hydrophobic/hydrophilic balance, leading to the fast and sustained release of physically encapsulated or covalently conjugated drugs. Moreover, it can promote the clearance and excretion of the nanocarriers from body because of formation of smaller fragments as consequence of linkage degradation. When SRD micelles are designed for intracellular drug delivery, the selection of stimuli and corresponding labile linkages become critical for controlled release of encapsulated therapeutics.[19-21]Among various stimuli that have been explored, acidic pH, glutathione (a tripeptide), and enzyme are the main endogenous stimuli found in tumoral environments.[22] Particularly, acidic pH gradient in tumor tissues has been regarded as a promising stimulus for controlled drug release, because pH is 6.5 - 6.9 in tumor microenvironments and further decreases to 4 - 6.0 in endosomes and lysosomes, compared to pH = 7.4 in normal tissues and blood.[23-25] This pH gradient in tumor

tissue is mainly originated from the dramatical accumulation of lactic acid produced by increased anaerobic glycolysis at hypoxic tumor environment, commonly known as Warburg effects.[26]

Owning to the possibility of biodegradation, numerous acid-labile linkages have been explored, including imine,[27] oxime,[28] hydrazone,[29] ketal and acetal,[30-31] 2,3-dialkylmaleamidic amide,[32] β-thiopropionate,[33] and orthoester.[34] Figure 1.3 illustrates that the incorporation of a series of acid-degradable linkages in ABPs enables the fabrication of micelles containing acid-labile linkage at the corona/core interfaces or hydrophobic cores.[24] These pH-sensitive polymer micelles have been designed to be stable at physiological pH = 7.4 during blood circulation, whereas can undergo rapid dissociation to release encapsulated drugs upon the acid-responsive cleavage of linkages while reaching to acidic tumor sites.

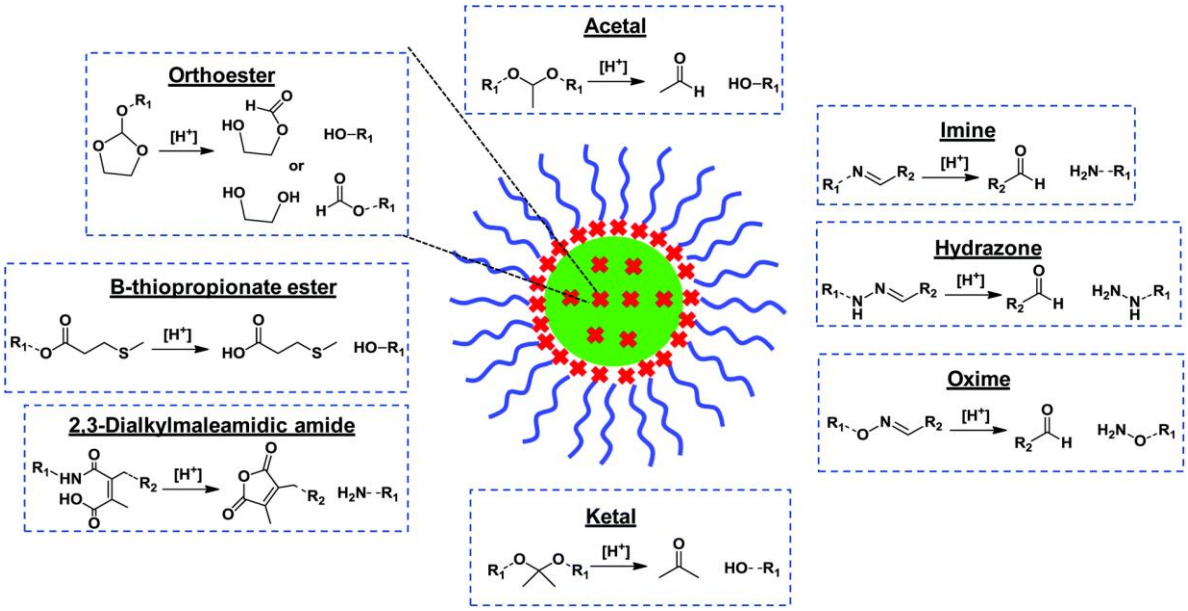

Figure 1.3. Chemical structures and acid-catalyzed hydrolysis of typical acid-labile linkages.[24] Copyright 2020 Royal Society of Chemistry.

1.5 Scope of my master thesis

My master thesis research has focused on exploration a novel strategy that enables the synthesis of imine-based block copolymers and their nanoassemblies for intracellular drug delivery applications. This strategy is distinct and beneficial to circumvent challenges associated with conventional multi-step post-modification approach to synthesize imine-based polymer for

drug delivery. Chapter 2 is a literature review to map out recent advances in development of imine-based acid-degradable polymeric nanoassemblies for intracellular drug delivery.

Chapter 3 describes the methods, including instrumentation, synthesis, and characterization of imine-containing methacrylate monomer and diblock copolymers, acid-triggered hydrolysis of imine linkages, aqueous micellization and disassembly, and *in vitro* release experiments of encapsulated doxorubicin.

In Chapter 4, the synthesis of novel imine monomer BzImMA and diblock copolymers PEG-b-PBzImMA bearing pendant imine linkages in hydrophobic block through direct polymerization approach is described. Furthermore, acid-catalyzed hydrolysis kinetics and mechanisms of imine linkages were systematically investigated with BzImMA and PEG-b-PBzImMA. For proof-of-concept demonstration of the versatility of our approach, aqueous micellization to fabricate empty micelles and Dox-loaded micelles as well as acid-triggered release of encapsulated Dox were systemically studied.

Finally, conclusion and future direction are presented in Chapter 5.

Chapter 2 Recent advances in development of imine-based acid-degradable polymeric nanoassemblies for intracellular drug delivery

2.1. Introduction

Recent decades have witnessed great advances in the development of nanometer-sized drug delivery systems (DDS)[35-37], particularly, polymeric DDS (PDDS) based on amphiphilic block copolymers (ABPs) for effective intracellular delivery of anticancer therapeutics to tumor sites.[38-43] PDDS possess great flexibility in chemical designs, unique core-shell structures for physical and chemical encapsulation of therapeutics, excellent colloidal stability upon dilution in blood, and tunable sizes with narrow size distribution. Furthermore, they can target tumor tissues during blood circulation through the Enhanced Permeability and Retention (EPR) effect[5, 44] and recent compelling mechanisms[45-48]. Therefore, PDDS can improve the biodistribution in tumor tissues and the efficacy of drug molecules to chemotherapy.[49-53] However, the dilemma associated with their colloidal stability during blood circulation and drug release profile in tumor tissues poses a key challenge for their *in vivo* and clinical anti-cancer performance.[54-59]

Stimuli-responsive degradation (SRD) is proven as a powerful approach to effectively tackle the challenges of PDDS by simultaneously achieving good colloidal stability during blood circulation and enhanced release of encapsulated drugs after reaching tumor tissues.[20-21, 25, 60-74] This promising approach involves the incorporation of stimuli-responsive cleavable linkages into the design of polymer precursors.[22] Well-defined ABPs undergo self-assembly to form aqueous micelles (named here as nanoassemblies) with cleavable linkages positioned in hydrophobic cores or at core/corona interfaces. In response to endogenous stimuli presented in tumor tissues and cancer cells, encapsulated or conjugated drugs are rapidly released through the SRD-induced disassembly process as a consequence of the cleavage of labile linkages. In particular, an acidic pH gradient is found in tumor tissues. Originated from the enhanced generation of lactic acid under anaerobic conditions, the tumor microenvironment is slightly acidic at pH = 6.6-6.9, compared with normal tissues being neutral at pH = 7.4.[23] Furthermore, endosomes and lysosomes are more acidic at pH = 4.0-6.0.[75-76]

To take advantage of tumoral and endo/lysosomal acidic environments and achieve biodegradation-induced controlled/enhanced drug release, various strategies have been proposed to synthesize acid-degradable copolymers and their nanoassemblies. These strategies explore the cleavage of a variety of acid-labile linkages such as ketal, acetal, orthoester, 2,3-dialkylmaleamidic amide, boronic ester, and β-thiopropionate.[24, 77-78] Particular interest is on imine and its families that offer tunable acid-catalyzed hydrolysis kinetics with varying substituents. Imine (C=N) bond, also known as Schiff base, is generally formed through condensation reaction between a carbonyl group (-C=O) and a primary amine group ($-NH_2$).[79] This reaction proceeds rapidly under a mild condition with high selectivity and yield. Furthermore, this reaction is versatile in that various imine families can be synthesized with varying carbonyl and amine groups. Typical families include benzoic imine ($-C_6H_4$-CH=N-) by the reaction of an aromatic aldehyde with primary amine as well as hydrazone (-CH=N-NH-) and oxime (-CH=N-O-) by the reaction of an aldehyde with hydrazide and aminoxyl groups, respectively.[27, 29, 80]

This review describes recent advances in the design and synthesis of imine-bearing block copolymers as building blocks for the development of acid-degradable nanoassemblies in three different forms as self-assembled nanoassemblies, core-crosslinked nanogels, and polymer-drug conjugates (polymer prodrugs) (Figure 2.1). These nanocarriers have been designed to disintegrate after the cleavage of imine bonds in acidic tumoral and endo/lysosomal environments, leading to the enhanced release of encapsulated drug molecules for tumor-targeting intracellular drug delivery. Note that the delivery of RNA and DNA is not included in this review. Several review articles have been reported with focuses on either individual hydrazone,[29] benzoic imine,[80] and oxime[81] chemistry, or their importance in polymer science[81-82]. This review focuses on the numerous synthetic strategies to synthesize nanoassemblies with different numbers and locations of imine linkages to elucidate their disassembly mechanism and enhanced drug release in acidic environments. In addition, this review discusses dual stimuli-responsive imine-based nanoassemblies containing a combination of imine bonds with other biological stimulus-cleavable linkages, typically disulfide and enzyme-cleavable linkages.

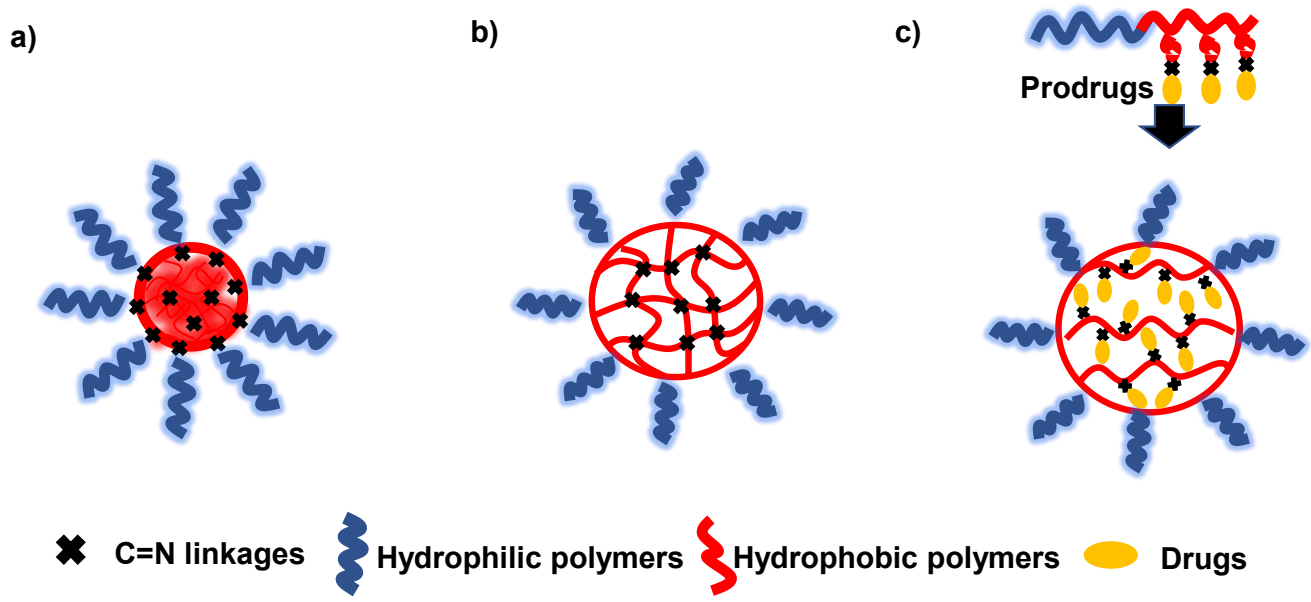

Figure 2.1. Acid-degradable imine-based polymeric nanocarriers, including self-assembled nanoassemblies (a), nanogels (b), and prodrug nanoassemblies (c) for intracellular drug delivery.

2.2 Imine formation and acid-catalyzed hydrolysis

Figure 2.2 shows the general mechanism for the formation of imine bond with five steps, including i) nucleophilic attack of a primary amine to a carbonyl group, ii) proton transfer, iii) protonation of hydroxyl group, iv) elimination of water, and v) deprotonation to form imine bond.[83-85] This mechanism is catalyzed with acid, and thus imine formation is greatly pH-dependent. Pioneering work by Jencks et al. suggests that the rate-determining step is acid-catalyzed dehydration of carbinolamine (step 4 in Figure 2.2) at neutral or slight acidic pH ranging at 3-7. However, it becomes nucleophilic attack (step 1) at pH < 3, as a result of the decreased nucleophilicity of primary amine upon protonation and the favor to backward reaction in acidic pH.[86]

In addition to mechanistic aspect with pH-dependence, the rate of imine formation is dependent on the intrinsic reactivity of carbonyl and amino groups. Their reactivity can be tuned with their structural features based on the electronic and steric effects of the substituents. In the aspect of electronic effect, electron-deficient carbonyl groups undergo rapid hydrazone formation due to their enhanced electrophilicity.[87] The nucleophilicity of amino groups plays a vital role in the attack of carbonyl groups to form a tetrahedral intermediate. For example,

aminoxy and hydrazide, compared to alkyl amine, have higher reactivity due to the α-effect of O and N substituents and thus undergo rapid imine formation with carbonyl groups.[87] Aldehyde possesses a relatively higher reactivity compared to ketone.[88] In term of the steric effect, sterically hindered aldehydes or ketones show slower imine formation rate, compared with unhindered counterparts.[89]

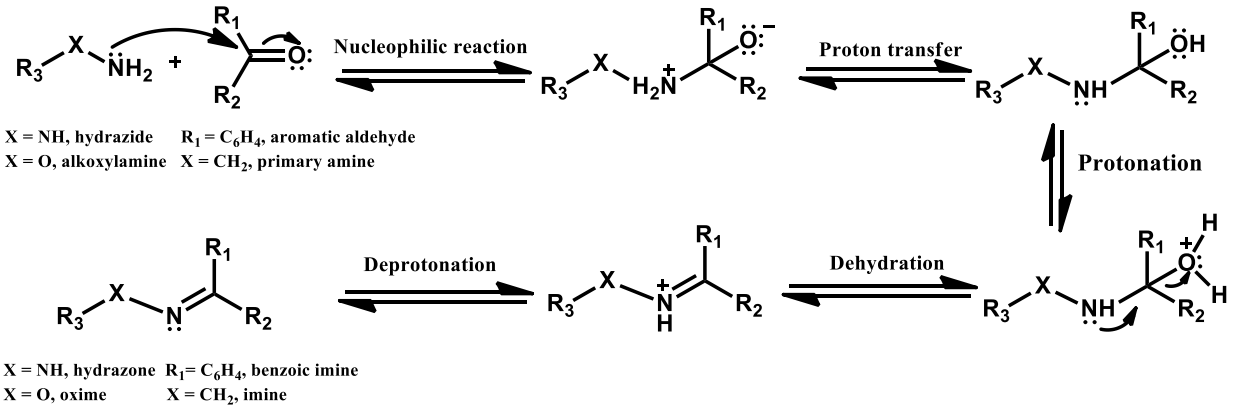

Figure 2.2. Proposed mechanism for formation of imine family, including imine, benzoic imine, oxime, and hydrazone.

In an acidic environment, imine (C=N) bonds are cleaved to the corresponding carbonyl and amine precursors. Their hydrolysis is initiated by the protonation of the N atom and followed by the nucleophilic attack of water molecule over C=N bond. Thus, their acid-catalyzed hydrolysis rate is dependent on pH and temperature. In general, the hydrolysis is rapid at lower pH and elevated temperature. Furthermore, the hydrolysis rate can be varied with the substituents attached to imine bonds through their inductive, resonance, and steric effects.[90] For example, imine bonds synthesized with alkyl amines and alkyl aldehydes are unstable even in a physiological condition (i.e. pH = 7.4 at 37 °C). Aromatic imines stabilized through π-π conjugation between aromatic substituents and C=N bonds exhibit enhanced stability to hydrolysis. As a typical example, benzoic imine is stable at pH = 7.4, while cleaved in response to slightly acidic pH ≈ 6.8.[80, 91] Similarly, aromatic hydrazone linkages show enhanced stability compared to alkyl counterparts.[92]

Hydrazones and oximes (imines substituted with electron-negative O and N atoms) substantially improve the resistance to hydrolysis because of their decreased electrophilicity by mesomeric effect. Seminal works by Raines group show that oximes are more stable than

hydrazones due to the better resistance to protonation by stronger inductive effect of O with higher electron-negativity.[93] Moreover, hydrazones bearing electron-withdrawing groups show better hydrolysis stability in the following order: alkyl hydrazone < acyl hydrazone < semicarbazone < oxime (Figure 2.3).

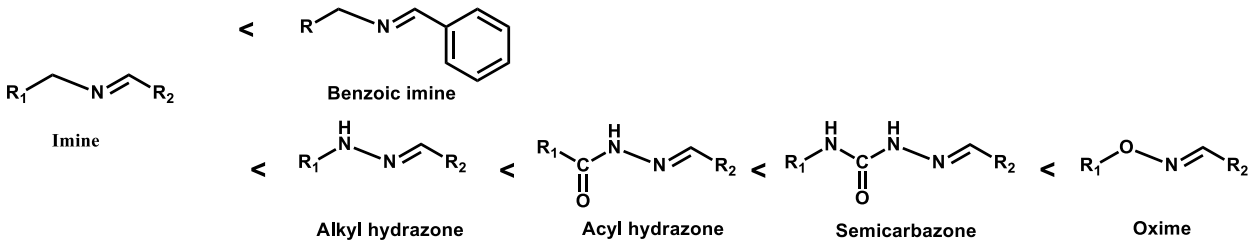

Figure 2.3. Comparison of the hydrolysis stability of imine family with different substituents.

2.3. Self-assembled nanoassemblies

Acid-degradable nanoassemblies have been designed with different numbers and locations of imine bonds in hydrophobic micellar cores or at core/corona interfaces. As illustrated in Figure 2.4, they have been fabricated through aqueous self-assembly of well-controlled ABPs. ABPs are functionalized with imine bonds at different positions, as on the main chain or pendant chains in the hydrophobic block or at the junction of hydrophilic/hydrophobic blocks. These imine-baring nanoassemblies are colloidally stable in physiological conditions (pH = 7.4) and during blood circulation. When being exposed to acidic pH, preferably tumoral pH = 6.6-6.9 and endo/lysosomal pH = 4.0-6.0, they are disintegrated through the distinct cleavage mechanisms of imine linkages, including degradation of main chain, change of hydrophobic/hydrophilic balance, or detachment of hydrophilic corona. Such pH-responsive degradation enables the enhanced release of encapsulated drugs and the improved biodistribution of drug molecules in body.

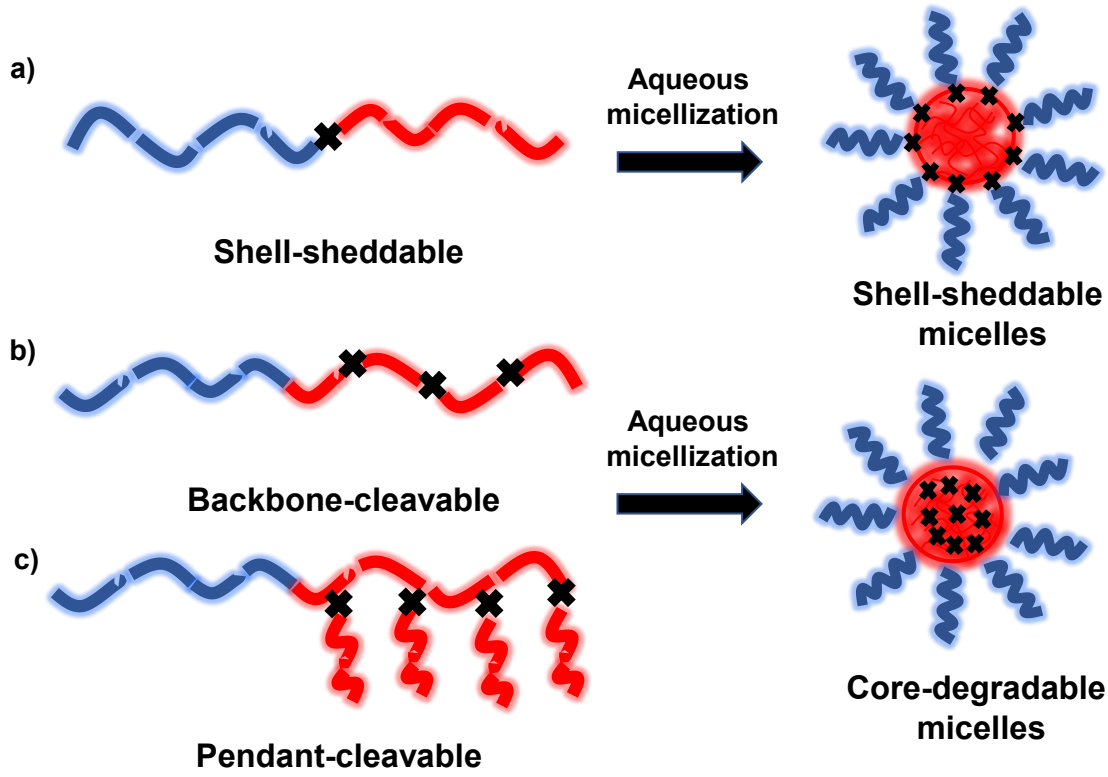

Figure 2.4. Illustration of strategies for the synthesis of acid-degradable ABPs and their nanoassemblies labeled with imine linkages located at core/corona interfaces or in hydrophobic cores.

2.3.1. Shell-sheddable nanoassemblies

Shell-sheddable nanoassemblies are featured with imine linkages located at the interfaces of hydrophobic cores and hydrophilic coronas. They are formed from ABPs bearing an imine linkage at the junction of hydrophobic/hydrophilic blocks. In an acidic environment, hydrophilic coronas are shed from hydrophobic cores, causing the disintegration of the shell-sheddable nanoassemblies and thereafter the aggregation of hydrophobic cores. These shell-sheddable block copolymers have been synthesized mainly by two approaches: post-polymerization modification and direct polymerization.

Post-polymerization modification utilizes the facile coupling reactions of two reactive homopolymers bearing functional groups. One approach explores *in situ* formation of imine bonds. This approach requires the synthesis of two reactive polymer precursors which are functionalized with terminal amino or aldehyde group, thus P1-NH_2 and P2-CHO. The two

reactive precursor polymers are conjugated through imine (Im) linkage to yield P1-Im-P2 ABPs. This approach has been extensively explored for the conjugation of a hydrophilic benzaldehyde-terminated PEG (PEG-BzCHO) with a variety of amine-terminated polymers[94-95] as well as oligomers, including peptides,[96] long alkyl chains,[97] and lipids[98]. The formed acid-sheddable PEG-based block polymers bearing benzoic imine linkage at block junction underwent self-assembly in aqueous solution. This process enabled the formation of nanoassemblies consisting of hydrophobic cores surrounded with PEG coronas and benzoic imine linkages located at interfaces. Owing to PEG corona, the nanoassemblies possess enhanced colloidal stability and reduced clearance by reticuloendothelial systems (RES) during blood circulation. In the tumoral extracellular environment at pH = 6.6-6.9, they were destabilized through the detachment of PEG corona upon the cleavage of benzoic imine bonds at the interfaces. This process can improve cellular uptake by overcoming the PEG dilemma.[99-100] After endocytosis, the nanoassemblies could degrade in endosomes and lysosomes at pH = 4.0-6.0, leading to the enhanced release of encapsulated drug molecules and significant improvement of anti-cancer efficacy.

An important advantage of imine-bearing shell-sheddable nanoassemblies is their ability to switch charge upon the cleavage of junction imine bonds in an acidic environment. The resultant cationic species promote cellular uptake through ionic interactions with anionic lipid membranes, thus improving the biodistribution of drug molecules. Tian et al. reported the synthesis of a triblock copolymer composed of a charge-switchable poly(vinyl imidazole) (PVIm) block and a hydrophobic poly(γ-benzyl-L-aspartate) (PBLA) conjugated through benzoic imine linkage (BzI) with a hydrophilic PEG block, thus forming PVIm-b-PBLA-BzI-PEG triblock copolymer.[94] As illustrated in Figure 2.5a, the first step was the synthesis of a block copolymer precursor bearing a terminal amine group (PVIm-b-PBLA-NH_2) by free radical polymerization of VIm in the presence of 2-aminoethanethiol as chain transfer agent, followed by the chain extension of PVIm with PBLA through ring opening polymerization (ROP). The next step was conjugation of PVIm-b-PBLA-NH_2 with PEG-BzCHO blocks via *in situ* imine formation. The synthesized triblock copolymer self-assembled to form colloidally stable nanoassemblies for co-delivery of paclitaxel/curcumin (PTX/CUR). In the acidic tumor microenvironment, benzoic imine linkages at interfaces were cleaved, causing the detachment of PEG coronas. As a consequence, their size decreased. Furthermore, this process resulted in the protonation of pendant imidazole groups, which changed the surface charge of nanoassemblies to be cationic and thus promoted cellular

uptake of the nanoassemblies (Figure 2.5b). Moreover, the cleavage of junction imine bonds resulted in the enhanced release of drug molecules (Figure 2.5c). *In vivo* (mouse model) results suggest that the PTX/CUR-loaded nanoassemblies had superior breast cancer stem cells-killing capacity and great tumor inhibition, compared with free drug formulations at equivalent dosage (Figure 2.5d).

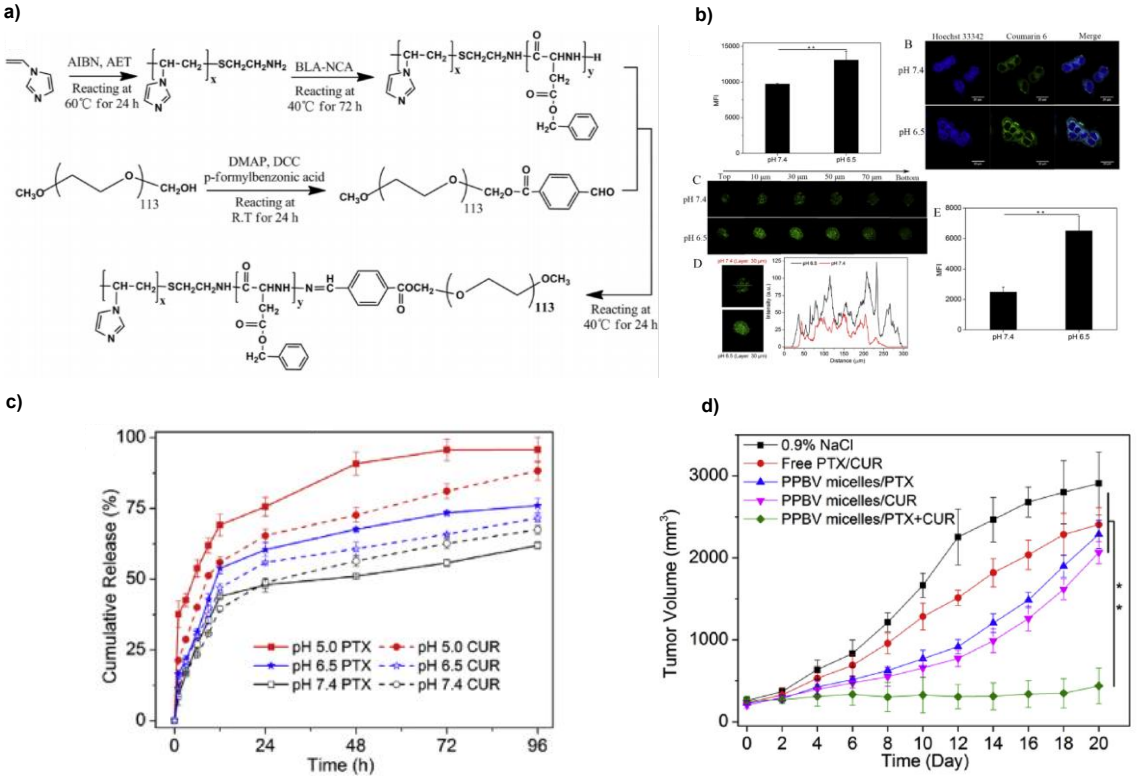

Figure 2.5. Synthesis of a triblock copolymer of PVIm-b-PBLA-BzI-PEG (a), promoted cellular uptake (b), enhanced release rates of encapsulated PTX/CUR in acidic pHs (c), and *in vivo* (mouse model) evolution of tumor volume with mice bearing MCF7 tumors being treated with different drug formulations (d).[94] Copyright 2018 Elsevier.

In addition, PEG detachment allows for effective nucleus-targeting drug delivery as a result of a significant decrease in size which enables deeper penetration to tumor tissues and diffusion into small nucleopores. This could exert a therapeutic effect in nuclei to effectively induce the apoptosis of cancer cells.[101] Chen et al. reported pH-activation strategy to decrease the size of nanoassemblies based on a PEG-based block copolymer labeled with benzoic imine junction and oligo-L-lysine/iridium(III), a metallo-drug. The nanoassemblies had a diameter of 150 nm at pH = 7.4, whereas their diameter decreased to 40 nm upon the cleavage of benzoic imine after being

internalized into endo/lysosomes in cancer cells. The degraded small species were translocated into nuclei and accelerated the release of encapsulated drug molecules, leading to 20-fold higher cytotoxicity compared to free drugs. Furthermore, the nanoassemblies exhibit significant improvement of tumor inhibition and lifespan of A549-cell-xenografted mice.

In addition to benzoic imine, hydrazone linkage has been incorporated at the block junction. Zhu et al. synthesized a PEG-based polystyrene block copolymer labeled with hydrazone at block junction by the coupling reaction of an aldehyde-functionalized polystyrene with a hydrazide-terminated PEG.[102] The block copolymer formed spherical micelles at neutral pH. When exposed to pH = 4, they were disassembled to smaller nanoparticles through the detachment of PEG corona. The acid-responsive disassembly caused the sustained release of encapsulated methyl porphyrin (a model drug) within 10 hrs at pH = 4. Further to linear ABPs, bottlebrush ABPs having imine linkages in side chains were constructed by the conjugation of PEG through *in situ* imine formation with hydrophobic copolymers with multiple pendants, including polypeptides,[91] polyesters,[103] and polymethacrylates[104].

Another approach to synthesize shell-sheddable PEG-based block copolymers having imine linkages at the block junction utilizes click-type reactions, typically including Michael addition reaction[105] and carbamate formation[106]. For this approach, the reactive polymer precursors should bear a functional group for click reaction, along with an imine bond. For example, Liu et al. reported the use of Michael addition reaction to synthesize a block copolymer consisting of PEG block connected through benzoic imine with cholesterol-grafted poly(β-amino ester) block (PAE-g-Ch), thus PEG-BzI-(PAE-g-Ch)-BzI-PEG.[105]

Direct polymerization has been also explored as an effective means to synthesize acid-shell-sheddable block copolymers. This strategy centers on the synthesis of imine-containing macroinitiators for ROP[107-108] and atom transfer radical polymerization (ATRP)[109] as well as a macro-mediator for reversible addition fragmentation chain transfer (RAFT) polymerization[110]. Huang et al. reported the synthesis of a benzoic imine-bearing PEG-based bromine (PEG-BzI-Br). As the synthetic route shown in Figure 2.6a, PEG-BzCHO was conjugated with ethanolamine via imine formation reaction, and further conjugated with α-bromoisobutyl bromide. The formed PEG-BzI-Br was then used as a macro-initiator for ATRP of ibuprofen-labelled methacrylate (HEI) to synthesize PEG-BzI-PHEI block copolymer. Enhanced drug

release was observed at pH = 5.0 with more than 55% of doxorubicin (Dox) release compared with 35% under physiological condition.[109] In another report, a combination of ROP and RAFT polymerization was explored to synthesize an amphiphilic diblock copolymer having benzoic imine at the junction (Figure 2.6b).[110]

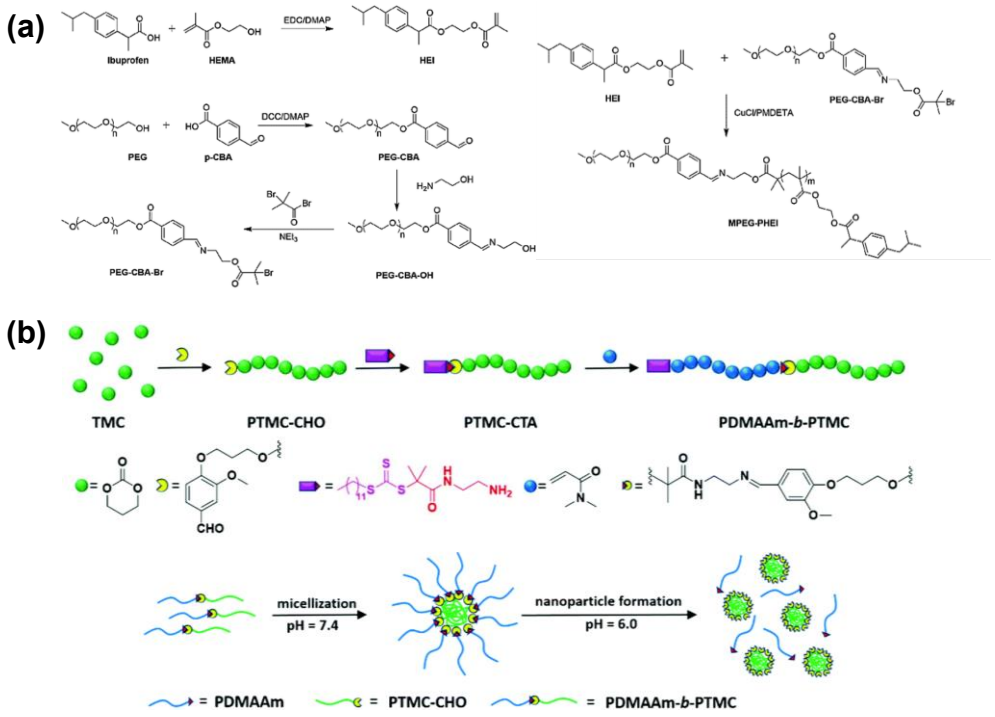

Figure 2.6. ATRP (a)[109] and RAFT polymerization (b)[110] to synthesize well-defined shell-sheddable ABPs containing a benzoic imine bond at the block junction. Copyright 2017 and 2018 Royal Society of Chemistry.

2.3.2. Core-degradable backbone-multicleavable nanoassemblies

These nanoassemblies with imine linkages in their hydrophobic cores are fabricated through self-assembly of ABPs with multiple imine linkages positioned on the backbones of hydrophobic blocks. In acidic pH, they undergo a main chain degradation mechanism, through which hydrophobic blocks degrade to the corresponding small fragments, leading to enhanced release of encapsulated therapeutics. Because small fragments are hydrophilic and water soluble, they could be easily excreted from body through renal clearance. Most backbone-multicleavable block copolymers have been synthesized by step-growth polymerization through either polycondensation or polyaddition reaction.

Step-growth polymerization through polycondensation reaction involves the reaction of dialdehydes with diamines through *in situ* imine formation [111-112] and with diaminooxys through *in situ* oxime formation,[28, 113] yielding hydrophobic copolymers labeled with multiple benzoic imine or oxime linkages on their backbone copolymers. The formed precursors are terminated with either amine, aminooxy, or aldehyde groups, which could be subjected to further modification with functional hydrophilic polymers to form ABPs.[113] The obtained ABPs could self-assemble to form core-degradable nanoassemblies. Zhu et al. reported the synthesis of a triblock copolymer consisting of hydrophobic oxime-labeled backbone polycaprolactone (OPCL) and hydrophilic PEG, thus PEG-OPCL-PEG. As shown in Figure 2.7, a facile polycondensation of a bisaminooxy monomer with a PCL bearing aldehyde terminals (CHO-PCL-CHO) yielded a hydrophobic OPCL, which was subsequently conjugated with PEG-CHO through the formation of oxime bonds. The formed triblock copolymer self-assembled into stable spherical nanoassemblies with a diameter of 250 nm. In acidic environment, they degraded and had the accelerated release of encapsulated Dox, i.e. 80% release at pH = 5.0, compared with <20% at pH = 7.4. The rapid Dox release was compared with < 5% at pH = 5.0 for PEG-b-PCL-b- PEG control without backbone oxime linkages. Furthermore, *in vitro* cell experiment demonstrates their facile internalization into HeLa cells and high anticancer efficacy.[113]

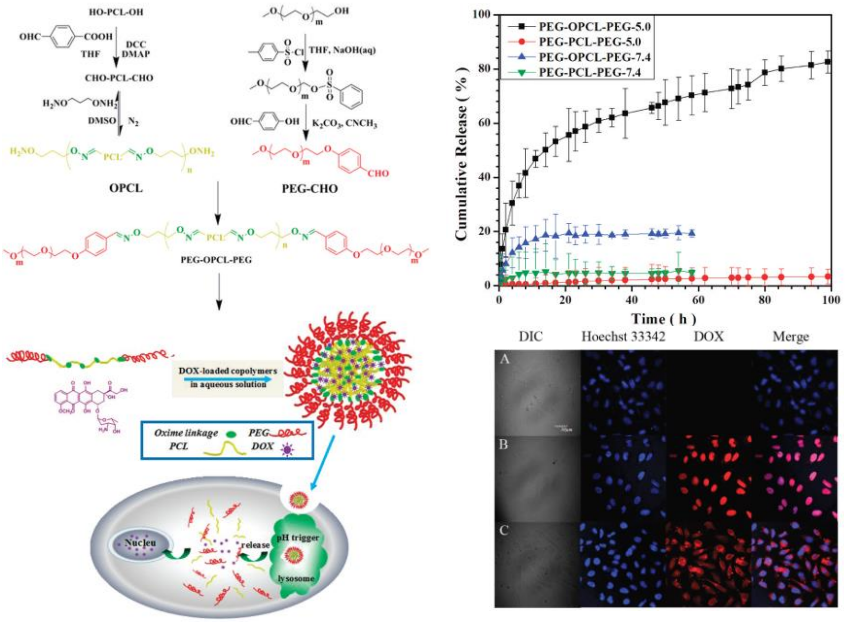

Figure 2.7. Synthetic route, *in vitro* drug release, schematic illustration to intracellular drug delivery, and cellular uptake of PEG-OPCL-PEG labeled with oxime linkages on the backbones.[113] Copyright 2011 American Chemical Society.

Step-growth polymerization through polyaddition reaction utilizes difunctional monomers bearing imine bonds through the formation of carbamate linkages, yielding isocyanate-terminated polyurethanes mostly labeled with hydrazone linkages. Following a facile coupling reaction with hydrophilic PEG allowed for the synthesis of amphiphilic PEG-based polyurethane block copolymers.[114-116] Tan et al. explored the ROP of caprolactone (CL) initiated with a hydrazone-labelled PEG to synthesize PCL-PEG-PCL triblock copolymer. The resulting copolymers labeled with terminal hydroxyl groups reacted with diisocyanates, yielding an amphiphilic multiblock polyurethane. When the copolymer was incubated at pH = 5.0, the hydrazone bonds embedded in the core-forming PCL block were cleaved, consequently disrupting the nanoassemblies. Furthermore, a significant decrease in molecular weights of polymers was confirmed by gel permeation chromatography analysis. The extent of degradation increased with increasing content of hydrazone linkages on the backbones. Such acid-responsive degradation significantly accelerated the release of encapsulated PTX at pH = 5.0.[116]

2.3.3. Core-degradable pendant-multicleavable nanoassemblies

Along with backbone-multicleavable systems, core-degradable nanoassemblies could be formed through self-assembly of ABPs bearing pendant imine linkages at side chains of hydrophobic blocks. They can be disintegrated (or destabilized) by a change in hydrophobic/hydrophilic balance upon the acid-triggered cleavage of imine pendants to the corresponding amines and aldehydes.

Post-polymerization modification through *in situ* imine formation has been extensively utilized to synthesize pendant-multicleavable ABPs and their nanoassemblies. This approach involves the conjugation of reactive polymer precursors mainly bearing pendant amine groups with small molecular hydrophobes bearing aldehyde groups, typically including 4-(decyloxy)benzaldehyde,[117] pyridoxal phosphate,[118] and recent cinnamaldehyde[119] and 1,1,2-triphenyl-2-(p-formyl)ethylene[120]. When anticancer drug molecules are used as hydrophobes, this approach yields polymer-drug conjugates described in Section 2.5. Owing to great biocompatibility and biodegradability, natural polysaccharides bearing pendant amino or carbonyl groups such as highly water-soluble dextran,[121] chitosan,[122] and hyaluronic acid[123] have attracted increasing attention for the construction of imine-based nanocarriers. As an example,

Jayakannan et al. reported a pH-responsive dextran amphiphile synthesized by the conjugation of an amine-labeled hydrophobe with an aldehyde-functionalized dextran through i*n situ* imine formation.[121] The cleavage of the benzoic imine linkages in response to acidic pH <6.0 resulted in the rupture of nanoassemblies, exhibiting the enhanced release of encapsulated drugs.

Direct polymerization strategy has been recently explored as a new means to the synthesis of novel acid-degradable ABPs bearing pendant imine linkages in the hydrophobic block.[124] The resultant PEG-based block copolymer (named PEG-b-PBzImMA) underwent self-assembly to form nanoassemblies composed of acid-degradable hydrophobic core bearing imine linkages surrounded with hydrophilic PEG corona. In response to the tumoral and endo/lysosomal acidic environment, they disassembled through a change in hydrophilic/hydrophobic balance upon the acid-catalyzed cleavage of pendant imine linkages to the corresponding primary amines. As a consequence, such acid-catalyzed hydrolysis of imine linkages in hydrophobic cores led to the enhanced release of encapsulated Dox.[124]

2.4. Core-crosslinked nanogels

Polymeric nanoassemblies fabricated through self-assembly (i.e. hydrophobic interaction) of ABPs in aqueous solutions suffer from undesired dissociation in the blood due to the dilution (4L) as their concentration reaches below CMC after intravenous injection. Such unexpected disassembly could cause the premature release of encapsulated drugs in blood, posing serious systemic toxicity. To circumvent this drawback, core-crosslinking strategy based on imine crosslinks has been employed to fabricate core-crosslinked nanogels. They can not only significantly improve colloidal stability during blood circulation owing to the stability of imine crosslinks at physiological pH = 7.4, but also enable the accelerated release of encapsulated drugs in acidic environments.

A general approach explores the self-assembly of block copolymers to form nanoassemblies, followed by crosslinking reaction inside cores. A variety of reactive block copolymers crosslinked with small molecule crosslinkers through the *in situ* formation of imine,[125-127] benzoic imine,[128-130] hydrazone,[131] and oxime linkages[132]. Because these linkages possess different stability to acid-catalyzed hydrolysis, their acid-responsive degradation rate and thus release kinetics could be tuned. As an example, Lee et al. recently reported a facile one-step

method to synthesize imine-crosslinked nanogels. As illustrated in Figure 2.8, PEG-b-poly[N-[N-(2-aminoethyl)-2-aminoethyl]-L-glutamate] (PEG-b-PLNG) diblock copolymer bearing pendant amine groups reacted with terephthalaldehyde as a crosslinker. The resulting nanogels retained excellent colloidal stability in the presence of a high concentration of salt and against extensive dilution at pH = 7.4. Under slightly acidic conditions (pH ≈ 6.4), encapsulated Dox was rapidly released as a result of the dissociation of cores upon the cleavage of benzoic imine crosslinks. Dox-loaded nanogels demonstrated better anti-cancer efficacy against human carcinoma cancer cells, compared to free Dox at an equivalent dose.[128]

Other approaches involve the use of reactive polysaccharide homopolymers for Cytochrome C (a protein therapeutic) delivery[133] and random copolymers for drug delivery[134]. These copolymers bearing pendant amino groups were subjected to crosslink with small molecular weight dialdehyde crosslinkers, yielding imine-crosslinked nanogels. Reports also describe the fabrication of imine-crosslinked nanogels from a mixture of reactive (co)polymers bearing pendant aldehyde groups and other reactive (co)polymers having amino pendants.[135-137]

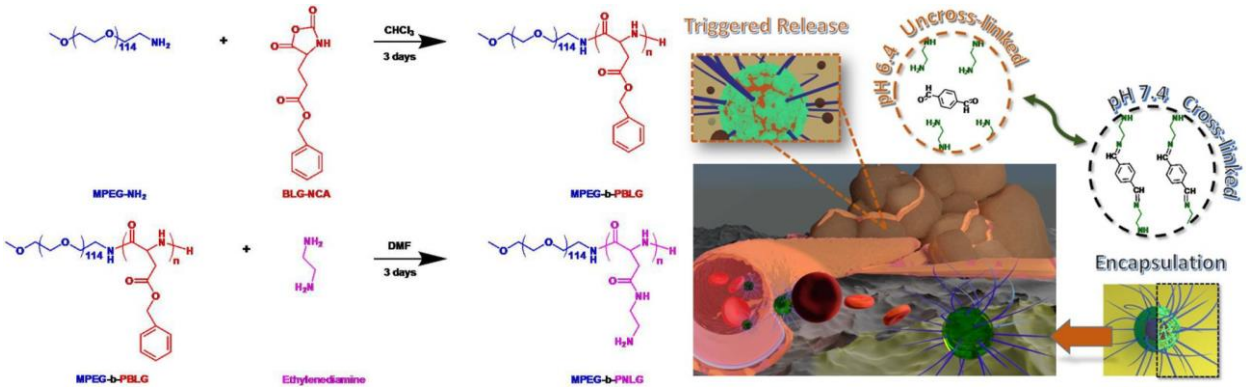

Figure 2.8. Synthesis of acid-degradable imine-core-crosslinked nanogels and schematic illustration for their tumor-targeting drug delivery.[128] Copyright 2018 American Chemical Society.

2.5. Polymer-drug conjugates

Most nanoassemblies self-assembled from ABPs utilize the physical encapsulation of drug molecules in hydrophobic cores mainly through hydrophobic-hydrophobic interactions. Such weak physical interactions often cause the undesired premature release of drug molecules during blood circulation before reaching tumor tissues. To circumvent this drawback, the covalent

conjugation of drug molecules to functional copolymers via acid-labile imine linkages has been extensively studied, forming acid-degradable polymer-drug conjugates or polymer prodrugs. This strategy could not only significantly reduce systemic toxicity of drug molecules, but also enable the rapid release of drug molecules upon the cleavage of imine linkages in acidic environments and thus improve anti-tumor activities.[8] Moreover, well-designed prodrug systems could have greater drug loading content and efficiency, compared with conventional nanoassemblies by physical encapsulation of drug molecules.[138]

Various anticancer drug molecules that bear reactive functional groups have been used to synthesize imine-labeled polymer prodrugs. Among various drugs such as paclitaxel[139] and platinum-based drugs,[140] Dox has received particular attention because it bears reactive carbonyl and primary amine groups. As illustrated in Figure 2.9, these functional groups can be utilized for conjugation of Dox molecules with functional copolymer precursors before and after their further modification with reactive small molecules. Importantly, pristine Dox molecules are generated upon acid-catalyzed hydrolysis of imine linkages, which exhibit similar pharmacological activities to original Dox molecules.

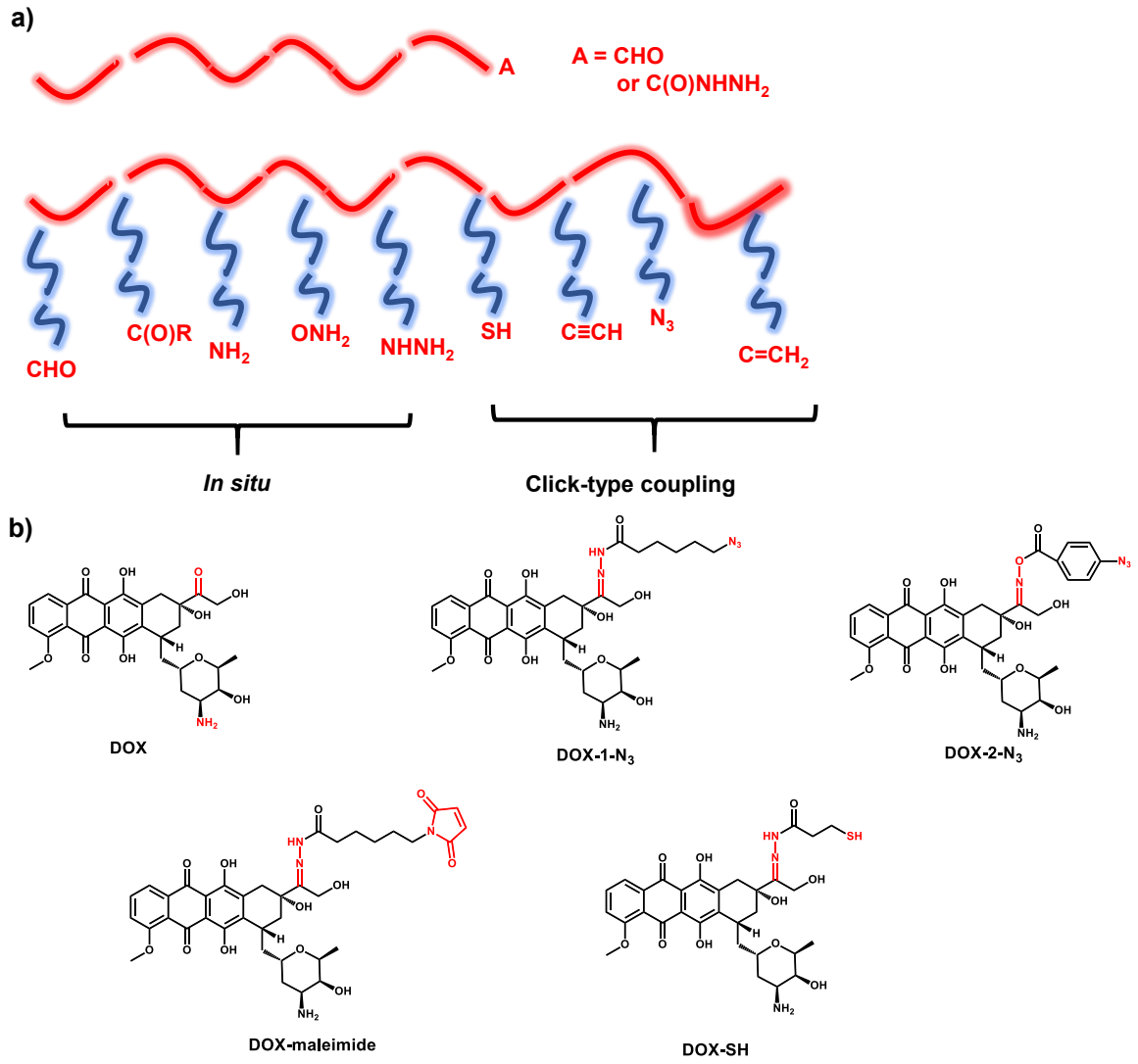

Figure 2.9. Schematic illustration of polymeric precursors with various reactive groups (a) and Dox and modified Dox molecules (b) for the construction of polymer-Dox conjugates with imine and its family linkages.

In situ imine formation has been considerably studied for functional polymers bearing terminal functional groups (Figure 2.9a). Typical polymers include PEG and ABPs bearing terminal aldehyde group that reacts with the amino group of Dox through *in situ* formation of imine bonds[141-145] or terminal hydrazide group that reacts with the carbonyl group of Dox through *in situ* formation of hydrazone bond[146]. For example, Liu et al. reported the conjugation of Dox molecules with polyoxazoline-b-PLA block copolymer through *in situ* formation of benzoic imine linkage.[147] The resultant Dox conjugates self-assembled in the presence of

honokiol (HNK) inhibitor, forming HNK-loaded prodrug nanoassemblies with a diameter of 21 nm. Acid-triggered degradation of benzoic imine bonds resulted in enhanced release of covalently conjugated Dox and physically encapsulated HNK, exhibiting synergistic suppression of growth and metastasis of cancer cells.

In addition to functional polymers bearing terminal reactive groups, various copolymers bearing pendant reactive groups such as aldehydes,[148-152] amines,[153], hydrazides,[154-160] and aminoxys[161] have been synthesized as functional polymer precursors (Figure 2.9a). These copolymer precursors enable the conjugation with more Dox molecules via *in situ* formations of benzoic imine, hydrazone, and oxime bonds, thus significantly improving Dox loading. Recently, Cui et al. reported the synthesis of poly(4-formylphenyl methacrylate-co-2-(diethylamino)ethyl methacrylate)-b-poly(oligo(ethylene glycol) methacrylate) conjugated with pendant Dox molecules through benzoic imine linkages. The block copolymer self-assembled in the presence of a photothermal agent IR780 for chemo-photothermal therapy. They exhibited the enhanced release of IR780 *in vitro* and *in vivo* through the acid-catalyzed cleavage of benzoic imine linkages in the tumoral acidic microenvironment. Owing to their high delivery efficiency and chemo-photothermal therapeutic efficacy, >97% tumor growth in tumor-bearing mice was suppressed with a low dose.[150] Pan et al. evaluated the effect of morphology and size of imine-labeled prodrug on intracellular drug delivery. Three types of nanoassemblies including spheres, nanorods, and vesicles were fabricated. Their morphologies and sizes had great impacts on cytotoxicity, cellular uptake, and intracellular release of conjugated Dox.[148]

Koyama et al. reported the synthesis of PEG-b-poly(aspartate) conjugated with Dox through hydrazone linkages. As illustrated in Figure 2.10, PEG-b-poly(aspartate) precursor was synthesized by four steps, including 1) ROP of α-benzyl-L-aspartate N-carboxyanhydride in the presence of PEG as a macroinitiator to generate PEG-b-poly(benzyl-L-aspartate), 2) deprotection of benzyl groups, 3) reaction with hydrazine hydrate to convert to the corresponding hydrazide groups, and 4) conjugation with Dox through the formation of hydrazone linkages. The self-assembled prodrug nanoassemblies were stable in physiological conditions with negligible leakage. However, they exhibited the selective release of Dox molecules at acidic pH equivalent to tumoral and endo/lysosomal acidic environments. Consequently, compared with free Dox, the synthesized prodrug nanoassemblies had enhanced tumor accumulation, infiltrating permeability, and effective antitumor activity with low cytotoxicity both *in vitro* and *in vivo*.[162]

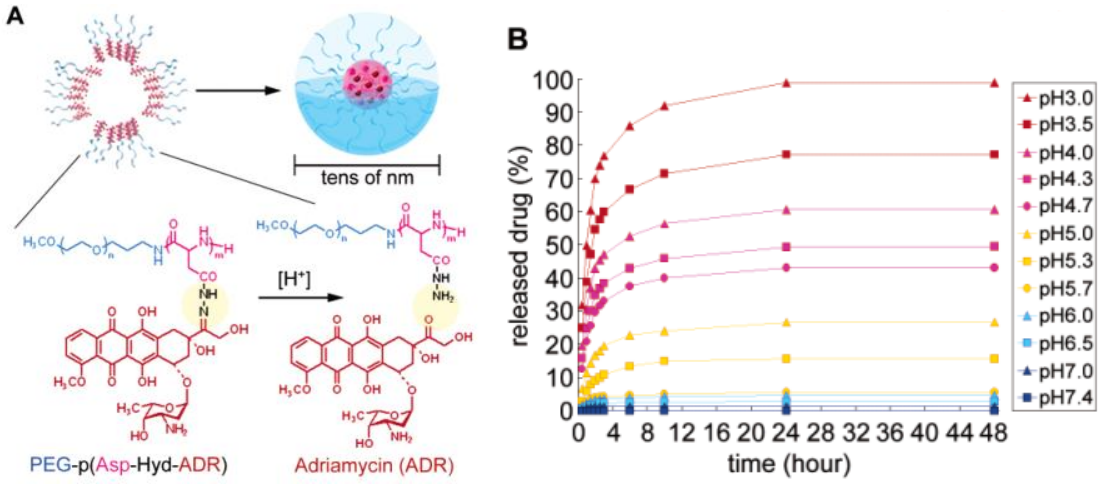

Figure 2.10. PEG-b-polyaspartate conjugated with Dox molecules through hydrazone linkages and their Dox release at different pHs.[162] Copyright 2005 American Chemical Society.

Facile coupling through click-type reactions has been also exploited. As summarized in Figure 2.9b, this approach involves the modification of Dox molecules with reactive functional groups such as azido (Dox-1-N_3 & Dox-2-N_3),[163-165] maleimide (Dox-maleimide),[166-168] and thiol (Dox-thiol)[169] to synthesize reactive Dox molecules labeled with either imine, hydrazone, or oxime bonds. These reactive Dox molecules were conjugated with functional copolymer precursors bearing reactive pendants, yielding acid-degradable Dox-polymer prodrugs. As an example, Shunmugam et al. synthesized a biocompatible and biodegradable polycarbonate-based ABP prodrug conjugated with Dox via oxime linkage by a combination of ROP and azide-alkyne click reaction. Due to the presence of stable oxime linkages, the release of conjugated Dox from self-assembled prodrug micelles remained negligible (<5%) at pH = 7.4 up to 48 hrs. However, a significantly enhanced release of free Dox >90% was observed for 7 hrs at pH = 5. Cellular uptake studies by confocal laser scanning microscopy (CLSM) show the high intracellular accumulation of Dox-conjugated nanocarriers inside cancer cells.[165]

2.6. Dual stimuli-responsive imine-based nanoassemblies

Further to single stimulus-cleavable systems with acid-labile imine bonds, its combination with other labile linkages that are cleavable to endogenous stimuli has provided synergistic

degradation of nanoassemblies. Glutathione (GSH) is over-expressed in cytosols of cancer cells at a greater concentration (4-5 times) than that in normal cells. Moreover, GSH is found 100–1000 times higher in intracellular compartments than extracellular compartments and blood.[170] Given these features of the important endogenous trigger, disulfide has been used as the most prominent example of GSH-responsive cleavable linkage, along with imine linkage, into the design and fabrication of block copolymer nanoassemblies exhibiting dual acid/GSH responses. It should be noted that the reports of imine-based dual acid-responsive copolymers containing combination of benzoic imine/hydrazone,[171] imine/amide,[172] and benzoic imine/acetal[173] are also reported in the literature.

For self-assembled nanoassemblies, a block copolymer having both imine and disulfide linkages positioned at the block junction of PEG and a polymethacrylate having pendant polylactide was synthesized by a combination of azide-alkyne click reaction and RAFT polymerization. The resulting nanoassemblies exhibit dual acid/GSH responses at core/corona interfaces.[174] Recently, polyDox was synthesized by step-growth polymerization of a disulfide-labeled Dox dimer (Dox-ss-Dox) with adipic dihydrazide, thus containing both disulfide and hydrazone linkages in a repeated manner on the backbones. The resultant polyDox nanoparticles showed dual acid/GSH responses to accelerate the release of Dox molecules.[175]

For dual acid/GSH-degradable crosslinked nanogels, an approach utilizes the *in situ* formation of imine or hydrazone group through the reaction of a reactive precursor block copolymer bearing pendant aldehyde groups with a diamine or dihydrazide crosslinker labelled with a disulfide linkage. Examples include shell-crosslinked diblock copolymer[176] and four-arm star copolymer for camptothecin delivery[177]. Another approach explores oxidation reaction of thiol groups to the corresponding disulfide linkages. Shuai et al. reported dual-degradable acid/GSH-responsive interlayer-crosslinked nanogels composed of sheddable PEG corona, imine block junction, disulfide-crosslinked interlayer based on poly(aspartic acid), and hydrophobic core of cholic acid. As illustrated in Figure 2.11, the nanogels were formed from the self-assembly of PEG-BzI-poly(aspartic acid) terminated with cholic acid (CA) hydrophobes, followed by the oxidation of pendant thiol groups to generate disulfide crosslinks in poly(aspartic acid) block. They degraded upon the cleavage of disulfide linkages in the interlayers, exhibiting the enhanced release of encapsulated Dox. Meanwhile, the cleavage of

imine linkages at interlayer/corona interfaces could improve cellular uptake through the detachment of PEG coronas.[178]

Further to nanoassemblies and crosslinked nanogels, polymer-drug conjugates exhibiting dual acid/GSH responses have been reported. For example, block copolymers were designed such that Dox molecules were attached to polymers through imine or hydrazone linkages, while disulfide linkages induced disassembly through GSH-driven degradation on copolymer backbones[169, 179] or crosslinks[164]. Other block copolymers were conjugated with pendant Dox through hydrazone linkage and terminal camptothecin through disulfide bond for rapid release of therapeutic cocktails[180] as well as Dox in pendant chain through both hydrazone and disulfide linkages to achieve more efficient and rapid drug release.[181]

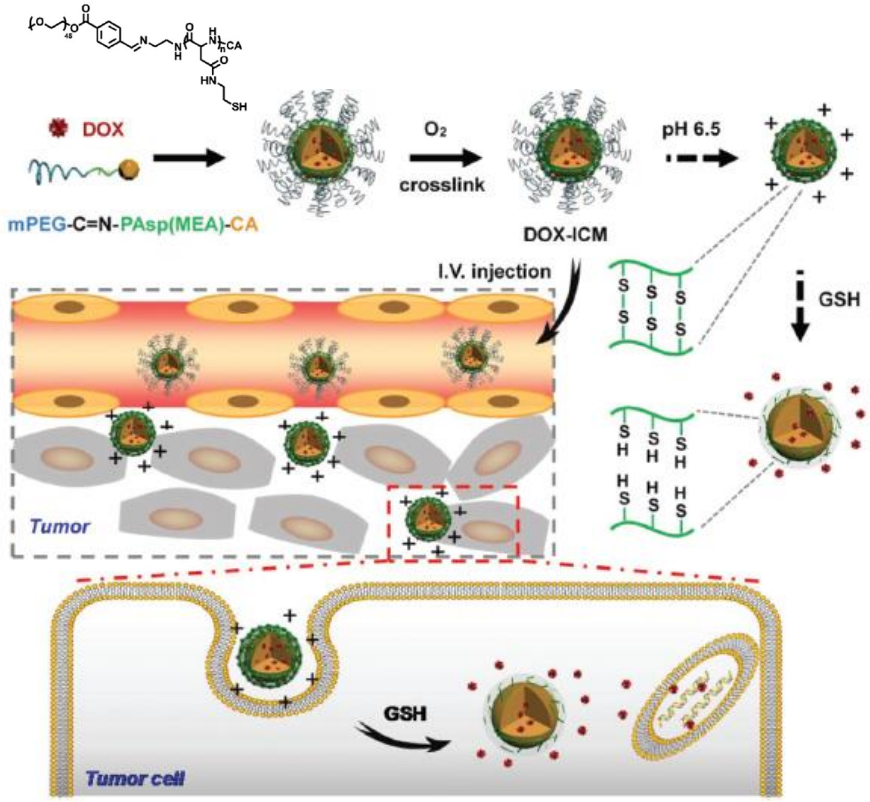

Figure 2.11. Schematic representation of dual acid/GSH responsive-degradable crosslinked-interlayered nanogels, their degradation in endocytic compartments, and cellular uptake.[178] Copyright 2019 Royal Society of Chemistry.

Enzymes, combined with acidic pH, can facilitate the degradation of nanoassemblies and the release of anticancer drugs in cancer cells. The high selectivity of peptidase, esterase, and phosphatase and their differential presence in the tumor environment have been utilized to disintegrate nanoassemblies and enhance the release of drugs covalently attached to copolymers.[182-183]

Several strategies have been reported to develop dual acid/enzyme-degradable nanoassemblies. These strategies center on the incorporation of enzyme cleavable linkages in the presence of targeted enzymes, along with imine linkages. One strategy involves the integration of a specific peptide linkage in dual acid/enzyme-degradable nanoassemblies. Zhu and his coworkers reported poly[N-(2-hydroxypropyl)-methacrylamide]-based highly branched copolymer nanoassemblies labeled with an enzyme-cleavable Gly-Phe-Leu-Gly tetrapeptide (GFLG) and conjugated with Dox through hydrazone bond. As illustrated in Figure 2.12, the hyperbranched copolymer was first synthesized by RAFT polymerization of a GFLG-labeled dimethacrylate in the presence of a GFLG-labeled RAFT mediator. The formed copolymer was then conjugated with Dox through *in situ* hydrazone formation. The resulting self-assembled nanoaggregates displayed greater drug release upon the cleavage of the peptide bonds in the presence of cathepsin (a peptidase) and upon the cleavage of hydrazone bonds at pH = 5.4.[184] Another strategy involves the incorporation of an ester or phosphate bond that can be cleaved by enzymes. For example, Jayakannan et al. reported the modification of dextran through imine and aliphatic ester bond (cleavable to esterase) with pentadecyl phenol. The formed nanoassemblies exhibited dual responses to acidic pH and esterase and were able to release 100% of encapsulated Dox in 50 hrs when pH reduced to 5.5 or esterase was introduced.[185] Zhang et al. reported the fabrication of dual acidic pH/phosphate-responsive nanoassemblies through the post-modification of a PEG-based poly(L-lysine) block copolymer with pyridoxal phosphate. The formed imine bonds were cleaved in acidic pH, releasing pyridoxal phosphate, while the phosphate bonds were cleaved in the presence of calf intestinal alkaline phosphatase, changing the polarity of the copolymers. Such dual responses caused the dissociation of the nanoassemblies.[118]

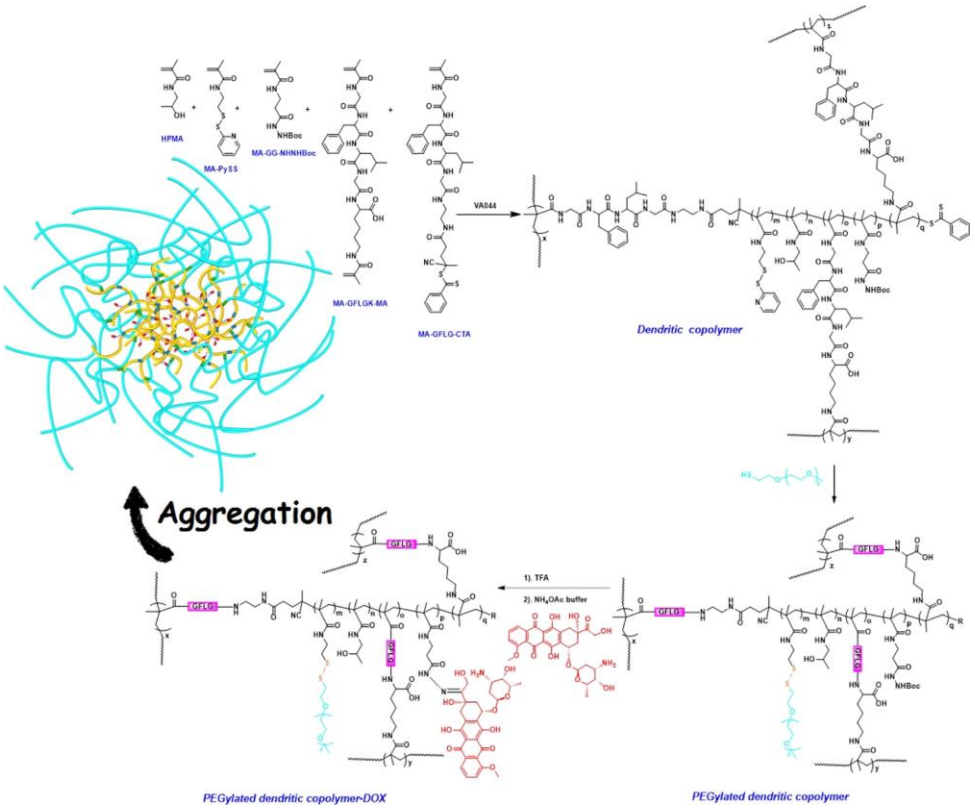

Figure 2.12. Synthesis, post-modification with Dox through hydrazone bonds, and self-assembly of a dual acid/enzyme-degradable highly branched copolymer.[184] Copyright 2018 American Chemical Society.

2.7. Summary and outlooks

Recent advances in various strategies that allow for the design and synthesis of imine-based acid-degradable block copolymers and their nanoassemblies are summarized. General strategies to integrate acid-labile imine bonds in acid-degradable copolymers have explored mainly *in situ* formation of imine bonds and click-type reactions of functional (co)polymers bearing imine linkages. A variety of synthetic strategies with the focus on the number and location of imine bonds in the copolymers and nanoassemblies offer varying disassembly mechanisms upon the cleavage of imine linkages in acidic environments, leading to enhanced release of encapsulated or conjugated drug molecules and thus improved anticancer efficacy.

Three typical forms of imine-bearing nanoassemblies including self-assembled nanoassemblies, core-crosslinked nanogels, and polymer-drug conjugates have been extensively explored for effective intracellular drug delivery. Self-assembled nanoassemblies enable the

physical encapsulation of hydrophobic drugs in the cores through physical interactions with hydrophobic blocks of ABPs. Such weak physical interactions may potentially cause the premature release of drug molecules during blood circulation and thereafter side effects. In an attempt to circumvent this undesired premature release, self-assembled nanoassemblies were crosslinked with imine bonds to form core-crosslinked nanogels. While well-defined nanogels retained excellent colloidal stability upon dilution, they exhibited the controlled/enhanced release of encapsulated drug molecules upon the cleavage of imine crosslinks in tumoral acidic pHs. However, their fabrication usually involved the sophisticated crosslinking process of self-assembled block copolymer precursors with functional crosslinks via either *in situ* imine formation or click-type reactions. Polymer prodrugs nanoassemblies were designed with drug molecules covalently conjugated to block copolymer precursors by imine linkages. Bioactive drugs were only generated and released upon after acid-responsive hydrolysis of imine linkages and disintegration of prodrug nanoassemblies. However, this method is limited to very few drugs (mostly Dox) or requires further chemical modification for the covalent conjugation, compared to facile physical encapsulation with wide choice of anticancer drugs.

Despite these tremendous progresses in the synthesis of imine-based block copolymers for drug delivery application, several major challenges still remain to be addressed for accelerating their successful clinical translation.[55-56] Comprehensive studies on the relationship between the structure of imine linkages and degradation of nanoassemblies are required for better understanding the mechanisms of acid-driven disassembly and drug release. These efforts can allow for the more rational and precise design of acid-degradable block copolymer nanoassemblies with the better selection of imine linkages to maximize therapeutic efficacy of encapsulated or conjugated drugs. Moreover, they enable the development of more effective dual or multiple acid/other stimuli-degradable block copolymer nanoassemblies for synergistic control over the release of drug molecules. As most of the current systems focus on the linear polymers, design and synthesis of imine-based polymers with different architecture and topology (e.g. bottlebrush, ring, and star polymers) presents opportunities to improve drug delivery performance. While a variety of imine-based nanoassemblies have been evaluated *in vitro* (with cell lines), many biological factors found *in vivo*, such as interactions with biomolecules, could significantly influence acid-catalyzed hydrolysis of imine bonds and thus enhanced drug release. Therefore, *in vivo* studies (animal models) could be followed to validate the *in vitro* performance

of these nanoassemblies. Furthermore, the fate and potential toxicity of degraded products upon the cleavage of imine bonds should be systematically studied both *in vitro* and *in vivo*.

Chapter 3 Method

3.1 Instrumentation

^{1}H- and ^{13}C-NMR spectra were recorded using a 500 MHz Varian spectrometer with the references at 7.26 ppm for $CDCl_3$, 2.50 ppm for DMSO-d_6, and 1.94 ppm for CD_3CN. Spectral features are tabulated in the following order: chemical shift (ppm), multiplicity (s = singlet, d = doublet, t = triplet, m = complex multiple), number of protons, and position of protons. Number average molecular weight (M_n) and dispersity ($Đ$) of polymers were analyzed by Agilent gel permeation chromatography (GPC) equipped with a 1260 Infinity isocratic pump and a RI detector. Two Agilent PLgel mixed-C and mixed-D columns were used with eluent solution DMF containing 0.1 mol % LiBr at 50 °C at a flow rate of 1.0 mL/min. Linear poly(methyl methacrylate) standards from Fluka were used for calibration. Aliquots of polymer samples dissolved in DMF with 0.1 mol % LiBr were filtered through 0.40 μm polytetrafluoroethylene filter to remove insoluble species before injecting into GPC columns. A drop of anisole was added as a flow rate marker. Dynamic light scattering (DLS) measurements were carried out to characterize the hydrodynamic sizes of aqueous micelles using a Malvern Instruments Nano S ZEN1600 equipped with a 633 nm He-Ne gas laser at a fixed scattering angle of 175° at 25 °C. For each measurement, date was collected from five repeated measurements for each sample by autocorrelation function using cumulant analysis. UV-vis spectra by Agilent Cary 60 UV/vis spectrometer and fluorescence spectra by Varian Cary Eclipse fluorometer were recorded using a 1 cm wide quartz cuvette.

3.2 Materials

Ethanolamine (EA, 99.5%), benzaldehyde (BA, 99.5%), 2-hydroxylethyl methacrylate (HEMA, 99%), 1,1′-carbonyldiimidazole (CDI, 97%), 1 ,8-diazabicyclo[5.4.0]undec-7-ene (DBU, 98%), 4-(methylamino)pyridine (DMAP, 99%), triethylamine (Et_3N, 99%), bromoisobutyryl bromide (Br-iBuBr, 98%), Tris(2-pyridylmethyl)amine (TPMA, 98%), copper(II) bromide ($Cu(II)Br_2$, 99%), tin(II) 2-ethylhexanoate ($Sn(EH)_2$, 95%), 4-cyano-4-(phenylcarbonothioylthio) pentanoic acid (CTA, 97%), Nile red (NR), and doxorubicin hydrochloride (Dox, -$NH_3^+Cl^-$ salt form, >98%) from Sigma-Aldrich; 1-ethyl-3-(3

dimethylaminopropyl) carbodiimide•HCl (EDC) A from Wako Chemicals were purchased and used as received. Methoxy poly(ethylene glycol) (PEG, MW = 5000 g/mol) from Sigma-Aldrich was dried by an azeotropic distillation with anhydrous toluene prior to use. PEG-Br was synthesized as described elsewhere.[186]

3.3 Synthesis of BzImMA

Synthesis of BzImOH. EA (5.2 g, 0.86 mol) dissolved in anhydrous dichloromethane (DCM, 10 mL) was mixed with a solution containing BA (9.1 g, 0.86 mol) dissolved in DCM (100 mL) in presence of sodium sulfate (3 g) under stirring at room temperature for 13 hr. After sodium sulfate were removed by vacuum filtration, the resulting mixture was dried over sodium sulfate. Solvent was removed by rotary evaporation, and the product was dried in a vacuum oven for 12 hr. Yield = 12.2 g (96%). ^{1}H-NMR ($CDCl_3$, ppm): 8.3 (s, 1H, -$CH_2N\underline{CH}C_6H_5$), 7.8 and 7.4 (m, 5H, $HOCH_2CH_2NCH\underline{C_6H_5}$), 3.9 (t, 2H, $HOCH_2\underline{CH_2}N$-), 3.7 (t, 2H, $HO\underline{CH_2}CH_2$-).^{13}C-NMR ($CDCl_3$, ppm): 163.1, 135.8, 130.8, 128.6, 128.1, 63.3, 62.4.

Synthesis of HEMA-CI. HEMA (6.5 g, 0.05 mol) dissolved in DCM (100 mL) was mixed with CDI (11.4 g, 0.07 mol) in an ice-bath under stirring at room temperature for 13 hr. The resultant mixture was washed with brine solution three times and dried over sodium sulfate. After the removal of solvent by rotary evaporation, oily residual was dried in a vacuum oven at room temperature for 13 hr. Yield = 7 g (89%). ^{1}H-NMR (500 MHz, $CDCl_3$, ppm): 7.1-8.1 (s, 3H, -$C_3N_2H_3$), 6.1 and 5.6 (s, 2H, $\underline{CH_2}C(CH_3)$-), 4.7 (t, 2H, -$\underline{CH_2}CH_2OC(O)$-), 4.5 (t, 2H, -$CH_2\underline{CH_2}O$-), 1.95 (s, 3H, $\underline{CH_3}$-). ^{13}C-NMR ($CDCl_3$, ppm): 166.7, 148.4, 136.9, 135.5, 130.5, 126.5, 117.1, 65.7, 61.5, 18.1.

Synthesis of BzImMA. BzImOH (1.4 g, 9 mmol) was mixed with a solution consisting of HEMA-CI (2.0 g, 9 mmol) and DBU (0.3 g, 1.8 mmol) dissolved in DCM (100 mL) under stirring at room temperature for 13 hr. The reaction mixture was washed with saturated $NaHCO_3$ solution three times and dried over sodium sulfate. After the removal of solvent, the product was dried in a vacuum oven for 13 hr. Yield = 2.6 g (95%). ^{1}H-NMR ($CDCl_3$, ppm): 8.3 (s, 1H, -$N\underline{CH}C_6H_5$), 7.8 and 7.4 (m, 5H, -$NCH\underline{C_6H_5}$), 6.1 and 5.5 (s, 2H, $\underline{CH_2}C(CH_3)$-), 4.5 (t, 2H, -$\underline{CH_2}CH_2OC(O)O$), 4.36 (m, 4H, -$\underline{CH_2}OC(O)O\underline{CH_2}$-), 3.9 (t, 2H, -$CH_2\underline{CH_2}NCH$-), 1.9 (s, 3H, $\underline{CH_3}$-). ^{13}C-NMR ($CDCl_3$, ppm): 166.9, 163.5, 154.9, 135.8, 130.8, 128.6, 128.1, 126.1, 67.2, 65.6, 62.2, 59.4, 18.2.

3.4 Synthesis of PEG-based macro-RAFT mediator (PEG-CTA)

EDC (0.3 g, 16.8 mmol) dissolved in anhydrous DCM (10 mL) was mixed with an organic solution containing PEG (2 g, 0.4 mmol), DMAP (0.02 g, 0.16 mmol) and CTA (0.56 g, 2 mmol) in anhydrous DCM (20 mL) in an ice-bath under stirring for 48 hr. The resultant mixture was washed with brine solution three times, dried over sodium sulfate, and then precipitated from cold diethyl ether to remove excess CTA. Pink solid product was isolated by vacuum filtration and dried in a vacuum oven at room temperature for 13 hr. Yield = 1.9 g (90%). ^{1}H-NMR ($CDCl_3$, ppm): 7.3-7.9 (m, 5H, -SC(S)$\underline{C_6H_5}$), 4.25 (t, 2H, -$\underline{CH_2}$OC(O)-), 3.5-3.8 (m, -$\underline{CH_2CH_2}$O- of PEG main chain), 3.38 (s, 3H, $\underline{CH_3}$O-), 2.7 (t, 2H, -$\underline{CH_2}CH_2(CH_3)C(CN)$-), 2.6 (t, 2H, -$CH_2\underline{CH_2}(CH_3)C(CN)$-), 1.94 (s, 3H, -($\underline{CH_3}$)C(CN)-).

3.5 Synthesis of PEG-b-PBzImMA by ATRP

BzImMA (1 g, 1.64 mmol), PEG-Br (0.17 g, 33 μmol), [Cu(II)TPMABr]Br (0.8 mg, 2 μmol), TPMA (1.4 mg, 5 μmol), and anhydrous anisole (1.5 mL) were mixed in a 10 mL Schlenk flask. The mixture was deoxygenated by purging with nitrogen (purity > 99.99%) for 45 min and then immersed in an oil-bath at 70 °C. A nitrogen purged solution of $Sn(EH)_2$ (5.3 mg, 13 μmol) dissolved in anisole (0.2 mL) was injected to initiate polymerization. For kinetics study, aliquots of the samples were taken out periodically to follow monomer conversion by ^{1}H-NMR and molecular weight by GPC. Polymerization was stopped by cooling the reaction mixture in an ice-bath and exposing to air.

For purification, as-synthesized polymer solutions were diluted with anisole and subsequently precipitated from cold hexane, and the precipitates were collected by vacuum filtration. The similar procedure was repeated twice to remove unreacted monomers and other impurities. The precipitates were then passed through basic alumina oxide column in an attempt to remove residual metal species. After the removal of the solvent by rotary evaporation, the product was dried in a vacuum oven at room temperature for 13 hr.

3.6 Synthesis of PEG-b-PBzImMA (ImP) by RAFT polymerization

As a typical procedure to synthesize ImP-1 (Table 4.1), BzImMA (0.5 g, 1.64 mmol), PEG-CTA (0.17 g, 32.8 μmol), AMBN (2 mg, 9.8 μmol) and anhydrous anisole (0.9 mL) were mixed in a 10 mL Schlenk flask. The mixture was deoxygenated by purging with nitrogen (purity >

99.99%) for 45 min, and then immersed into an oil bath at 70 °C to initiate polymerization. For kinetics study, aliquots of the samples were taken out periodically to follow monomer conversion by ^{1}H-NMR and molecular weight by GPC. Polymerization was stopped by cooling the reaction mixture in an ice-bath and exposing to air.

For the synthesis of ImP-2 and ImP-3, this similar procedure was applied except for the use of BzImMA (1 g, 3.3 mmol), PEG-CTA (0.17 g, 32.8 μmol), AMBN (2 mg, 9.8 μmol), and anhydrous anisole (1.7 mL).

3.7 Investigation of acid-triggered imine degradation using ^{1}H-NMR spectroscopy

Phosphate buffered (PB) solutions (0.2 M) in D_2O at pD = 5, 6.8, and 7.4 were prepared by mixing aqueous stock solutions of NaH_2PO_3 (0.2 M) with Na_2HPO_3 (0.2 M) in D_2O at various volume ratios. pH was measured using a pH meter with a glass electrode standardized with aqueous buffer solutions (pH = 4, 6 and 10). pD values were calculated using the equation of: pD = $pH_{(measured)}$ + 0.41.[187]

For the hydrolysis study of monomer, BzImMA (3.1 mg, 10.0 μmol) was dissolved in CD_3CN (0.3 mL) and resulting solution was mixed with the as-prepared PB solutions in D_2O (0.1 mL, 0.2 M, pD = 5, 6.8 and 7.4). For PEG-b-PBzImMA block copolymer, the purified ImP-3 (10 mg) was dissolved in CD_3CN (0.3 mL) and then mixed with the PB solutions in D_2O (0.1 mL, 0.2 M, pD = 5). The resultant mixtures were subjected to ^{1}H-NMR analysis at 25 °C for given periods of time.

In a separated experiment, an organic solution of ImP (0.1 g) dissolved in THF (10 mL) was mixed with excess concentrated HCl (72 μL, 5 mol equivalents to imine linkages) under stirring at room temperature for 20 hr. The resultant mixture was subjected to centrifugation (10000 rpm x 25 °C x 1 hr). Precipitate was washed with THF three times and dried in a vacuum oven at room temperature for 12 hr. Supernatant was dried over sodium sulfate, and then solvent was removed by rotary evaporation. The obtained degraded products were analyzed by ^{1}H-NMR spectroscopy.

3.8 Determination of critical micelle concentration

A stock solution of NR in THF at 1 mg/mL and stock solutions of ImP-3 in THF at 1 mg/mL and 0.1 μg/mL were prepared. Phosphate buffer saline (PBS) solution (10 mL, pH = 7.4) was

added dropwise into mixtures (2 mL) consisting of the same amount of the stock solution of NR (0.5 mL, 0.5 mg) and various amounts of ImP-3. The resulting mixtures were stirred at room temperature for 40 hr to remove THF, and subsequently filtered through a 0.45 μm PES filter to remove free (not encapsulated) NR molecules. A series of aqueous NR-loaded micelle solutions were obtained at concentrations ranging from 10^{-6} to 0.1 mg/mL. Their fluorescence spectra were recorded at λ_{ex} = 480 nm, and the fluorescence intensities at λ_{em} = 620 nm were plotted over the concentration to determine CMC value.

3.9 Aqueous micellization of PEG-b-PBzImMA by nanoprecipitation method

PBS solution (10 mL, pH = 7.4) was dropwise added to an organic solution of ImP-3 (10 mg) dissolved in THF (2 mL) at a rate of 1 mL/min using a syringe pump under stirring. The resultant mixture was kept stirring at room temperature for 40 hr to remove THF, yielding an aqueous micelle solution at 1 mg/mL.

3.10 Investigation of colloidal stability and acid-responsive degradation of micelles

Aliquots of empty micelles (1 mL, 1 mg/mL) were mixed with acetic buffer solution (3 mL, 0.2 M, pH = 5) under stirring at room temperature. In parallel, empty micelles were kept on bench at room temperature. Aliquots of samples were taken out of the mixtures for DLS analysis for given periods of time.

3.11 Preparation of Dox-loaded micelles by dialysis method

PBS solution (10 mL, pH = 7.4) was added dropwise to an organic solution consisting of Dox (2 mg), Et_3N (5 uL) and ImP-3 (20 mg) dissolved in DMF (2 mL) at a rate of 1 mL/min using a syringe pump under stirring for 1 hr. The resulting mixture was transferred to a dialysis tubing (MWCO = 11–13 kDa) for dialysis against PBS solution (1 L, pH = 7.4) at room temperature for 24 hr to remove free (not encapsulated) Dox molecules and residual DMF. The resulting dispersion was passed through a 0.45 μm PES filter, yielding an aqueous Dox-loaded micelles (Dox-NPs) at 1.6 mg/mL.

To determine the loading level of Dox in micelles, aliquots of aqueous Dox-NPs (1 mL) were mixed with DMF (5 mL). The resultant mixture was subjected to filtration using a 0.45 μm PTFE filter to remove insoluble salts and was analyzed by UV/vis spectroscopy.

3.12 Acidic pH-responsive drug release from Dox-NPs

Aliquots of Dox-NPs (1.7 mg/mL, 2 mL) were mixed with buffer solutions (2 mL) at different pHs = 5, 6.8 and 7.4. The mixtures were transferred to a dialysis tubing (MWCO = 11–13 kDa) and immersed into corresponding buffer solutions (40 mL) at 25 °C under stirring. Aliquots of outer solutions (3 mL) were taken out at given interval to record fluorescence spectra excited at λ_{ex} = 480 nm. Equivalent amounts of fresh buffer solutions were added back to keep sink condition.

Chapter 4 Direct polymerization approach to synthesize acid-degradable block copolymers bearing imine pendants for tunable pH-sensitivity and enhanced drug release

4.1 Synthesis of an imine-bearing methacrylate monomer (BzImMA)

Figure 4.1 depicts our approach with two steps to synthesize a novel BzImMA, a methacrylate bearing an imine linkage.

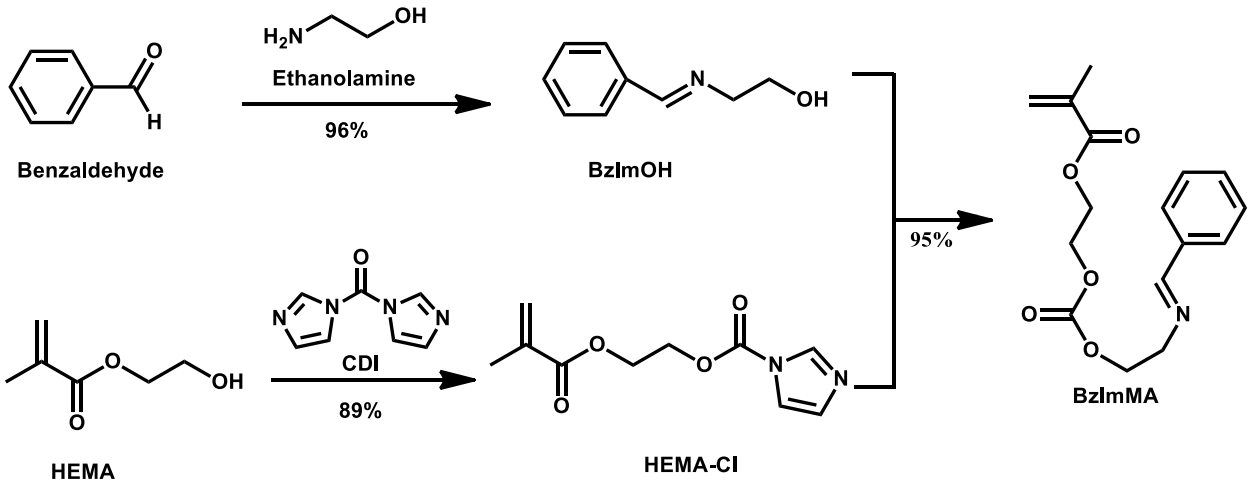

Figure 4.1. Synthetic scheme of BzImMA, a methacrylate bearing a benzoic imine linkage.

The first step was the synthesis of BzImOH precursor bearing a benzoic imine linkage by a facile coupling reaction of BA with EA at 1/1 mole ratio in a gram scale. Sodium sulfate was used to remove water molecules formed during reactions as a biproduct in order to promote forward reaction. ^{1}H-NMR spectrum of BzImOH (Figure 4.2a) shows no peak at 10 ppm corresponding to aldehyde proton in benzaldehyde (a reactant). It shows the appearance of a new peak at 8.3 ppm (c) corresponding to imine proton and the peak at 7.4-7.8 ppm (d) to conjugated benzyl protons. Their integral ratio is quantitative to that of their protons. Combined with ^{13}C-NMR spectrum (Figure A1), our NMR analysis confirms the synthesis of BzImOH with a yield as high as 96%.

In a separated experiment, a carbonylimidazole (CI)-activated 2-hydroxyethylmethacrylate (HEMA-CI) was synthesized by the reaction of HEMA with 1,1′-carbonyldiimidazole (CDI),

followed by a workup purification at 89% yield. Its chemical structure was confirmed by both ^{1}H-NMR (Figure 4.2b) and ^{13}C-NMR (Figure A2) spectra.

Given the successful synthesis of BzImOH and HEMA-CI, the next step was the synthesis of BzImMA by the reaction of BzImOH with HEMA-CI. A 1/1 molar ratio was examined in the presence of DBU as a base catalyst. ^{1}H-NMR spectrum in Figure 4.2c shows the presence of characteristic peak at 8.3 ppm (g) corresponding to an imine proton, 7.4-7.8 ppm (h) to benzyl protons, and 5.5-6.1 ppm (a) to methacrylate protons. Their integral ratio is quantitative to that of their protons. Combined with ^{13}C-NMR analysis (Figure A3), these results confirm the successful synthesis of BzImMA.

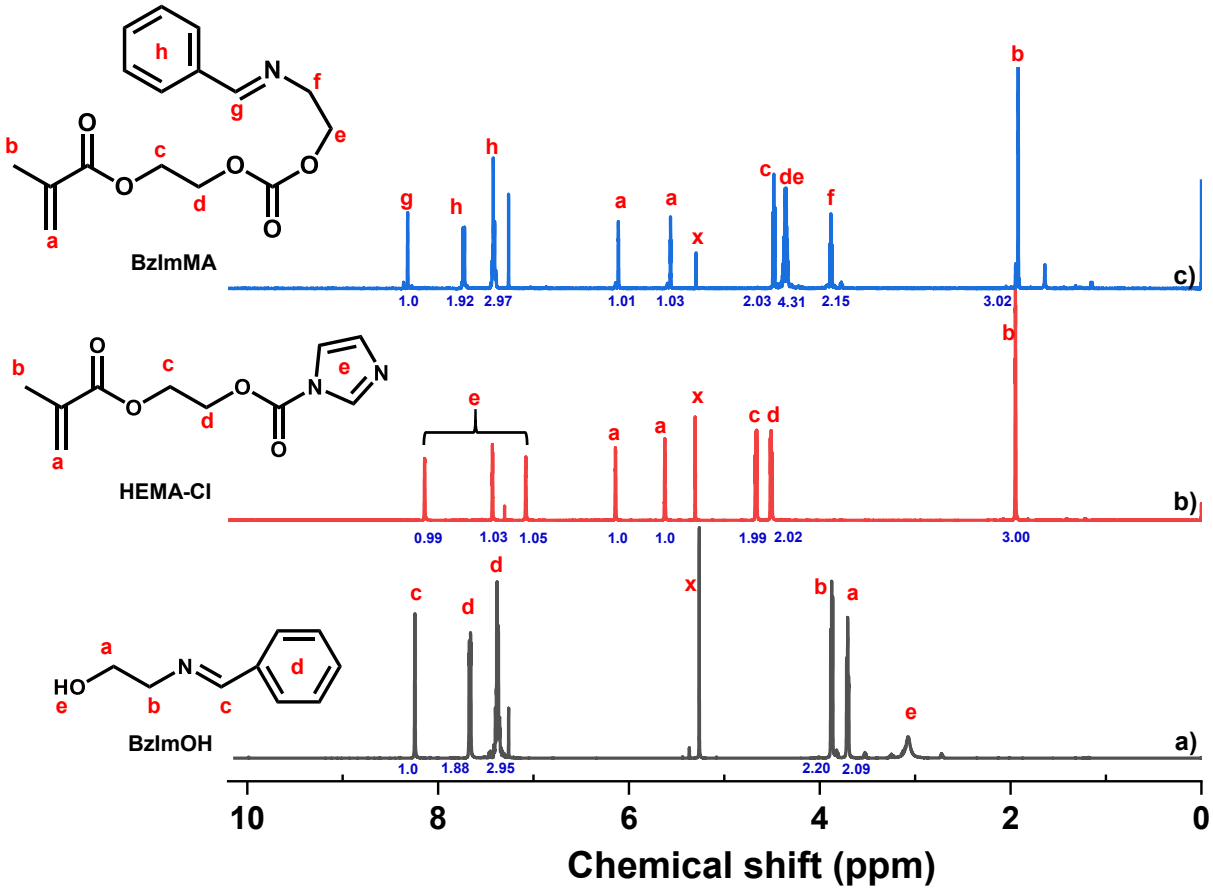

Figure 4.2. ^{1}H-NMR spectra of BzImOH (a), HEMA-CI (b), and BzImMA (c) in $CDCl_3$. x denotes residual solvents or impurities.

4.2 ATRP in an attempt to synthesize PEG-b-PBzImMA

As depicted in Figure 4.3a, the synthesized BzImMA was first examined for atom transfer radical polymerization (ATRP)[188-189] in an attempt to synthesize PEG-b-PBzImMA.

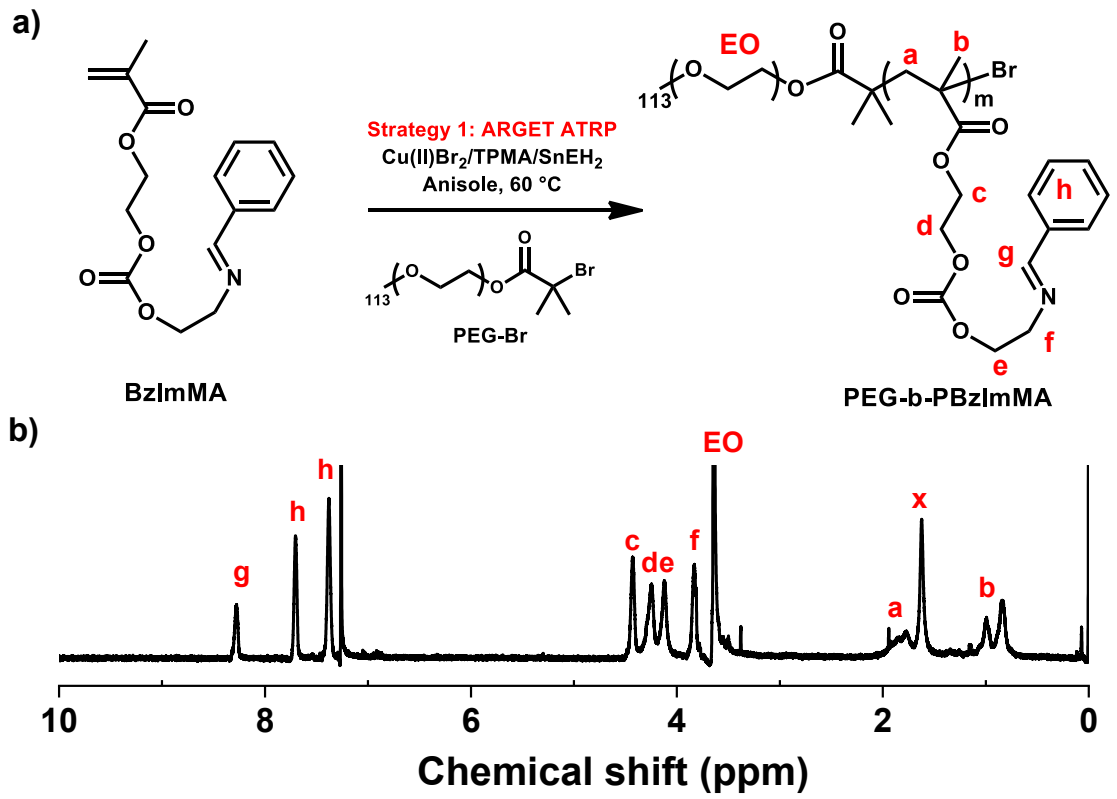

Figure 4.3. Scheme for ATRP of BzImMA in an attempt to synthesize PEG-b-PBzImMA diblock copolymer (a) and ^{1}H-NMR spectrum of PEG-b-PBzImMA precipitate in $CDCl_3$ (b). x denotes residual solvents or impurities.

A PEG-based bromine (PEG-Br) was synthesized and used as a macroinitiator for activator regenerated by electron transfer (ARGET) ATRP [190], where only a few ppm Cu-based catalyst is required. Under the condition of $[BzImMA]_0/[PEG\text{-}Br]_0 = 50/1$ as targeted degree of polymerization (DP) = 50 at complete consumption of monomer, an ATRP was conducted for BzImMA with Cu(II)Br_2/TPMA complexes in anisole at 60 °C. $Sn(EH)_2$ was used as a reducing agent to convert Cu(II) species to active Cu(I) species to initiate ATRP. As seen in Figure A4, the ATRP of BzImMA is well-controlled, with first-order kinetics up to 60% conversion, linear increase of molecular weight over conversion, and narrow molecular weight distribution.

After the stop of polymerization at 60% conversion, the product was attempted to be purified by our standard procedure with two steps. First step was the precipitation of the formed mixture from hexane to remove unreacted monomers and solvents. As seen in Figure 4.3b, ^{1}H-NMR spectrum of precipitate shows the presence of imine linkage at 8.3 ppm (g), benzyl group at 7.4-7.7 ppm (h), backbone methyl group at 0.7-1.1 ppm (b), and PEG block at 3.6 ppm (EO). Using their integral with the DP = 113 for PEG block as a reference, DP of PBzImMA block is determined to be 26 at conversion = 0.6. GPC analysis with PMMA standards shows the formed product has the number average molecular weight (Mn) = 18.3 kg/mol with narrow molecular weight distribution as Đ= 1.24 (Figure A5). These results from ^{1}H-NMR and GPC analysis after precipitation suggest the synthesis of well-controlled PEG-b-PBzImMA diblock copolymer.

The other step of the purification was to pass the mixture through basic aluminum oxide column to remove residual Cu and Sn (metal) species. Unexpectedly, ^{1}H-NMR spectrum in Figure A6 shows disappearance of the peak at 0.7-1.1 ppm equivalent to backbone methyl groups, but a new peak at 10 ppm corresponding to aldehyde protons. This result could suggest the possible cleavage of imine linkages of PEG-b-PBzImMA in basic aluminum oxide column. The cleaved polymer products having pendant amino groups generated as a consequence of the cleavage of imine linkages could not be eluted through column.

To further confirm the potential cleavage of imine linkage with basic aluminum oxide column, BzImMA monomer was treated with basic aluminum oxide in column. As seen in Figure 4.4, ^{1}H-NMR spectrum shows the presence aldehyde peak at 10 ppm owning to the degradation of imine linkages. Given unsuccessful removal of metal residue in PEG-b-PBzImMA by ATRP approach, which may pose potential cytotoxicity for biomedical application, we have turned our attention to RAFT polymerization technique.

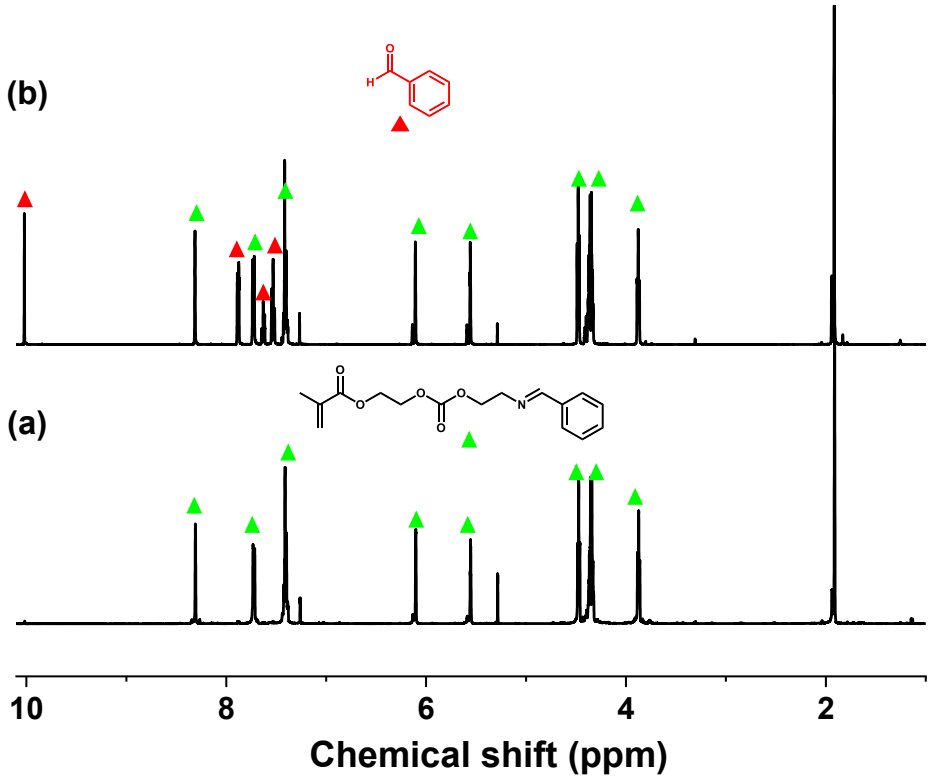

Figure 4.4. ^{1}H-NMR spectra of BzImMA before (a) and after (b) treatment with basic aluminum oxide in $CDCl_3$.

4.3 RAFT polymerization to synthesize well-controlled PEG-b-PBzImMA

Figure 4.5a illustrates RAFT polymerization of BzImMA to synthesize well-controlled PEG-b-PBzImMA (ImP). A poly(ethylene glycol)-labeled dithiocarbonyl RAFT macro-mediator (PEG-CTA) was synthesized and characterized by ^{1}H-NMR analysis with >98% conjugation efficiency (Figure A7). As mediated with PEG-CTA, RAFT polymerization of BzImMA was initiated with 2,2′-azodi(2-methylbutyronitrile) in anisole at 70 °C. Under the condition of $[PEG\text{-}CTA]_0/[AMBN]_0 = 1/0.3$, the initial mole ratio of $[BzImMA]_0/[PEG\text{-}CTA]_0$ as the targeted DP was varied with 100/1 and 50/1 to demonstrate the direct polymerization approach as an effective means to the synthesis of well-controlled ImPs.

After being purified by precipitation from hexane, the formed PEG-b-PBzImMA were characterized for chemical structure by NMR and molecular weight by GPC. With an example of ImP-1 synthesized under $[BzImMA]_0/[PEG\text{-}CTA]_0 = 50/1$, ^{1}H-NMR spectrum in Figure 4.5b

shows the presence of characteristic peaks at 8.3 ppm (g′) for imine linkage, 7.4-7.7 ppm (h′) for benzyl group, 0.7-1.1 ppm (b′) for backbone methyl group of PBzImMA block, and 3.6 ppm (EO) for PEG block. Their integral ratio was used to determine the DP of PBzImMA block to be 29, which is close to that (DP = 36) theoretically calculated with monomer conversion. GPC analysis confirms that ImP-1 had M_n = 16.7 kg/mol with narrow dispersity as $Đ$ = 1.30. As seen in Figure A8, the molecular weight distribution shifted to high molecular region; however, it had two shoulders in both low and high molecular weight regions. One in low molecular region could be attributed to trace of unreacted PEG-CTA residue. The other in high molecular weight region could be caused by undesired side reactions caused in a complicated manner. Possible side reactions could include the undesired chain termination by mainly disproportionation due to methacrylate polymerization, the presence of residual PEG-diol as an impurity contained in commercially available PEG which eventually results in the formation of triblock copolymer as a side product, and possible cleavage of imine linkage during polymerization. With $[BzImMA]_0/[PEG\text{-}CTA]_0$ = 100/1, the similar procedure was used to synthesize ImP-2 and ImP-3 at different monomer conversions. The results are summarized in Table 4.1.

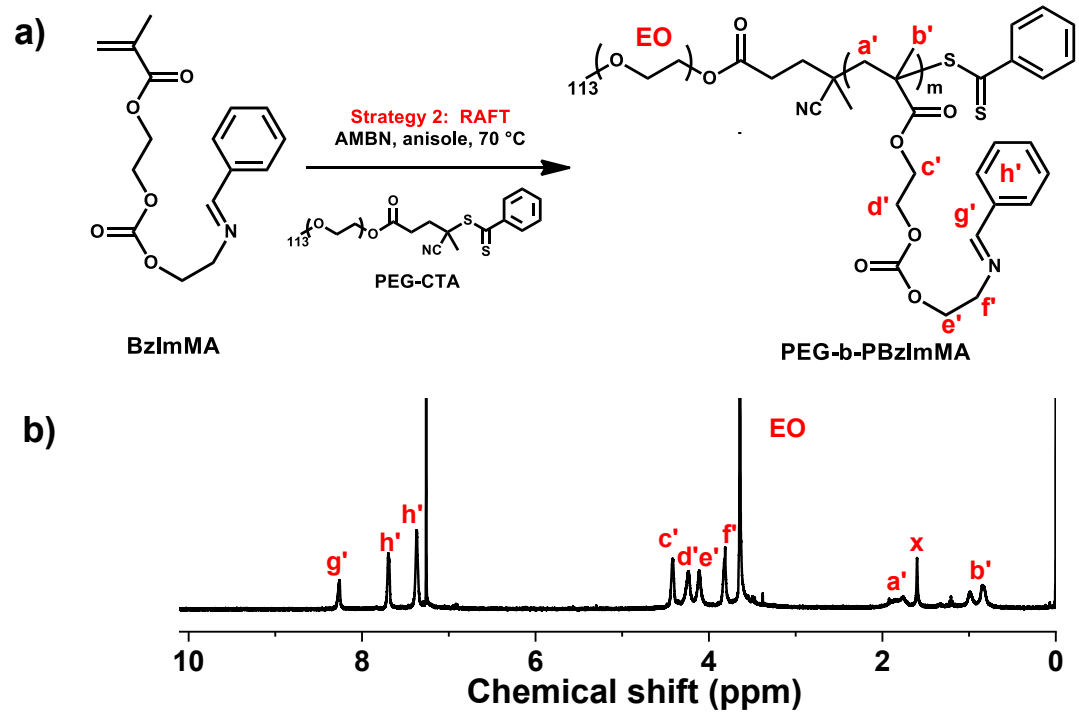

Figure 4.5. Scheme for RAFT polymerization of BzImMA to synthesize PEG-b-PBzImMA in presence PEG-CTA (a), ^{1}H-NMR spectrum of ImP-1 in $CDCl_3$ as an example(b). x denotes residual solvents.

Table 4.1. Characteristics and results for PEG-b-PBzImMA (ImP) block copolymers synthesized by RAFT polymerization.[a]

ImP	$[BzImMA]_0/[PEG\text{-}CTA]_0$	Time (hr)	Conv [b]	DP_{theo} [c]	DP_{NMR} [b]	M_n [d] (kg/mol)	$Đ$ [d]
ImP-1	50	7	0.72	36	29	16.7	1.30
ImP-2	100	5	0.33	33	34	20	1.25
ImP-3	100	10	0.72	72	58	25.2	1.29

[a]$[PEG\text{-}CTA]_0/[AMBN]_0$= 1/0.3 in anisole at 70 °C and $[BzImMA]_0$/anisole = 0.6 wt/wt; [b]By ^{1}H-NMR; [c]DP_{theo}= $[BzImMA]_0/[PEG\text{-}CTA]_0$ × conversion; [d]GPC with PMMA standards.

To get an insight into kinetics of RAFT polymerization of BzImMA in the presence of PEG-CTA, aliquots were taken periodically during polymerization of ImP-1 to analyze their conversion and molecular weight data (Figure A9). The polymerization was first order, suggesting the constant concentration of active centers during polymerization up to 70% conversion. An induction period was observed for 3 hrs. Molecular weight increased linearly with conversion. Molecular weight distribution was narrow with Đ <1.30 and GPC traces were evolved to high molecular weight region over conversion; however, two shoulders in both low and high molecular weight region were observed for all samples.

4.4 Investigation of acidic pH-triggered imine degradation

Imine bond could be cleaved to corresponding primary amine and aldehyde in acidic environment. The formed PEG-b-PBzImMA (ImP-3) contain pendant imine linkages through the polymerization of BzImMA, a methacrylate labelled with an imine bond. Here, acidic pH-responsive cleavage of imine bonds was systemically investigated with BzImMA and PEG-b-PBzImMA using ^{1}H-NMR spectroscopy in a homogenous $CDCN_3$/PB-D_2O mixture.

First, small molecule BzImMA was incubated at different pDs. As illustrated in Figure 4.6a, the cleavage of imine bond in BzImMA generates the corresponding primary amine-labeled methacrylate (AM) and BA as degraded products. As an example, Figure 4.6b shows overlaid ^{1}H-NMR spectra of BzImMA over incubation time at pD = 6.8. A new peak at 10 ppm (g′) corresponding to aldehyde proton of degraded product BA was observed after 0.5 hr incubation. Its integral increased over incubation time, whereas the integral of the imine peak (g) decreased. Its integral ratio to that of the peak vinyl peaks (a, a′) was used to estimate %hydrolysis rate of

imine linkages. As seen in Figure 4.6c, %hydrolysis increased over incubation time and further reached to completion in acidic conditions (i.e. pD = 6.8 and 5.0). The rate is much faster, compared to physiological pD = 7.4. As compared in Figure 4.6d, the time when a half concentration of imine linkages is cleaved ($t_{1/2}$) was 118.5 hr at pD = 7.4, while it significantly decreased to 6.4 hr at pD = 6.8, and further to 1.5 hr at pD = 5.

The cleavage of 50% imine linkages at pD = 6.8 in 6–7 h is promising in that it can occur in extracellular microenvironment of tumor tissues after extravasation during blood circulation. The cleavage could generate the corresponding amine groups and following quaternary ammonium salts in mild acidic environment, which can facilitate the endocytosis of drug-loaded nanoassemblies into cancer cells.[191]

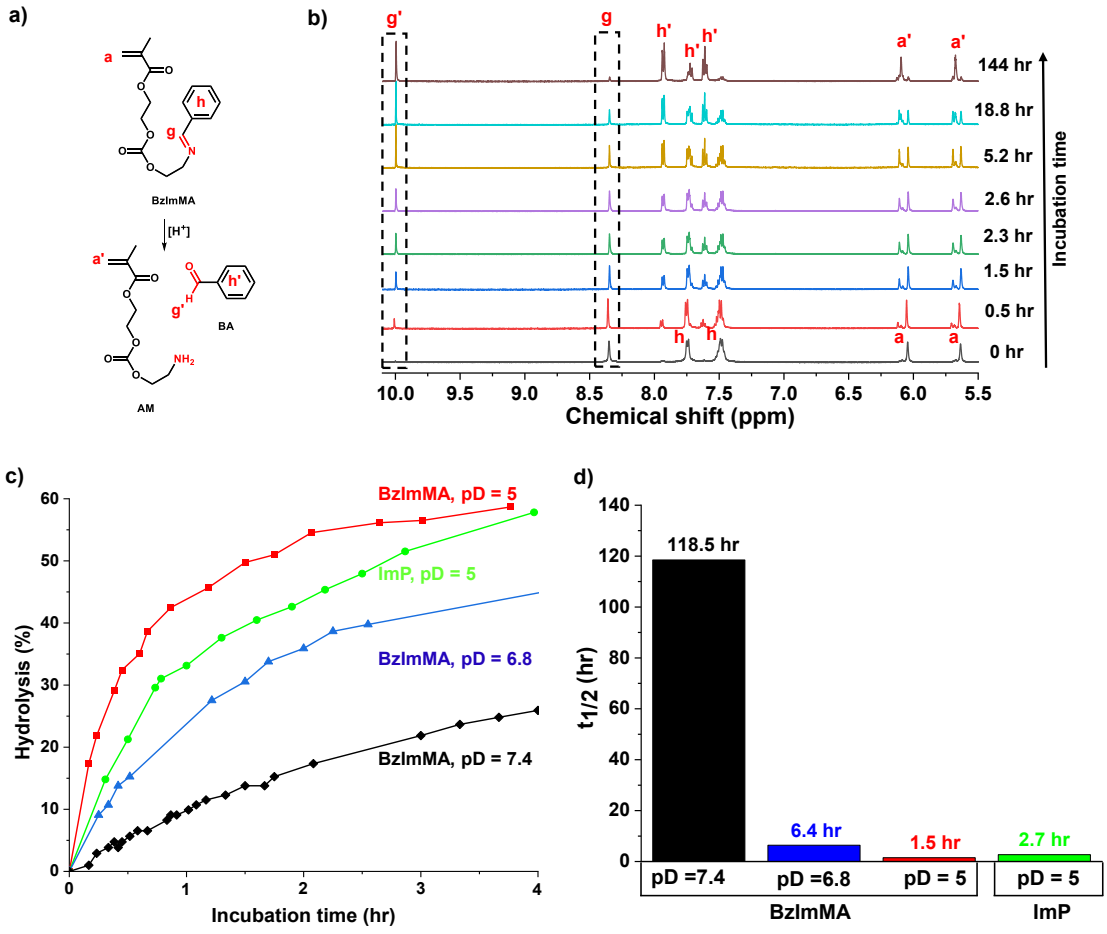

Figure 4.6. Scheme for cleavage of imine linkage (a) and overlaid ^{1}H-NMR in $CDCN_3$/PB-D_2O over time incubated at pD = 6.8 as an example (b) for BzImMA; evolution of %hydrolysis of imine linkages over incubation time (c) and $t_{1/2}$ (d) for BzImMA at pDs = 7.4, 6.8, and 5.0 as well as ImP-3 at pD = 5.0.

For comparison with BzImMA, ImP copolymer was examined with a choice of ImP-3 at pD = 5. Note that ImP refers ImP-3 hereafter. As illustrated in Figure 4.7a, PEG-b-PAM and BA were generated as degraded products upon the cleavage of imine linkages in the PBzImMA block. With overlaid ^{1}H-NMR spectra in Figure 4.7b, %hydrolysis was plotted over incubation time. Similar to BzImMA, %hydrolysis of pendant imine linkages increased over incubation time. The $t_{1/2}$ of ImP was determined to be 2.7 hr, which is slightly larger than that (1.5 hr) for BzImMA. This is plausibly due to longer chain length and amphiphilic nature of ImP in aqueous buffer. Overall, the cleavage of imine bonds is confirmed to be greatly enhanced at acidic condition.

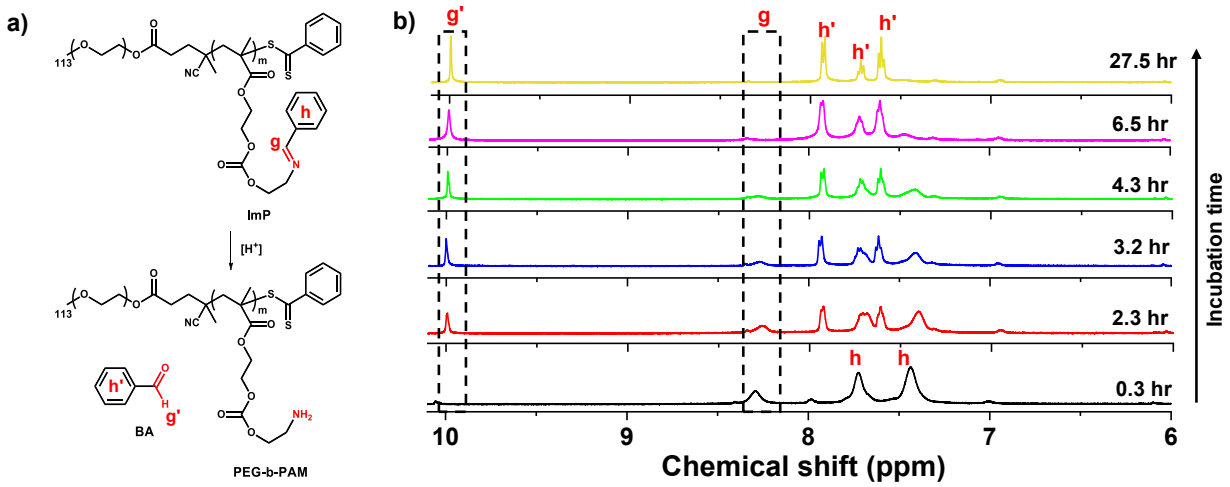

Figure 4.7. Scheme for cleavage of imine bonds (a) and overlaid ^{1}H-NMR over time incubation pD = 5.0 (b) for ImP-3.

The acid-responsive degradation of PEG-b-PBzImMA was further examined by being treated with excess concentrated HCl in THF. The resultant mixture became turbid (Figure 4.8a) and was subjected for centrifugation to separate supernatant from precipitates (Figure 4.8b). ^{1}H-NMR spectrum of supernatant shows the typical peaks at 10 ppm (a) and 7.5–8 ppm corresponding to aldehyde and benzyl protons respectively, confirming the presence of BA (Figure 4.8c). ^{1}H-NMR spectrum of precipitates (Figure 4.8d) presents two new peaks at 8.5 ppm (g) and 3.1 ppm (f) corresponding to the amino and adjacent methylene groups, respectively. These results confirm the generation of PEG-b-PAM as a consequence of the detachment of BA from PEG-b-PBzImMA upon the cleavage of imine linkages.

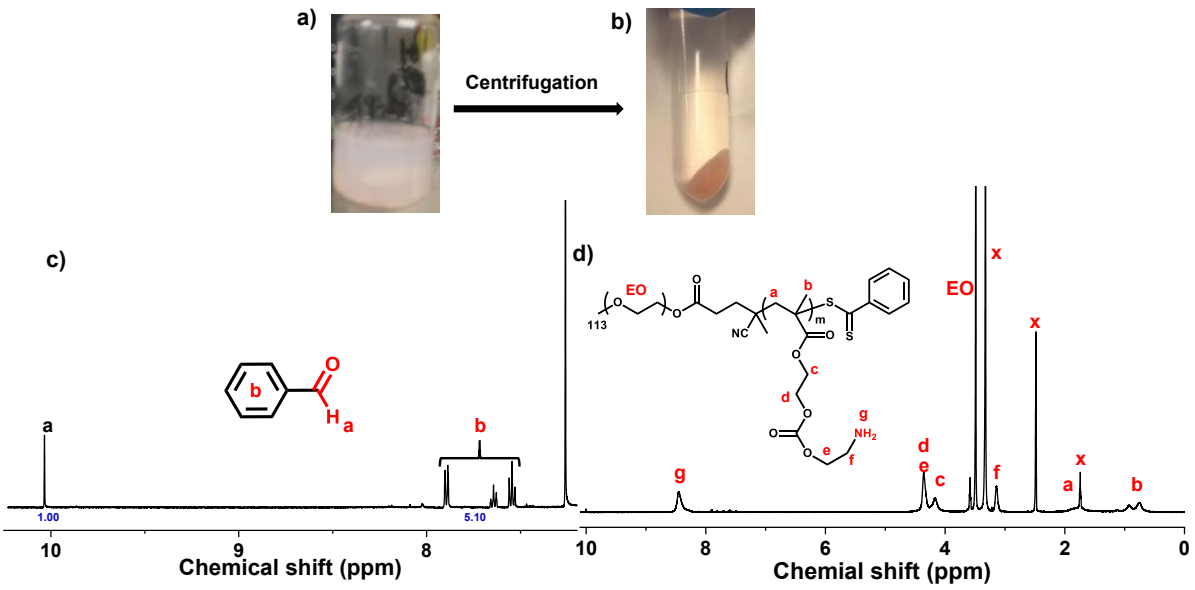

Figure 4.8. Digital image of a mixture consisting of ImP and HCl in THF before (a) and after (b) centrifugation; ^{1}H-NMR for isolated supernatant BA in $CDCl_3$ (c) and precipitates PEG-b-PAM in DMSO-d_6 (d). x denotes solvent residue.

4.5 Aqueous micellization and acid-responsive disassembly

The synthesized diblock copolymer ImP consists of a hydrophilic PEG block and a hydrophobic PBzImMA block bearing multiple imine pendants. Its amphiphilicity was examined with the determination of its CMC by fluorescence spectroscopy using a hydrophobic NR probe. This method is based on the fact that the fluorescence intensity of NR dramatically increases when NR molecules are encapsulated in hydrophobic micellar cores. However, fluorescence intensity is lower when they exist in aqueous solution due to their poor water solubility.[192-193] A series of aqueous mixtures containing same amount of NR but various amounts of ImP were prepared and filtered to remove free (not encapsulated) NR molecules. From their fluorescence spectra (Figure 4.9a), the fluorescence intensity at λ_{em} = 620 nm was plotted over the concentration of ImP (Figure 4.9b). Fluorescence intensity remained low at lower concentration of ImP; however, upon further increase in ImP concentration, it rapidly increased owning to an increasing concentration of NR molecules encapsulated in micellar cores. By regression analysis of the two linear regions of the data, the CMC of ImP was determined to be 24 µg/mL equivalent to 1.1 µM, which is within the range of typical CMC values of amphiphilic block copolymers.

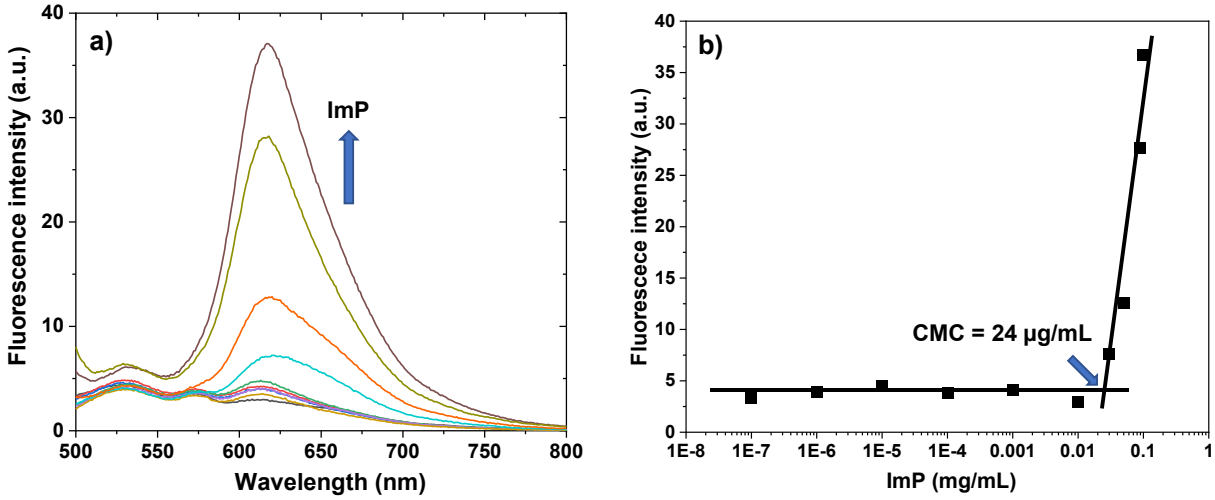

Figure 4.9. Overlaid fluorescence spectra of a series of aqueous mixtures consisting of NR and ImP (a) and fluorescence intensity at 620 nm over the amount of ImP (b).

At concentration above the CMC, amphiphilic ImP self-assembled to form micellar aggregates that are composed of imine-containing hydrophobic PBzImMA cores, surrounded with hydrophilic PEG corona (Figure 4.10a). For instance, the nanoassemblies formed at 1 mg/mL had the z-average diameter of 86 ± 0.7 nm with monomodal distribution (Figure 4.10b). Their colloidal stability and acid-responsive degradation were investigated by DLS with evolution of z-average diameter (Figure 4.10c) and count rate (Figure A10). At physiological pH = 7.4, their z-average diameters and count rates kept unchanged at room temperature, suggesting good colloidal stability over 40 days. When the micelles were incubated at pH = 5, both z-average diameter and count rates increased rapidly within 190 hr with the occurrence of aggregates (diameter >1 µm). As illustrated in Figure 4.10a, the acid-triggered cleavage of imine pendants causes the detachment of hydrophobic benzyl groups, generating PEG-b-PAM degraded products over time. ImP becomes hydrophilic through the change in hydrophobic/hydrophilic balance. However, the degraded PEG-b-PAM chains could have a limited solubility even in aqueous acidic solution. Furthermore, the degradation took place in micellar cores. These combinations could result in the formation of large aggregates in acidic environment.

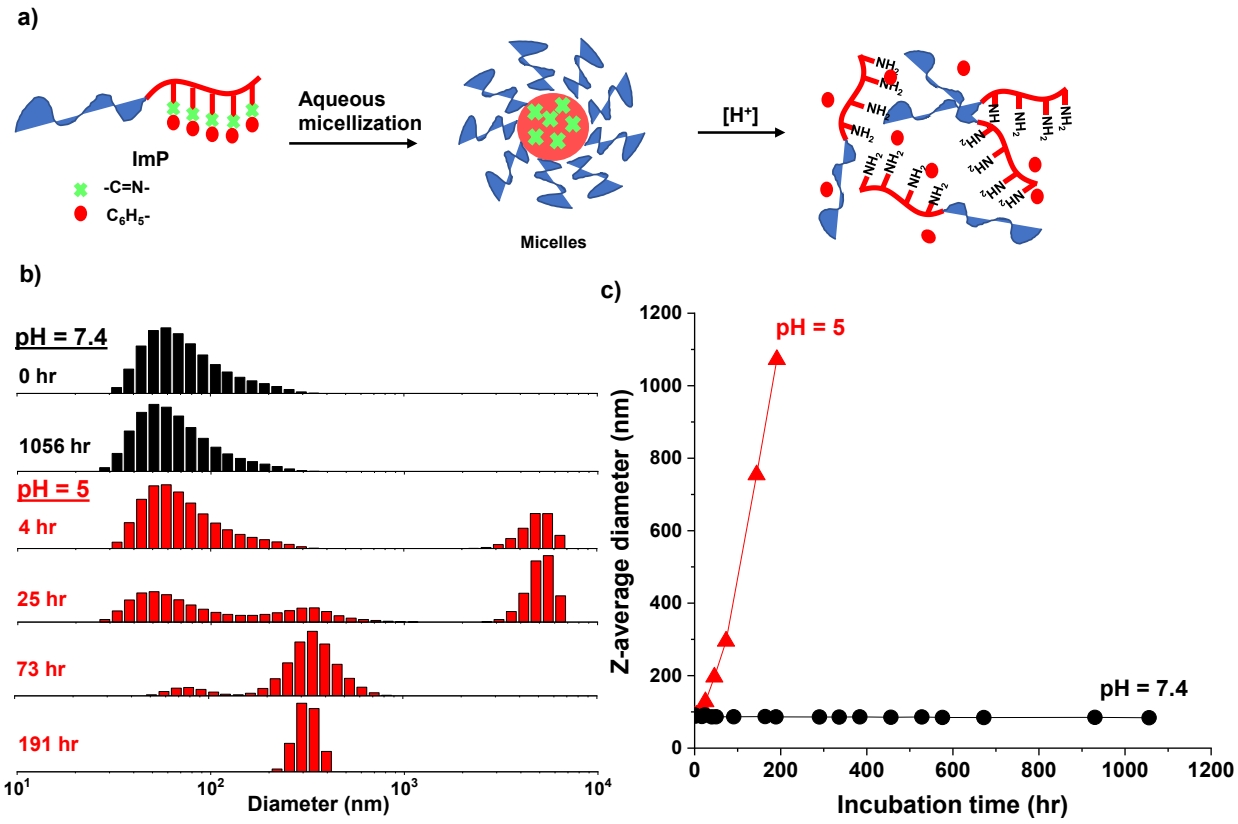

Figure 4.10. Schematic illustration of acid-responsive dissociation of self-assembled micelles (a); overlaid DLS diagrams (b), and evolution of z-average diameter of ImP micelles at 1 mg/mL, incubated at physiological pH = 7.4 and acidic pH = 5.0 (c).

4.6 Preparation of Dox-loaded micelles

To preliminarily investigate the ImP-based micelles as an intracellular delivery nanocarrier of anticancer drugs, Dox (a clinically used anticancer drug) was selected to fabricate Dox-loaded ImP micelles (Dox-NPs) in aqueous solution. Dialysis method with neutral form of Dox (after treating with Et_3N) and ImP at Dox/P3 = 1:10 wt/wt was selected to fabricate Dox-NPs in PBS solution (pH = 7.4) at 1.6 mg/mL. The resultant Dox-NPs had the z-average diameter of 106 ± 0.6 nm by DLS (Figure 4.11a). Next, the loading level of Dox in Dox-NPs were determined by UV-vis spectroscopy. Figure 4.11b shows UV-vis spectrum of aqueous Dox-NPs mixed with DMF at 1/5 v/v. With the predetermined extinction coefficient of Dox (12,400 M^{-1} cm^{-1}) in water/DMF =1/5 v/v at λ_{em} = 497 nm,[194] the loading level was determined to be 5.2% with a loading efficiency as high as 46%. These relatively high Dox loading content and efficiency could be attributed to π- π interaction of aromatic moieties in Dox with benzyl groups in

hydrophobic PBzImMA cores. Furthermore, our DLS analysis confirms excellent shelf stability of Dox-NPs over 21 days (Figure A11).

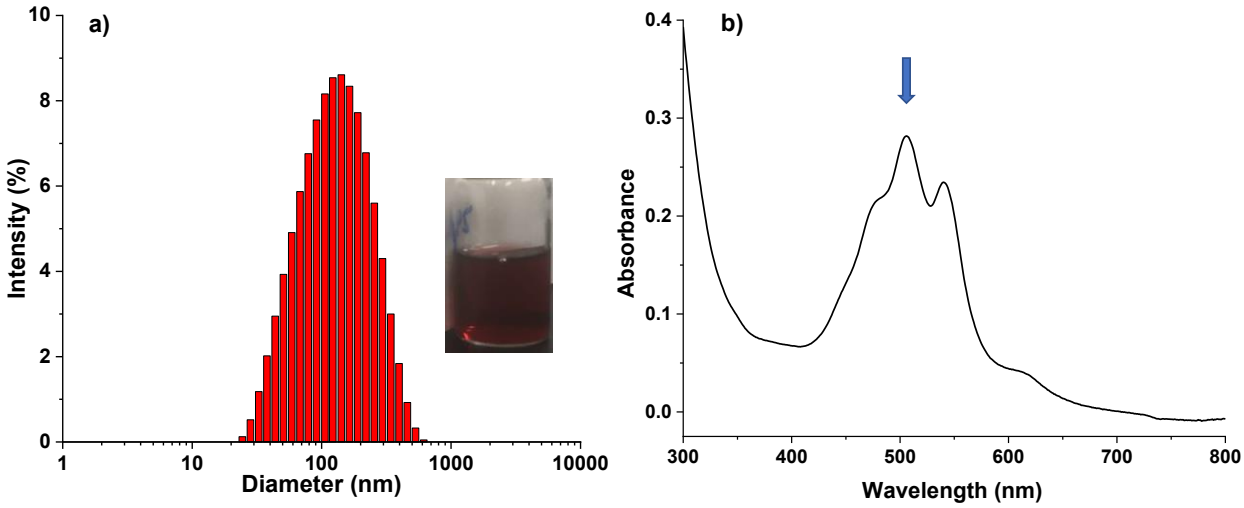

Figure 4.11. DLS diagram and digital image (inset) of formed Dox-NPs at 1.6 mg/mL (a) and UV/vis spectrum (b) of a mixture consisted of Dox-NPs (1 mL) with DMF (5 mL).

4.7 Acid-responsive release of encapsulated Dox from Dox-NPs

Aqueous Dox-NPs could be disintegrated upon acid-catalyzed hydrolysis of pendant imine linkages in hydrophobic cores through disrupting the hydrophilic/hydrophobic balance. Such acidic pH-responsive degradation could accelerate the release of encapsulated Dox from micelles in tumoral and endo/lysosomal acid conditions. Here, fluorescence spectroscopy technique was used to investigate the release of Dox. This technique involves the determination of Dox in outer buffer solutions that are diffused through dialysis tubing upon being released from Dox-NPs inside tubing. The amount of accumulated Dox was quantified to %Dox release using the predetermined Dox calibration curves at desired pH ranges.[194]

Figure 4.12 shows the accumulated Dox release over incubation time in acidic pHs to mimic tumoral extracellular pH = 6.8 and endosomal/lysosomal pH = 5.0, compared with that at physiological pH = 7.4. At pH = 7.4 (in absence of acid stimulus), Dox was gradually released to reach plateau at 30% up to 210 h. This is probably attributed to mainly natural leak of Dox from micelles and possibly the partial cleavage of imine linkages (see Figure 4.6). When Dox-NPs was incubated in acidic pHs, Dox was rapidly released and the release rate appeared to be pH-dependent. For example, sustained Dox release reached to 53% at pH = 6.8, further to >85% at

pH = 5.0, which is almost three folds faster compared with pH= 7.4. Such enhanced Dox release in acidic condition is consistent with acid-catalyzed imine hydrolysis kinetics found by NMR spectroscopy, suggesting acid-responsive cleavage of imine linkages in micellar cores could control and enhance the Dox release by causing disintegration or dissociation of micelles.

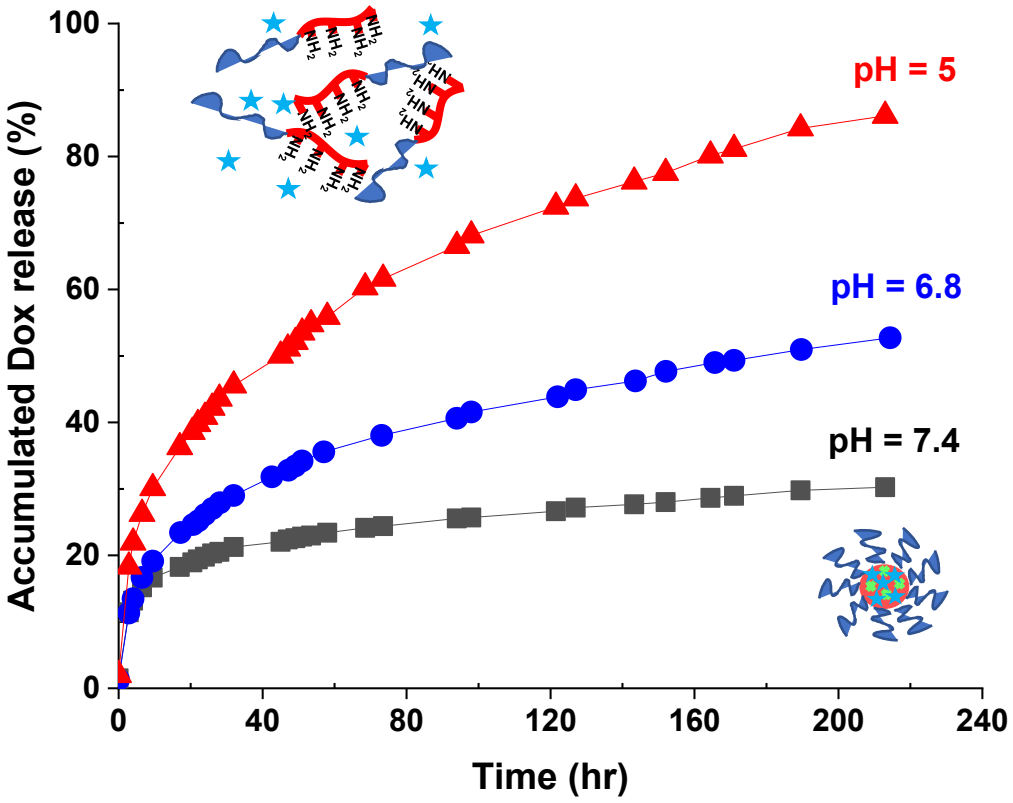

Figure 4.12. %Dox release over incubation time at acidic pHs = 5.0 and 6.8, compared with physiological pH = 7.4.

Chapter 5 Conclusion and future direction

5.1 Conclusion

My master research explored a new strategy that enabled the synthesis of well-controlled PEG-b-PBzImMA (ImP) diblock copolymers having pendant imine linkages for enhanced drug release upon acid-responsive degradation. We developed direct polymerization approach by exploring both ATRP and RAFT polymerization as a new means for the synthesis of well-defined acid-degradable diblock copolymers with imine pendants. A novel methacrylate monomer bearing imine linkage was successfully synthesized by two-step facile coupling reactions. RAFT polymerization of the imine monomer was controlled in a living manner, based on kinetic investigation, enabling the well control over molecular weight and narrow molecular weight distribution. Interestingly, our results suggest the instability of imine bonds when the copolymers synthesized by ATRP were treated with basic alumina during purification process. Acid-catalyzed hydrolysis of imine bonds were systematically investigated with BzImMA monomer and its ImP block copolymers by ^{1}H-NMR analysis. The results revealed that acid-catalyzed hydrolysis of imine linkage to corresponding the aldehyde and amine was rapid in tumoral and endo/lysosomal acidic pHs, compared to physiological pH. Such accelerated cleavage of imine linkages incorporated in hydrophobic cores caused the dissociation of fabricated Dox-loaded micelles, leading to enhanced release of Dox in acidic environment. These combined results demonstrate that our developed direct polymerization approach can be a robust and versatile means to the synthesis of imine-based block copolymers for enhanced drug delivery.

5.2 Future direction and up-to-date progress

Built on newly developed strategy based on direct polymerization through controlled radical polymerization to synthesize acid-degradable block copolymer-based nanoassemblies with pendant imine linkages, we aim to expand our scope by further developing advanced drug delivery systems through two strategies: tunable acid-responsive degradation and dual location dual acid/reduction responsive degradation.

5.2.1 Tunable acid-responsive degradation

Description. Novel imine-bearing methacrylates denoted as R-N=CH-C_6H_4-X, where R is methacryl functionality, are varied with substituents X. Noting that X is hydrogen for BzImMA. Acid-catalyzed hydrolysis rate of imine linkages is well known to be controlled with varying N-substituents of imine moieties by their inductive and resonance effects.[90, 93, 111] We have hypothesized that hydrolysis rate of C=N bond can be varied with X groups with different electronic properties. As a proof-of-concept demonstration, p-nitro as electron withdrawing group, p-methoxy as electron denoting group, and pyryl as resonance group will be examined. Three methacryates (named RImMA) will be synthesized using similar procedure to synthesis of BzImMA. Their RAFT polymerization will be followed to construct a series of diblock copolymers as PEG-b-PRImMA. Degradation in acidic pHs will be systematically investigated by ^{1}H-NMR to elucidate the substituent effects over imine hydrolysis, compared with those of BzImMA and PEG-b-PBzImMA. These efforts will enable the development of a promising imine-based polymeric delivery platform with tunable drug release, aiming to further improve anticancer efficacy.

Progress. Figure 5.1 illustrates our synthetic route to novel imine-bearing methacrylate monomers substituted with different R groups (RImMA). The same synthetic procedure for BzImMA was used. ^{1}H-NMR spectra in Figure 5.2 confirm the synthesis of RImOH. Given the successful synthesis of RImOH, the next step was the synthesis of RImMA by the coupling reaction of RImOH with HEMA-CI. ^{1}H-NMR spectra in Figure 5.3 confirm the successful synthesis of PyImMA, MBzImMA, and NBzImMA monomers.

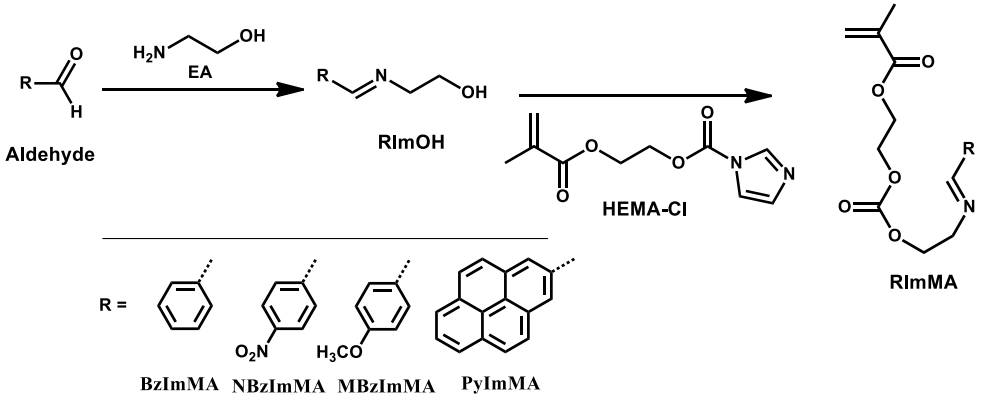

Figure 5.1. Schematic illustration to synthesis of imine-bearing methacrylate monomers with different substituents (R = benzyl, p-nitrobenzyl, p-methoxybenzyl, or pyryl group).

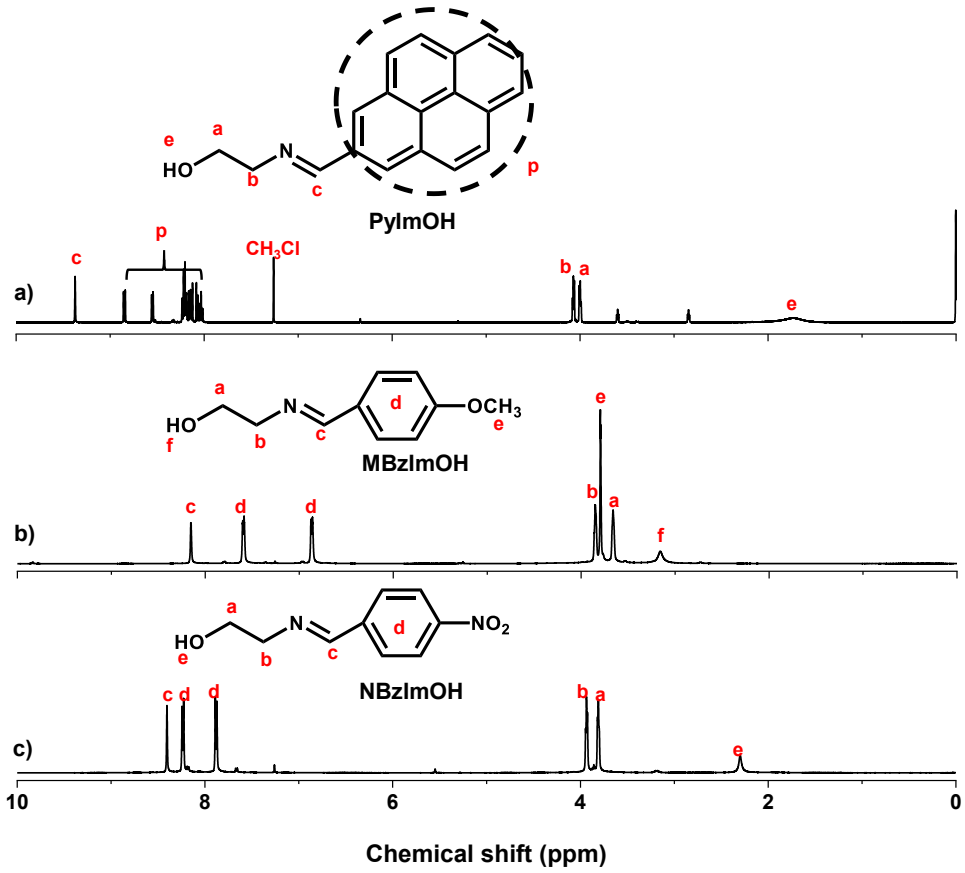

Figure 5.2. Overlaid ^{1}H-NMR spectra of PyImOH (a), MBzImOH (b), and NBzImOH (c).

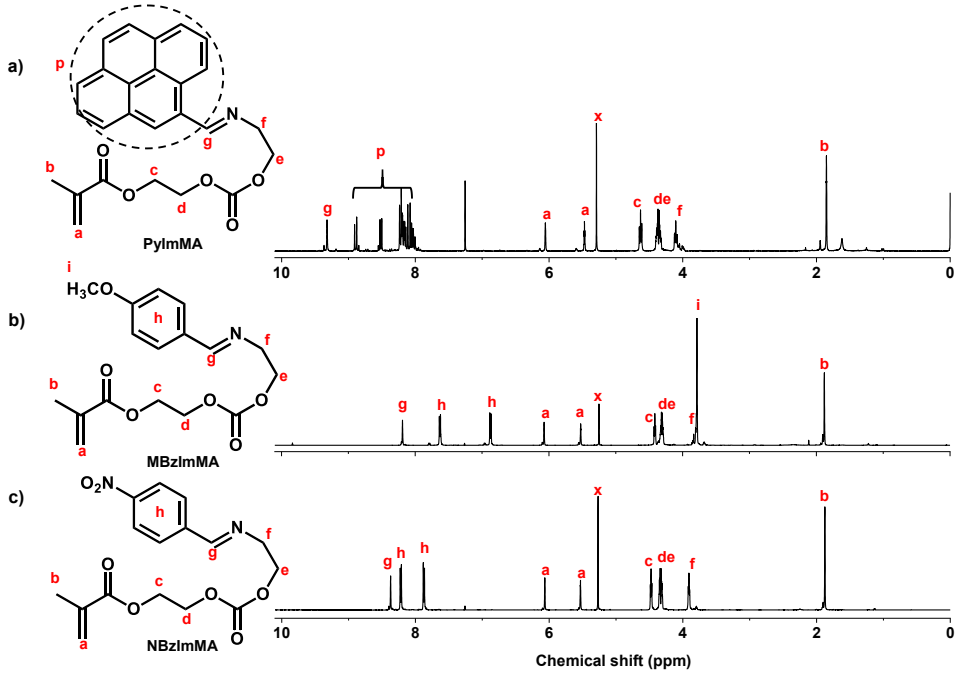

Figure 5.3. Overlaid ^{1}H-NMR spectra of PyImMA (a), MBzImMA (b), and NBzImMA (c).

Experimental.

NBzImOH: EA (1.22 g, 0.02 mol) dissolved in DCM (5 mL) was mixed with a solution containing 4-nitrobenzaldehyde (3.02 g, 0.02 mol) dissolved in DCM (50 mL) in presence of sodium sulfate (5 g) under stirring at room temperature for 13 hr. Yield = 3.8 g (98%). ^{1}H-NMR ($CDCl_3$, ppm): 8.4 (s, 1H, -N<u>CH</u>$C_6H_4NO_2$), 8.22 and 7.88 (d, 4H, - <u>C_6H_4</u>NO_2), 3.93 (t, 2H, $HOCH_2$<u>CH_2</u>-), 3.81 (t, 2H, HO<u>CH_2</u>CH_2-).

MBzImOH: Similar procedure was applied except for the use of EA (1.22 g, 0.02 mol), 1-methoxybenzaldehyde (2.72 g, 0.02 mol), DCM (50 mL), and sodium sulfate (5 g). Yield = 3.4 g (96%). ^{1}H-NMR ($CDCl_3$, ppm): 8.15 (s, 1H, -N<u>CH</u>C_6H_4-), 7.6 and 6.9 (d, 4H, -NCH<u>C_6H_4</u>OCH_3), 3.85 (t, 2H, $HOCH_2$<u>CH_2</u>NCH-), 3.8 (S, 3H, -C_6H_4O<u>CH_3</u>) 3.66 (t, 2H, HO<u>CH_2</u>CH_2NCH-).

PyImOH: Similar procedure was applied except for the use of EA (1.0 g, 16.5 mmol), 1-pyrenecarboxaldehyde (3.8 g, 16.5 mmol), DCM (100 mL), and sodium sulfate (0.3 g). Yield = 4.28 g (95%). ^{1}H-NMR ($CDCl_3$, ppm): 9.4 (s, 1H, -N<u>CH</u>$C_{16}H_{10}$), 7.97-8.86 (m, 10H, -$HOCH_2CH_2NCH$<u>$C_{16}H_{10}$</u>), 4.1 (t, 2H, $HOCH_2$<u>CH_2</u>N-), 4.0 (t, 2H, HO<u>CH_2</u>CH_2N-).

NBzImMA: NBzImOH (1.74 g, 9 mmol) was mixed with a solution consisting of HEMA-CI (2.02, 9 mmol) and DBU (0.27 g, 0.2 mmol) dissolved in DCM (100 mL) under stirring at room temperature for 13 hr. The reaction mixture was washed with saturated $NaHCO_3$ solution three times and dried over sodium sulfate. After the removal of solvent, the product was dried in a vacuum oven for 13 hr. Yield = 3.1 g (98 %). ^{1}H-NMR ($CDCl_3$, ppm): 8.4 (s, 1H, -N<u>CH</u>C_6H_4-), 8.2 and 7.9 (d, 4H, -NCH<u>C_6H_4</u>NO_2), 6.1 and 5.5 (s, 2H, <u>CH_2</u>$C(CH_3)$-), 4.5 (t, 2H, -<u>CH_2</u>$CH_2OC(O)O$), 4.36 (t, 2H, -CH_2<u>CH_2</u>$OC(O)O$), 4.3 (t, 2H, -<u>CH_2</u>CH_2NCH-), 3.9 (t, 2H, -CH_2<u>CH_2</u>NCH-), 1.9 (s, 3H, <u>CH_3</u>-).

MBzImMA: Similar procedure was applied except for the use of MBzImOH (0.16 g, 0.9 mmol), HEMA-CI (0.20 g, 0.9 mmol), DBU (0.27 g, 0.18 mmol), and DCM (10 mL). Yield = 0.3 g (99 %). ^{1}H-NMR ($CDCl_3$, ppm): 8.2 (s, 1H, -N<u>CH</u>C_6H_4-), 7.6 and 6.9 (d, 4H, -NCH<u>C_6H_4</u>OCH_3), 6.1 and 5.5 (s, 2H, <u>CH_2</u>$C(CH_3)$-), 4.4 (t, 2H, -<u>CH_2</u>$CH_2OC(O)O$), 4.3 (t, 2H, -CH_2<u>CH_2</u>$OC(O)O$), 4.33 (t, 2H, -<u>CH_2</u>CH_2NCH-), 3.8 (m, 5H, -CH_2<u>CH_2</u>$NCHC_6H_4O$<u>CH_3</u>), 1.9 (s, 3H, CH_2C(<u>CH_3</u>)-).

PyImMA: Similar procedure was applied except for the use of PyImOH (1.4 g, 5 mmol), HEMA-CI (1.1 g, 5 mmol), DBU (0.15 g, 1 mmol), and DCM (100 mL). Yield = 1.82 g (85 %).

^{1}H-NMR ($CDCl_3$, ppm): 9.4 (s, 1H, -NCHC$_{16}$H$_{10}$), 8-8.9 (m, 10H, -NCHC$_{16}$H$_{10}$), 6.1 and 5.5 (s, 2H, $CH_2C(CH_3)$-), 4.6 (t, 2H, -$CH_2CH_2OC(O)O$), 4.4 (t, 2H, -$CH_2CH_2OC(O)O$-), 4.3 (t, 2H, -CH_2CH_2NCH-), 4.1 (t, 2H, -CH_2CH_2NCH-), 1.8 (s, 3H, CH_3-).

5.2.2 Dual location dual acid/reduction responsive degradation (DL-DSRD) strategy

Description. Our research group has made significant efforts to explore DL-DSRD strategy as design and synthesis of block copolymers and their nanoassemblies exhibiting dual stimuli response in dual locations, as in micellar cores and core/corona interfaces. This strategy enables synergistically controlled and enhanced drug release as well as independent regulation on the release of encapsulated drugs in response to each stimulus. Built on our initial design of PEG-b-PBzImMA block copolymer, we aim to explore DL-DSRD strategy with the synthesis of PEG-ss-PBzImMA having disulfide linkage at the block junction and imine linkage in hydrophobic block. Figure 5.4 illustrates synthesis of PEG-ss-PBzImMA by RAFT polymerization as a promising nanocarrier for intracellular drug delivery.

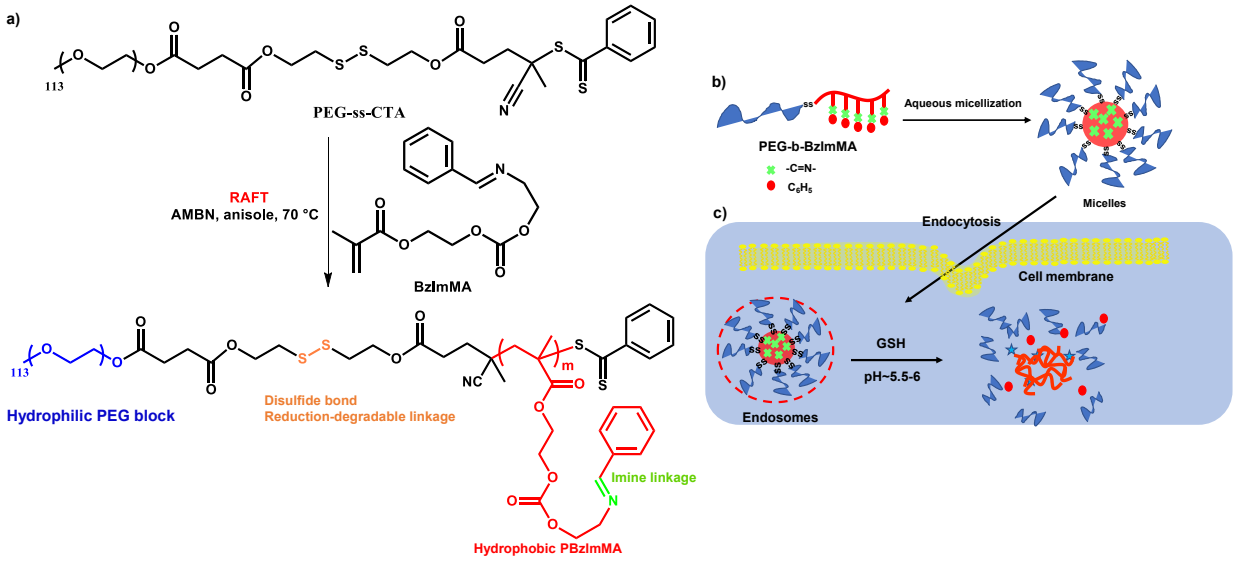

Figure 5.4. Synthetic scheme for PEG-ss-PBzImMA (a), aqueous micellization to fabricate DL-DSRD nanoassemblies (b), and illustration of intracellular drug release in presence of GSH and acidic pH (c).

Progress. To employ the RAFT polymerization technique for the synthesis of PEG-ss-PBzImMA, a novel PEG-based macro-mediator bearing a disulfide linkage (PEG-ss-CTA) was synthesized as depicted in Figure 5.5.

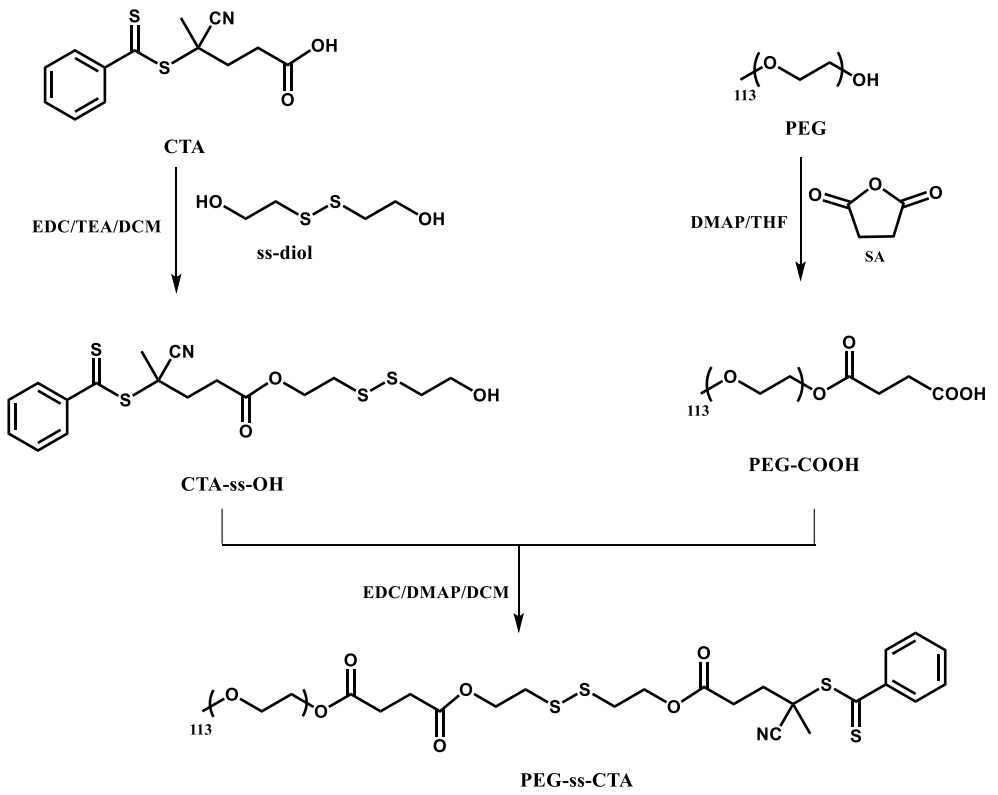

Figure 5.5. Synthetic scheme for PEG-ss-CTA.

The first step is to synthesize CTA-ss-OH by EDC coupling reaction of ss-diol with CTA. The product was purified and collected as the 3rd out of total 5 bands by silica gel column chromatography with eluent solution ethyl acetate/hexane = 1/1 v/v at yield of 30%. Its chemical structure was confirmed by ^{1}H-NMR (Figure 5.6a). In a separated batch, carboxylic acid-capped PEG (PEG-COOH) was synthesized by the reaction of PEG with succinic anhydride. ^{1}H-NMR spectrum in Figure 5.6b reveals the presence of characteristic peaks at 2.6 ppm (b) corresponding to methylene group adjacent to ester group. Based on the integral ratio (b/a), high conjugation efficiency at ≈100% was determined at a yield of 65%. Given the synthesis of PEG-COOH and CTA-ss-OH, EDC coupling reaction was carried out to synthesize PEG-ss-CTA. ^{1}H-NMR in Figure 5.6c shows the appearance of characteristic peak at 7.3-8.0 ppm (h) corresponding to benzyl group adjacent to thiocarbonate. Integral ratio of h and a allows to determine the conjugation efficiency to be >99% at a yield of 70% after purification.

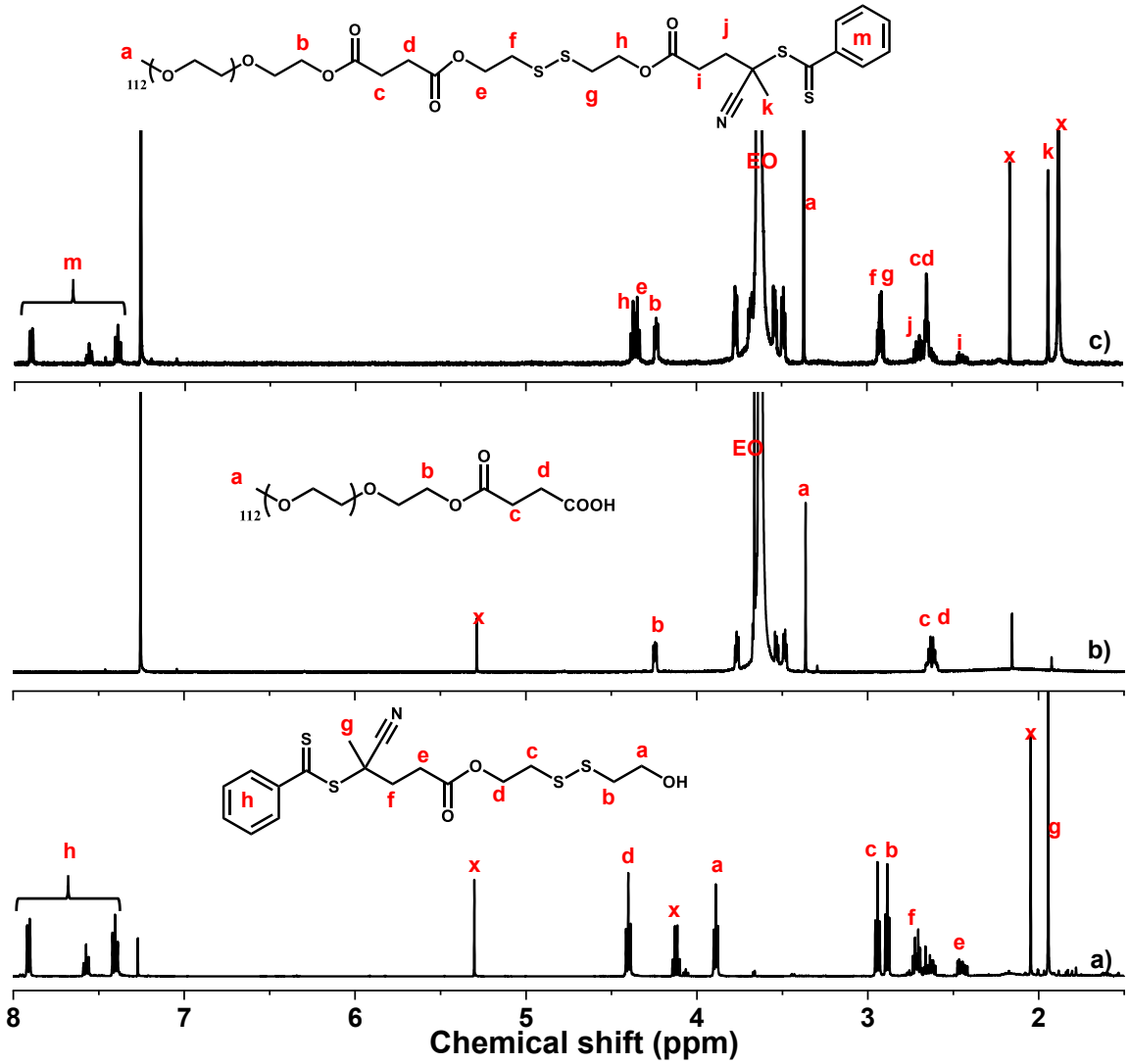

Figure 5.6. Overlaid ^{1}H-NMR spectra of CTA-ss-OH (a), PEG-COOH (b) and PEG-ss-RAFT (c).

Experimental.

Synthesis of CTA-ss-OH. CTA (0.2 g, 0.72 mmol) dissolved in anhydrous DCM (15 mL) was mixed with an organic solution containing ss-diol (166 mg, 1.1 mmol), EDC (270 mg, 1.4 mmol) and TEA (145 mg, 2 mmol) in DCM (85 mL) in an ice-bath under stirring. After proceeding at room temperature for 48h, the solvent was evaporated, and the product was purified by silica gel column chromatography. The product, a red oil, was collected as the third band of total five bands. Yield= 0.06 g (30%); Rf = 0.35 (ethyl acetate/hexane = 1/1, v/v).^{1}H-NMR ($CDCl_3$, ppm): 7.9-7.3 (m, 5H, -SC(S)$\underline{C_6H_5}$), 4.4 (t, 2H, -$\underline{CH_2}$OC(O)-), 3.9 (t, 2H, -$CH_2\underline{CH_2}$OH), 2.94 (t, 2H, -

$\underline{CH_2}SSCH_2CH_2OH$), 2.88 (t, 2H, -SS$\underline{CH_2}CH_2OH$), 2.7 (t, 2H, -$\underline{CH_2}CH_2(CH_3)C(CN)$-), 2.4 (t, 2H, -$CH_2\underline{CH_2}(CH_3)C(CN)$-), 1.94 (s, 3H, -($\underline{CH_3}$)C(CN)-).

Synthesis of PEG-COOH. Succinic anhydride (0.22 g, 2.2 mmol) dissolved in anhydrous DCM (5 mL) was mixed with an organic solution containing PEG (2 g, 0.4 mmol) and DMAP (49 mg, 0.4 mmol) in DCM (15 mL) in an ice-bath under stirring for 48 hr. The resultant mixture was washed with brine solution three times, dried over sodium sulfate, and then precipitated from cold diethyl ether to remove excess succinic anhydride. White solid product was isolated by vacuum filtration and dried in a vacuum oven at room temperature for 13 hr. Yield = 1.35 g (65%). ^{1}H-NMR ($CDCl_3$, ppm): 4.25 (t, 2H, -$\underline{CH_2}OC(O)$-), 3.5-3.8 (m, -$\underline{CH_2CH_2}$O- of PEG main chain), 3.36 (s, 3H, CH_3-), 2.6 (m, 4H, -$\underline{CH_2CH_2}$COOH).

Synthesis of PEG-ss-CTA. EDC (79 mg, 0.41 mmol) dissolved in anhydrous DCM (20 mL) was mixed with an organic solution containing PEG-COOH (0.5 g, 98 μmol), DMAP (3.6 g, 29 μmol) and CTA-ss-OH (0.16 g, 0.39 mmol) in DCM (80 mL) in an ice-bath under stirring for 24 hr. The resultant mixture was washed with brine solution three times, dried over sodium sulfate, and then precipitated from cold diethyl ether to remove excess CTA. Pink solid product was isolated by vacuum filtration and dried in a vacuum oven at room temperature for 13 hr. Yield = 0.46 g (70%). ^{1}H-NMR ($CDCl_3$, ppm): 7.9-7.3 (m, 5H, -SC(S)$\underline{C_6H_5}$), 4.34 (m, 4H, -$\underline{CH_2}OC(O)$-), 4.24 (t, 2H, -$OCH_2\underline{CH_2}OC(O)$-), 3.5-3.8 (m, -$\underline{CH_2CH_2}$O- of PEG main chain), 3.38 (s, 3H, $\underline{CH_3}$O-), 2.92 (t, 4H, -$\underline{CH_2}SS\underline{CH_2}$), 2.7 (m, 2H, -$\underline{CH_2}CH_2(CH_3)C(CN)$-), 2.69 (m, 4H, -$OC(O)\underline{CH_2CH_2}$ C(O)O-), 2.4 (t, 2H, -$CH_2\underline{CH_2}(CH_3)C(CN)$-), 1.94 (s, 3H, -($\underline{CH_3}$)C(CN)-).

References

1. DeVita, V. T.; Chu, E., A history of cancer chemotherapy. *Cancer Res.* **2008,** *68* (21), 8643-8653.
2. Cho, K.; Wang, X.; Nie, S.; Shin, D. M., Therapeutic nanoparticles for drug delivery in cancer. *Clin. Cancer Res.* **2008,** *14* (5), 1310-1316.
3. Sun, T.; Zhang, Y. S.; Pang, B.; Hyun, D. C.; Yang, M.; Xia, Y., Engineered nanoparticles for drug delivery in cancer therapy. *Angew. Chem. Int. Ed.* **2014,** *53* (46), 12320-12364.
4. Langer, R., Polymer-controlled drug delivery systems. *Acc. Chem. Res.* **1993,** *26* (10), 537-542.
5. Maeda, H.; Wu, J.; Sawa, T.; Matsumura, Y.; Hori, K., Tumor vascular permeability and the EPR effect in macromolecular therapeutics: a review. *J. Control. Release* **2000,** *65* (1-2), 271-284.
6. Peer, D., Nanocarriers as an emerging platform for cancer therapy. *Nat. Nanotechnol.* **2007,** *2*.
7. Bazak, R.; Houri, M.; El Achy, S.; Kamel, S.; Refaat, T., Cancer active targeting by nanoparticles: a comprehensive review of literature. *J. Cancer Res. Clin. Oncol.* **2015,** *141* (5), 769-784.
8. Seidi, F.; Jenjob, R.; Crespy, D., Designing smart polymer conjugates for controlled release of payloads. *Chem. Rev.* **2018,** *118* (7), 3965-4036.
9. Kataoka, K.; Harada, A.; Nagasaki, Y., Block copolymer micelles for drug delivery: design, characterization and biological significance. *Adv. Drug Deliv. Rev.* **2012,** *64*, 37-48.
10. Mora-Huertas, C. E.; Fessi, H.; Elaissari, A., Polymer-based nanocapsules for drug delivery. *Int. J. Pharm.* **2010,** *385* (1-2), 113-142.
11. Oh, J. K.; Lee, D. I.; Park, J. M., Biopolymer-based microgels/nanogels for drug delivery applications. *Prog. Polym. Sci.* **2009,** *34* (12), 1261-1282.
12. Kim, T.-Y.; Kim, D.-W.; Chung, J.-Y.; Shin, S. G.; Kim, S.-C.; Heo, D. S.; Kim, N. K.; Bang, Y.-J., Phase I and pharmacokinetic study of Genexol-PM, a cremophor-free, polymeric micelle-formulated paclitaxel, in patients with advanced malignancies. *Clin. Cancer Res.* **2004,** *10* (11), 3708-3716.
13. Valle, J. W.; Armstrong, A.; Newman, C.; Alakhov, V.; Pietrzynski, G.; Brewer, J.; Campbell, S.; Corrie, P.; Rowinsky, E. K.; Ranson, M., A phase 2 study of SP1049C, doxorubicin in P-glycoprotein-targeting pluronics, in patients with advanced adenocarcinoma of the esophagus and gastroesophageal junction. *Invest. New Drugs* **2011,** *29* (5), 1029-1037.
14. Matsumura, Y.; Hamaguchi, T.; Ura, T.; Muro, K.; Yamada, Y.; Shimada, Y.; Shirao, K.; Okusaka, T.; Ueno, H.; Ikeda, M., Phase I clinical trial and pharmacokinetic evaluation of NK911, a micelle-encapsulated doxorubicin. *Br. J. Cancer* **2004,** *91* (10), 1775-1781.
15. Weiss, G. J.; Chao, J.; Neidhart, J. D.; Ramanathan, R. K.; Bassett, D.; Neidhart, J. A.; Choi, C. H. J.; Chow, W.; Chung, V.; Forman, S. J., First-in-human phase 1/2a trial of CRLX101, a cyclodextrin-containing polymer-camptothecin nanopharmaceutical in patients with advanced solid tumor malignancies. *Invest. New Drugs* **2013,** *31* (4), 986-1000.
16. Hrkach, J.; Von Hoff, D.; Ali, M. M.; Andrianova, E.; Auer, J.; Campbell, T.; De Witt, D.; Figa, M.; Figueiredo, M.; Horhota, A., Preclinical development and clinical translation of a PSMA-targeted docetaxel nanoparticle with a differentiated pharmacological profile. *Sci. Transl. Med.* **2012,** *4* (128), 128ra39.

17. He, H.; Liu, L.; Morin, E. E.; Liu, M.; Schwendeman, A., Survey of Clinical Translation of Cancer Nanomedicines—Lessons Learned from Successes and Failures. *Acc. Chem. Res.* **2019,** *52* (9), 2445-2461.
18. Fleige, E.; Quadir, M. A.; Haag, R., Stimuli-responsive polymeric nanocarriers for the controlled transport of active compounds: concepts and applications. *Adv. Drug Deliv. Rev.* **2012,** *64* (9), 866-884.
19. Zhang, Q.; Re Ko, N.; Kwon Oh, J., Recent advances in stimuli-responsive degradable block copolymer micelles: synthesis and controlled drug delivery applications. *Chem. Commun.* **2012,** *48* (61), 7542-7552.
20. Rijcken, C.; Soga, O.; Hennink, W.; Van Nostrum, C., Triggered destabilisation of polymeric micelles and vesicles by changing polymers polarity: an attractive tool for drug delivery. *J. Control. Release* **2007,** *120* (3), 131-148.
21. Oh, J. K., Disassembly and tumor-targeting drug delivery of reduction-responsive degradable block copolymer nanoassemblies. *Polym. Chem.* **2019,** *10* (13), 1554-1568.
22. Kamaly, N.; Yameen, B.; Wu, J.; Farokhzad, O. C., Degradable Controlled-Release Polymers and Polymeric Nanoparticles: Mechanisms of Controlling Drug Release. *Chem. Rev.* **2016,** *116* (4), 2602-2663.
23. Tannock, I. F.; Rotin, D., Acid pH in tumors and its potential for therapeutic exploitation. *Cancer Res.* **1989,** *49* (16), 4373-4384.
24. Jazani, A. M.; Oh, J. K., Development and disassembly of single and multiple acid-cleavable block copolymer nanoassemblies for drug delivery. *Polym. Chem.* **2020,** *11* (17), 2934-2954.
25. Mura, S.; Nicolas, J.; Couvreur, P., Stimuli-responsive nanocarriers for drug delivery. *Nat. Mater.* **2013,** *12* (11), 991-1003.
26. Kato, Y.; Ozawa, S.; Miyamoto, C.; Maehata, Y.; Suzuki, A.; Maeda, T.; Baba, Y., Acidic extracellular microenvironment and cancer. *Cancer Cell Int.* **2013,** *13* (1), 1-8.
27. Layer, R. W., The chemistry of imines. *Chem. Rev.* **1963,** *63* (5), 489-510.
28. Collins, J.; Xiao, Z.; Espinosa-Gomez, A.; Fors, B. P.; Connal, L. A., Extremely rapid and versatile synthesis of high molecular weight step growth polymers via oxime click chemistry. *Polym. Chem.* **2016,** *7* (14), 2581-2588.
29. Sonawane, S. J.; Kalhapure, R. S.; Govender, T., Hydrazone linkages in pH responsive drug delivery systems. *Eur. J. Pharm. Sci.* **2017,** *99*, 45-65.
30. Liu, B.; Thayumanavan, S., Substituent Effects on the pH Sensitivity of Acetals and Ketals and Their Correlation with Encapsulation Stability in Polymeric Nanogels. *J. Am. Chem. Soc.* **2017,** *139* (6), 2306-2317.
31. Gillies, E. R.; Goodwin, A. P.; Fréchet, J. M., Acetals as pH-sensitive linkages for drug delivery. *Bioconjug. Chem.* **2004,** *15* (6), 1254-1263.
32. Du, J.-Z.; Li, H.-J.; Wang, J., Tumor-Acidity-Cleavable Maleic Acid Amide (TACMAA): A Powerful Tool for Designing Smart Nanoparticles To Overcome Delivery Barriers in Cancer Nanomedicine. *Acc. Chem. Res.* **2018,** *51* (11), 2848-2856.
33. Dan, K.; Ghosh, S., One-Pot Synthesis of an Acid-Labile Amphiphilic Triblock Copolymer and its pH-Responsive Vesicular Assembly. *Angew. Chem. Int. Ed.* **2013,** *125* (28), 7441-7446.
34. Masson, C.; Garinot, M.; Mignet, N.; Wetzer, B.; Mailhe, P.; Scherman, D.; Bessodes, M., pH-sensitive PEG lipids containing orthoester linkers: new potential tools for nonviral gene delivery. *J. Control. Release* **2004,** *99* (3), 423-434.
35. Pelaz, B.; Alexiou, C.; Alvarez-Puebla, R. A.; Alves, F.; Andrews, A. M.; Ashraf, S.; Balogh, L. P.; Ballerini, L.; Bestetti, A.; Brendel, C.; Bosi, S.; Carril, M.; Chan, W. C. W.; Chen,

C.; Chen, X.; Chen, X.; Cheng, Z.; Cui, D.; Du, J.; Dullin, C.; Escudero, A.; Feliu, N.; Gao, M.; George, M.; Gogotsi, Y.; Gruenweller, A.; Gu, Z.; Halas, N. J.; Hampp, N.; Hartmann, R. K.; Hersam, M. C.; Hunziker, P.; Jian, J.; Jiang, X.; Jungebluth, P.; Kadhiresan, P.; Kataoka, K.; Khademhosseini, A.; Kopecek, J.; Kotov, N. A.; Krug, H. F.; Lee, D. S.; Lehr, C.-M.; Leong, K. W.; Liang, X.-J.; Ling Lim, M.; Liz-Marzan, L. M.; Ma, X.; Macchiarini, P.; Meng, H.; Moehwald, H.; Mulvaney, P.; Nel, A. E.; Nie, S.; Nordlander, P.; Okano, T.; Oliveira, J.; Park, T. H.; Penner, R. M.; Prato, M.; Puntes, V.; Rotello, V. M.; Samarakoon, A.; Schaak, R. E.; Shen, Y.; Sjoeqvist, S.; Skirtach, A. G.; Soliman, M. G.; Stevens, M. M.; Sung, H.-W.; Tang, B. Z.; Tietze, R.; Udugama, B. N.; VanEpps, J. S.; Weil, T.; Weiss, P. S.; Willner, I.; Wu, Y.; Yang, L.; Yue, Z.; Zhang, Q.; Zhang, Q.; Zhang, X.-E.; Zhao, Y.; Zhou, X.; Parak, W. J., Diverse Applications of Nanomedicine. *ACS Nano* **2017,** *11* (3), 2313-2381.
36. Marques, M. R. C.; Choo, Q.; Ashtikar, M.; Rocha, T. C.; Bremer-Hoffmann, S.; Wacker, M. G., Nanomedicines - Tiny particles and big challenges. *Adv. Drug Deliv. Rev.* **2019,** *151-152*, 23-43.
37. Prokop, A.; Davidson, J. M., Nanovehicular intracellular delivery systems. *J. Pharm. Sci.* **2008,** *97* (9), 3518-3590.
38. Harada, A.; Kataoka, K., Supramolecular assemblies of block copolymers in aqueous media as nanocontainers relevant to biological applications. *Prog. Polym. Sci.* **2006,** *31* (11), 949-982.
39. Mikhail, A. S.; Allen, C., Block copolymer micelles for delivery of cancer therapy: Transport at the whole body, tissue and cellular levels. *J. Control. Release* **2009,** *138* (3), 214-223.
40. Nishiyama, N.; Kataoka, K., Nanostructured Devices Based on Block Copolymer Assemblies for Drug Delivery:Designing Structures for Enhanced Drug Function. In *Polymer Therapeutics II*, 2006; 67-101.
41. Xiong, X.-B.; Falamarzian, A.; Garg, S. M.; Lavasanifar, A., Engineering of amphiphilic block copolymers for polymeric micellar drug and gene delivery. *J. Control. Release* **2011,** *155* (2), 248-261.
42. Ding, J.; Chen, L.; Xiao, C.; Chen, L.; Zhuang, X.; Chen, X., Noncovalent interaction-assisted polymeric micelles for controlled drug delivery. *Chem. Commun.* **2014,** *50* (77), 11274-11290.
43. Kakkar, A.; Traverso, G.; Farokhzad, O. C.; Weissleder, R.; Langer, R., Evolution of macromolecular complexity in drug delivery systems. *Nat. Rev. Chem.* **2017,** *1* (8), 1-17.
44. Matsumura, Y.; Maeda, H., A new concept for macromolecular therapeutics in cancer chemotherapy: mechanism of tumoritropic accumulation of proteins and the antitumor agent smancs. *Cancer Res.* **1986,** *46* (12), 6387-6392.
45. Sindhwani, S.; Syed, A. M.; Ngai, J.; Kingston, B. R.; Maiorino, L.; Rothschild, J.; MacMillan, P.; Zhang, Y.; Rajesh, N. U.; Hoang, T.; Wu, J. L. Y.; Wilhelm, S.; Zilman, A.; Gadde, S.; Sulaiman, A.; Ouyang, B.; Lin, Z.; Wang, L.; Egeblad, M.; Chan, W. C. W., The entry of nanoparticles into solid tumours. *Nat. Mater.* **2020,** *19* (5), 566-575.
46. Setyawati, M. I.; Tay, C. Y.; Chia, S. L.; Goh, S. L.; Fang, W.; Neo, M. J.; Chong, H. C.; Tan, S. M.; Loo, S. C.; Ng, K. W.; Xie, J. P.; Ong, C. N.; Tan, N. S.; Leong, D. T., Titanium dioxide nanomaterials cause endothelial cell leakiness by disrupting the homophilic interaction of VE-cadherin. *Nat. Commun.* **2013,** *4*, 1-12.
47. Nakamura, Y.; Mochida, A.; Choyke, P. L.; Kobayashi, H., Nanodrug Delivery: Is the Enhanced Permeability and Retention Effect Sufficient for Curing Cancer? *Bioconjug. Chem.* **2016,** *27* (10), 2225-2238.

48. Tee, J. K.; Yip, L. X.; Tan, E. S.; Santitewagun, S.; Prasath, A.; Ke, P. C.; Ho, H. K.; Leong, D. T., Nanoparticles' interactions with vasculature in diseases. *Chem. Soc. Rev.* **2019,** *48* (21), 5381-5407.
49. Wang, J.; Mao, W.; Lock, L. L.; Tang, J.; Sui, M.; Sun, W.; Cui, H.; Xu, D.; Shen, Y., The Role of Micelle Size in Tumor Accumulation, Penetration, and Treatment. *ACS Nano* **2015,** *9* (7), 7195-7206.
50. Nichols, J. W.; Bae, Y. H., Odyssey of a cancer nanoparticle: From injection site to site of action. *Nano Today* **2012,** *7* (6), 606-618.
51. Bae, Y. H.; Park, K., Targeted drug delivery to tumors: Myths, reality and possibility. *J. Control. Release* **2011,** *153* (3), 198-205.
52. Cabral, H.; Matsumoto, Y.; Mizuno, K.; Chen, Q.; Murakami, M.; Kimura, M.; Terada, Y.; Kano, M. R.; Miyazono, K.; Uesaka, M.; Nishiyama, N.; Kataoka, K., Accumulation of sub-100 nm polymeric micelles in poorly permeable tumors depends on size. *Nat. Nanotechnol.* **2011,** *6* (12), 815-823.
53. Farokhzad, O. C.; Langer, R., Impact of Nanotechnology on Drug Delivery. *ACS Nano* **2009,** *3* (1), 16-20.
54. Salvioni, L.; Rizzuto, M. A.; Bertolini, J. A.; Pandolfi, L.; Colombo, M.; Prosperi, D., Thirty years of cancer nanomedicine: success, frustration, and hope. *Cancers* **2019,** *11* (12), 1855.
55. He, H.; Liu, L.; Morin, E. E.; Liu, M.; Schwendeman, A., Survey of Clinical Translation of Cancer Nanomedicines-Lessons Learned from Successes and Failures. *Acc. Chem. Res.* **2019,** *52* (9), 2445-2461.
56. Shi, J.; Kantoff, P. W.; Wooster, R.; Farokhzad, O. C., Cancer nanomedicine: progress, challenges and opportunities. *Nat. Rev. Cancer.* **2017,** *17* (1), 20-37.
57. Gothwal, A.; Khan, I.; Gupta, U., Polymeric Micelles: Recent Advancements in the Delivery of Anticancer Drugs. *Pharm. Res.* **2016,** *33* (1), 18-39.
58. Cabral, H.; Kataoka, K., Progress of drug-loaded polymeric micelles into clinical studies. *J. Control. Release* **2014,** *190*, 465-476.
59. Houdaihed, L.; Evans, J. C.; Allen, C., Overcoming the Road Blocks: Advancement of Block Copolymer Micelles for Cancer Therapy in the Clinic. *Mol. Pharm.* **2017,** *14* (8), 2503-2517.
60. Wei, H.; Zhuo, R.-X.; Zhang, X.-Z., Design and development of polymeric micelles with cleavable links for intracellular drug delivery. *Prog. Polym. Sci.* **2013,** *38* (3-4), 503-535.
61. Alvarez-Lorenzo, C.; Concheiro, A., Smart drug delivery systems: from fundamentals to the clinic. *Chem. Commun.* **2014,** *50* (58), 7743-7765.
62. Loomis, K.; McNeeley, K.; Bellamkonda, R. V., Nanoparticles with targeting, triggered release, and imaging functionality for cancer applications. *Soft Matter* **2011,** *7* (3), 839-856.
63. Delplace, V.; Nicolas, J., Degradable vinyl polymers for biomedical applications. *Nat. Chem.* **2015,** *7* (10), 771-784.
64. Wang, Y.; Xu, H.; Zhang, X., Tuning the Amphiphilicity of Building Blocks: Controlled Self-Assembly and Disassembly for Functional Supramolecular Materials. *Adv. Mater.* **2009,** *21* (28), 2849-2864.
65. Jackson, A. W.; Fulton, D. A., Making polymeric nanoparticles stimuli-responsive with dynamic covalent bonds. *Polym. Chem.* **2013,** *4* (1), 31-45.
66. Bawa, K. K.; Oh, J. K., Stimulus-Responsive Degradable Polylactide-Based Block Copolymer Nanoassemblies for Controlled/Enhanced Drug Delivery. *Mol. Pharm.* **2017,** *14* (8), 2460-2474.

67. Deng, C.; Jiang, Y.; Cheng, R.; Meng, F.; Zhong, Z., Biodegradable polymeric micelles for targeted and controlled anticancer drug delivery: Promises, progress and prospects. *Nano Today* **2012,** *7* (5), 467-480.
68. Cheng, R.; Feng, F.; Meng, F.; Deng, C.; Feijen, J.; Zhong, Z., Glutathione-responsive nano-vehicles as a promising platform for targeted intracellular drug and gene delivery. *J. Control. Release* **2011,** *152* (1), 2-12.
69. Quinn, J. F.; Whittaker, M. R.; Davis, T. P., Glutathione responsive polymers and their application in drug delivery systems. *Polym. Chem.* **2017,** *8* (1), 97-126.
70. Ding, Y.; Kang, Y.; Zhang, X., Enzyme-responsive polymer assemblies constructed through covalent synthesis and supramolecular strategy. *Chem. Commun.* **2015,** *51* (6), 996-1003.
71. Segal, M.; Avinery, R.; Buzhor, M.; Shaharabani, R.; Harnoy, A. J.; Tirosh, E.; Beck, R.; Amir, R. J., Molecular Precision and Enzymatic Degradation: From Readily to Undegradable Polymeric Micelles by Minor Structural Changes. *J. Am. Chem. Soc.* **2017,** *139* (2), 803-810.
72. de Gracia Lux, C.; Joshi-Barr, S.; Nguyen, T.; Mahmoud, E.; Schopf, E.; Fomina, N.; Almutairi, A., Biocompatible Polymeric Nanoparticles Degrade and Release Cargo in Response to Biologically Relevant Levels of Hydrogen Peroxide. *J. Am. Chem. Soc.* **2012,** *134* (38), 15758-15764.
73. Deng, Z.; Hu, J.; Liu, S., Reactive Oxygen, Nitrogen, and Sulfur Species (RONSS)-Responsive Polymersomes for Triggered Drug Release. *Macromol. Rapid Commun.* **2017,** *38* (11), 1600685.
74. Zhang, W.; Hu, X.; Shen, Q.; Xing, D., Mitochondria-specific drug release and reactive oxygen species burst induced by polyprodrug nanoreactors can enhance chemotherapy. *Nat. Commun.* **2019,** *10* (1), 1-14.
75. Watson, P.; Jones, A. T.; Stephens, D. J., Intracellular trafficking pathways and drug delivery: fluorescence imaging of living and fixed cells. *Adv. Drug Deliv. Rev.* **2005,** *57* (1), 43-61.
76. Bazban-Shotorbani, S.; Hasani-Sadrabadi, M. M.; Karkhaneh, A.; Serpooshan, V.; Jacob, K. I.; Moshaverinia, A.; Mahmoudi, M., Revisiting structure-property relationship of pH-responsive polymers for drug delivery applications. *J. Control. Release* **2017,** *253*, 46-63.
77. Binauld, S.; Stenzel, M. H., Acid-degradable polymers for drug delivery: a decade of innovation. *Chem. Commun.* **2013,** *49* (21), 2082-2102.
78. Kocak, G.; Tuncer, C.; Butun, V., pH-Responsive polymers. *Polym. Chem.* **2017,** *8* (1), 144-176.
79. Schiff, H., Sur quelques dérivés phéniques des aldéhydes. *Annali Di Chimica* **1864,** *131*, 118.
80. Qu, X.; Yang, Z., Benzoic-Imine-Based Physiological-pH-Responsive Materials for Biomedical Applications. *Chem. Asian J.* **2016,** *11* (19), 2633-2641.
81. Collins, J.; Xiao, Z.; Müllner, M.; Connal, L. A., The emergence of oxime click chemistry and its utility in polymer science. *Polym. Chem.* **2016,** *7* (23), 3812-3826.
82. Xin, Y.; Yuan, J., Schiff's base as a stimuli-responsive linker in polymer chemistry. *Polym. Chem.* **2012,** *3* (11), 3045-3055.
83. Cordes, E. H.; Jencks, W. P., The mechanism of hydrolysis of Schiff bases derived from aliphatic amines. *J. Am. Chem. Soc.* **1963,** *85* (18), 2843-2848.
84. Jencks, W. P., Studies on the mechanism of oxime and semicarbazone formation1. *J. Am. Chem. Soc.* **1959,** *81* (2), 475-481.

85. Jencks, W. P., Mechanism and catalysis of simple carbonyl group reactions. *Prog. Phys. Org. Chem* **1964,** *2*, 63-128.
86. Cordes, E.; Jencks, W., General acid catalysis of semicarbazone formation. *J. Am. Chem. Soc.* **1962,** *84* (22), 4319-4328.
87. Ren, Y.; Yamataka, H., G2 (+) Investigation on the α-Effect in the SN2 Reactions at Saturated Carbon. *Chem. Eur. J.* **2007,** *13* (2), 677-682.
88. Kool, E. T.; Park, D.-H.; Crisalli, P., Fast hydrazone reactants: electronic and acid/base effects strongly influence rate at biological pH. *J. Am. Chem. Soc.* **2013,** *135* (47), 17663-17666.
89. Daasch, L., Infrared Spectra and Structure of Reaction Products of Ketones and Ethanolamine1. *J. Am. Chem. Soc.* **1951,** *73* (10), 4523-4525.
90. Neuvonen, K.; Fülöp, F.; Neuvonen, H.; Koch, A.; Kleinpeter, E.; Pihlaja, K., Comparison of the Electronic Structures of Imine and Hydrazone Side-Chain Functionalities with the Aid of 13C and 15N NMR Chemical Shifts and PM3 Calculations. The Influence of C N-Substitution on the Sensitivity to Aromatic Substitution. *J. Org. Chem.* **2003,** *68* (6), 2151-2160.
91. Gu, J.; Cheng, W.-P.; Liu, J.; Lo, S.-Y.; Smith, D.; Qu, X.; Yang, Z., pH-triggered reversible "stealth" polycationic micelles. *Biomacromolecules* **2008,** *9* (1), 255-262.
92. Kale, A. A.; Torchilin, V. P., Design, synthesis, and characterization of pH-sensitive PEG− PE conjugates for stimuli-sensitive pharmaceutical nanocarriers: The effect of substitutes at the hydrazone linkage on the pH stability of PEG− PE conjugates. *Bioconjug. Chem.* **2007,** *18* (2), 363-370.
93. Kalia, J.; Raines, R. T., Hydrolytic stability of hydrazones and oximes. *Angew. Chem. Int. Ed.* **2008,** *47* (39), 7523-7526.
94. Yang, Z.; Sun, N.; Cheng, R.; Zhao, C.; Liu, Z.; Li, X.; Liu, J.; Tian, Z., pH multistage responsive micellar system with charge-switch and PEG layer detachment for co-delivery of paclitaxel and curcumin to synergistically eliminate breast cancer stem cells. *Biomaterials* **2017,** *147*, 53-67.
95. Babikova, D.; Kalinova, R.; Momekova, D.; Ugrinova, I.; Momekov, G.; Dimitrov, I., Multifunctional polymer nanocarrier for efficient targeted cellular and subcellular anticancer drug delivery. *ACS Biomater. Sci. Eng.* **2019,** *5* (5), 2271-2283.
96. Fan, Y.; Li, C.; Li, F.; Chen, D., pH-activated size reduction of large compound nanoparticles for in vivo nucleus-targeted drug delivery. *Biomaterials* **2016,** *85*, 30-39.
97. Ding, C.; Gu, J.; Qu, X.; Yang, Z., Preparation of multifunctional drug carrier for tumor-specific uptake and enhanced intracellular delivery through the conjugation of weak acid labile linker. *Bioconjug. Chem.* **2009,** *20* (6), 1163-1170.
98. Zhao, C.; Deng, H.; Xu, J.; Li, S.; Zhong, L.; Shao, L.; Wu, Y.; Liang, X.-j., "Sheddable" PEG-lipid to balance the contradiction of PEGylation between long circulation and poor uptake. *Nanoscale* **2016,** *8* (20), 10832-10842.
99. Kong, L.; Campbell, F.; Kros, A., DePEGylation strategies to increase cancer nanomedicine efficacy. *Nanoscale Horiz.* **2019,** *4* (2), 378-387.
100. Jiang, W.; Kim, B. Y.; Rutka, J. T.; Chan, W. C., Nanoparticle-mediated cellular response is size-dependent. *Nat. Nanotechnol.* **2008,** *3* (3), 145-150.
101. Chen, W. H.; Luo, G. F.; Zhang, X. Z., Recent advances in subcellular targeted cancer therapy based on functional materials. *Adv. Mater.* **2019,** *31* (3), 1802725.
102. He, L.; Jiang, Y.; Tu, C.; Li, G.; Zhu, B.; Jin, C.; Zhu, Q.; Yan, D.; Zhu, X., Self-assembled encapsulation systems with pH tunable release property based on reversible covalent bond. *Chem. Commun.* **2010,** *46* (40), 7569-7571.

103. Wu, S.; Zheng, L.; Li, C.; Xiao, Y.; Huo, S.; Zhang, B., Grafted copolymer micelles with pH triggered charge reversibility for efficient doxorubicin delivery. *J. Polym. Sci. A. Polym. Chem.* **2017,** *55* (12), 2036-2046.
104. Yang, X.; An, J.; Luo, Z.; Yang, R.; Yan, S.; Liu, D.-E.; Fu, H.; Gao, H., A cyanine-based polymeric nanoplatform with microenvironment-driven cascaded responsiveness for imaging-guided chemo-photothermal combination anticancer therapy. *J. Mater. Chem. B* **2020,** *8* (10), 2115-2122.
105. Xu, M.; Zhang, C. Y.; Wu, J.; Zhou, H.; Bai, R.; Shen, Z.; Deng, F.; Liu, Y.; Liu, J., PEG-detachable polymeric micelles self-assembled from amphiphilic copolymers for tumor-acidity-triggered drug delivery and controlled release. *ACS Appl. Mater. Interfaces* **2019,** *11* (6), 5701-5713.
106. Song, N.; Ding, M.; Pan, Z.; Li, J.; Zhou, L.; Tan, H.; Fu, Q., Construction of targeting-clickable and tumor-cleavable polyurethane nanomicelles for multifunctional intracellular drug delivery. *Biomacromolecules* **2013,** *14* (12), 4407-4419.
107. Liu, B.; Chen, H.; Li, X.; Zhao, C.; Liu, Y.; Zhu, L.; Deng, H.; Li, J.; Li, G.; Guo, F., pH-responsive flower-like micelles constructed via oxime linkage for anticancer drug delivery. *RSC Adv.* **2014,** *4* (90), 48943-48951.
108. Xu, J.; Luan, S.; Qin, B.; Wang, Y.; Wang, K.; Qi, P.; Song, S., Backbone-hydrazone-containing biodegradable copolymeric micelles for anticancer drug delivery. *J. Nanopart. Res.* **2016,** *18* (11), 1-15.
109. Zeng, Z.; Wei, Z.; Ma, L.; Xu, Y.; Xing, Z.; Niu, H.; Wang, H.; Huang, W., pH-Responsive nanoparticles based on ibuprofen prodrug as drug carriers for inhibition of primary tumor growth and metastasis. *J. Mater. Chem. B* **2017,** *5* (33), 6860-6868.
110. Sun, J.; Fransen, S.; Yu, X.; Kuckling, D., Synthesis of pH-cleavable poly (trimethylene carbonate)-based block copolymers via ROP and RAFT polymerization. *Polym. Chem.* **2018,** *9* (23), 3287-3296.
111. Che, J.; Xue, Y.; Feng, J.; Bai, G.; Yuan, W., Comparison of Biological Responses of Polymers Based on Imine and Disulfide Backbones for siRNA Delivery. *ACS Appl. Mater. Interfaces* **2018,** *10* (6), 5196-5202.
112. Zhang, X.; Kang, Y.; Liu, G.-t.; Li, D.-d.; Zhang, J.-y.; Gu, Z.-p.; Wu, J., Poly (cystine–PCL) based pH/redox dual-responsive nanocarriers for enhanced tumor therapy. *Biomater. Sci.* **2019,** *7* (5), 1962-1972.
113. Jin, Y.; Song, L.; Su, Y.; Zhu, L.; Pang, Y.; Qiu, F.; Tong, G.; Yan, D.; Zhu, B.; Zhu, X., Oxime linkage: a robust tool for the design of pH-sensitive polymeric drug carriers. *Biomacromolecules* **2011,** *12* (10), 3460-3468.
114. Pan, Z.; Ren, Y.; Song, N.; Song, Y.; Li, J.; He, X.; Luo, F.; Tan, H.; Fu, Q., Multifunctional mixed micelles cross-assembled from various polyurethanes for tumor therapy. *Biomacromolecules* **2016,** *17* (6), 2148-2159.
115. Zhou, L.; Yu, L.; Ding, M.; Li, J.; Tan, H.; Wang, Z.; Fu, Q., Synthesis and characterization of pH-sensitive biodegradable polyurethane for potential drug delivery applications. *Macromolecules* **2011,** *44* (4), 857-864.
116. Ding, M.; Song, N.; He, X.; Li, J.; Zhou, L.; Tan, H.; Fu, Q.; Gu, Q., Toward the next-generation nanomedicines: design of multifunctional multiblock polyurethanes for effective cancer treatment. *ACS Nano* **2013,** *7* (3), 1918-1928.
117. Wang, C.; Wang, G.; Wang, Z.; Zhang, X., A pH-responsive superamphiphile based on dynamic covalent bonds. *Chem. Eur. J.* **2011,** *17* (12), 3322-3325.

118. Wang, C.; Kang, Y.; Liu, K.; Li, Z.; Wang, Z.; Zhang, X., pH and enzymatic double-stimuli responsive multi-compartment micelles from supra-amphiphilic polymers. *Polym. Chem.* **2012,** *3* (11), 3056-3059.
119. Han, S.; Lee, J.; Jung, E.; Park, S.; Sagawa, A.; Shibasaki, Y.; Lee, D.; Kim, B.-S., Mechanochemical Drug Conjugation via pH-Responsive Imine Linkage for Polyether Prodrug Micelles. *ACS Appl. Bio. Mater.* **2021,** *4* (3), 2465-2474.
120. Wang, M.; Xu, L.; Lin, M.; Li, Z.; Sun, J., Fabrication of reversible pH-responsive aggregation-induced emission luminogens assisted by a block copolymer via a dynamic covalent bond. *Polym. Chem.* **2021,** *12* (19), 2825-2831.
121. Pramod, P.; Shah, R.; Jayakannan, M., Dual stimuli polysaccharide nanovesicles for conjugated and physically loaded doxorubicin delivery in breast cancer cells. *Nanoscale* **2015,** *7* (15), 6636-6652.
122. Wang, Y.; Khan, A.; Liu, Y.; Feng, J.; Dai, L.; Wang, G.; Alam, N.; Tong, L.; Ni, Y., Chitosan oligosaccharide-based dual pH responsive nano-micelles for targeted delivery of hydrophobic drugs. *Carbohydr. Polym.* **2019,** *223*, 115061.
123. Kang, Y.; Ju, X.; Wang, L.; Ding, L.-S.; Liu, G.-T.; Zhang, S.; Li, B.-J., pH and glutathione dual-triggered supramolecular assemblies as synergistic and controlled drug release carriers. *Polym. Chem.* **2017,** *8* (46), 7260-7270.
124. Hu, X.; Oh, J. K., Direct Polymerization Approach to Synthesize Acid-Degradable Block Copolymers Bearing Imine Pendants for Tunable pH-Sensitivity and Enhanced Release. *Macromol. Rapid Commun.* **2020,** *41* (22), 2000394.
125. Cai, X.; Dong, C.; Dong, H.; Wang, G.; Pauletti, G. M.; Pan, X.; Wen, H.; Mehl, I.; Li, Y.; Shi, D., Effective gene delivery using stimulus-responsive catiomer designed with redox-sensitive disulfide and acid-labile imine linkers. *Biomacromolecules* **2012,** *13* (4), 1024-1034.
126. Hartlieb, M.; Bus, T.; Kubel, J.; Pretzel, D.; Hoeppener, S.; Leiske, M. N.; Kempe, K.; Dietzek, B.; Schubert, U. S., Tailoring Cellular Uptake and Fluorescence of Poly(2-oxazoline)-Based Nanogels. *Bioconjug. Chem.* **2017,** *28* (4), 1229-1235.
127. Tao, Y.; Liu, S.; Zhang, Y.; Chi, Z.; Xu, J., A pH-responsive polymer based on dynamic imine bonds as a drug delivery material with pseudo target release behavior. *Polym. Chem.* **2018,** *9* (7), 878-884.
128. Li, Y.; Bui, Q. N.; Duy, L. T. M.; Yang, H. Y.; Lee, D. S., One-step preparation of pH-responsive polymeric nanogels as intelligent drug delivery systems for tumor therapy. *Biomacromolecules* **2018,** *19* (6), 2062-2070.
129. Azuma, Y.; Terashima, T.; Sawamoto, M., Precision synthesis of imine-functionalized reversible microgel star polymers via dynamic covalent cross-linking of hydrogen-bonding block copolymer micelles. *Macromolecules* **2017,** *50* (2), 587-596.
130. Liao, S. C.; Ting, C. W.; Chiang, W. H., Functionalized polymeric nanogels with pH-sensitive benzoic-imine cross-linkages designed as vehicles for indocyanine green delivery. *J. Colloid Interface Sci.* **2020,** *561*, 11-22.
131. Wang, X.; Wang, L.; Yang, S.; Zhang, M.; Xiong, Q.; Zhao, H.; Liu, L., Construction of multifunctionalizable, core-cross-linked polymeric nanoparticles via dynamic covalent bond. *Macromolecules* **2014,** *47* (6), 1999-2009.
132. Mukherjee, S.; Bapat, A. P.; Hill, M. R.; Sumerlin, B. S., Oximes as reversible links in polymer chemistry: dynamic macromolecular stars. *Polym. Chem.* **2014,** *5* (24), 6923-6931.

133. Yang, H. Y.; Li, Y.; Jang, M.-S.; Fu, Y.; Wu, T.; Lee, J. H.; Lee, D. S., Green preparation of pH-responsive and dual targeting hyaluronic acid nanogels for efficient protein delivery. *Eur. Polym. J.* **2019,** *121*, 109342.
134. Raghupathi, K.; Li, L.; Ventura, J.; Jennings, M.; Thayumanavan, S., pH responsive soft nanoclusters with size and charge variation features. *Polym. Chem.* **2014,** *5* (5), 1737-1742.
135. Jackson, A. W.; Stakes, C.; Fulton, D. A., The formation of core cross-linked star polymer and nanogel assemblies facilitated by the formation of dynamic covalent imine bonds. *Polym. Chem.* **2011,** *2* (11), 2500-2511.
136. Jackson, A. W.; Fulton, D. A., pH triggered self-assembly of core cross-linked star polymers possessing thermoresponsive cores. *Chem. Commun.* **2011,** *47* (24), 6807-6809.
137. Jackson, A. W.; Fulton, D. A., Triggering polymeric nanoparticle disassembly through the simultaneous application of two different stimuli. *Macromolecules* **2012,** *45* (6), 2699-2708.
138. Delplace, V.; Couvreur, P.; Nicolas, J., Recent trends in the design of anticancer polymer prodrug nanocarriers. *Polym. Chem.* **2014,** *5* (5), 1529-1544.
139. Su, Z.; Liang, Y.; Yao, Y.; Wang, T.; Zhang, N., Polymeric complex micelles based on the double-hydrazone linkage and dual drug-loading strategy for pH-sensitive docetaxel delivery. *J. Mater. Chem. B* **2016,** *4* (6), 1122-1133.
140. Binauld, S.; Scarano, W.; Stenzel, M. H., pH-Triggered release of platinum drugs conjugated to micelles via an acid-cleavable linker. *Macromolecules* **2012,** *45* (17), 6989-6999.
141. Zhu, L.; Zhao, L.; Qu, X.; Yang, Z., pH-sensitive polymeric vesicles from coassembly of amphiphilic cholate grafted poly (L-lysine) and acid-cleavable polymer–drug conjugate. *Langmuir* **2012,** *28* (33), 11988-11996.
142. Sun, N.; Zhao, C.; Cheng, R.; Liu, Z.; Li, X.; Lu, A.; Tian, Z.; Yang, Z., Cargo-free nanomedicine with pH sensitivity for codelivery of DOX conjugated prodrug with SN38 to synergistically eradicate breast cancer stem cells. *Mol. Pharm.* **2018,** *15* (8), 3343-3355.
143. Zhang, Y.; Yang, C.; Wang, W.; Liu, J.; Liu, Q.; Huang, F.; Chu, L.; Gao, H.; Li, C.; Kong, D.; Liu, Q.; Liu, J., Co-delivery of doxorubicin and curcumin by pH-sensitive prodrug nanoparticle for combination therapy of cancer. *Sci. Rep.* **2016,** *6*, 21225.
144. Chen, D.; Tang, Q.; Zou, J.; Yang, X.; Huang, W.; Zhang, Q.; Shao, J.; Dong, X., pH-Responsive PEG–Doxorubicin-Encapsulated Aza-BODIPY Nanotheranostic Agent for Imaging-Guided Synergistic Cancer Therapy. *Adv. Funct. Mater.* **2018,** *7* (7), 1701272.
145. Zhou, Y.; Zhou, C.; Zou, Y.; Jin, Y.; Han, S.; Liu, Q.; Hu, X.; Wang, L.; Ma, Y.; Liu, Y., Multi pH-sensitive polymer-drug conjugate mixed micelles for efficient co-delivery of doxorubicin and curcumin to synergistically suppress tumor metastasis. *Biomater. Sci.* **2020,** *8* (18), 5029-5046.
146. Li, J.; Zhou, Y.; Li, C.; Wang, D.; Gao, Y.; Zhang, C.; Zhao, L.; Li, Y.; Liu, Y.; Li, X., Poly(2-ethyl-2-oxazoline)-doxorubicin conjugate-based dual endosomal pH-sensitive micelles with enhanced antitumor efficacy. *Bioconjug. Chem.* **2015,** *26* (1), 110-119.
147. Zou, Y.; Zhou, Y.; Jin, Y.; He, C.; Deng, Y.; Han, S.; Zhou, C.; Li, X.; Zhou, Y.; Liu, Y., Synergistically enhanced antimetastasis effects by honokiol-loaded pH-sensitive polymer–doxorubicin conjugate micelles. *ACS Appl. Mater. Interfaces* **2018,** *10* (22), 18585-18600.
148. Qiu, L.; Xu, C.-R.; Zhong, F.; Hong, C.-Y.; Pan, C.-Y., Fabrication of functional nano-objects through RAFT dispersion polymerization and influences of morphology on drug delivery. *ACS Appl. Mater. Interfaces* **2016,** *8* (28), 18347-18359.

149. Mao, J.; Li, Y.; Wu, T.; Yuan, C.; Zeng, B.; Xu, Y.; Dai, L., A simple dual-pH responsive prodrug-based polymeric micelles for drug delivery. *ACS Appl. Mater. Interfaces* **2016,** *8* (27), 17109-17117.
150. Song, C.; Li, Y.; Li, T.; Yang, Y.; Huang, Z.; de la Fuente, J. M.; Ni, J.; Cui, D., Long-Circulating Drug-Dye-Based Micelles with Ultrahigh pH-Sensitivity for Deep Tumor Penetration and Superior Chemo-Photothermal Therapy. *Adv. Funct. Mater.* **2020,** *30* (11), 1906309.
151. Dong, Y.; Du, P.; Pei, M.; Liu, P., Design, postpolymerization conjugation and self-assembly of a di-block copolymer-based prodrug for tumor intracellular acid-triggered DOX release. *J. Mater. Chem. B* **2019,** *7* (37), 5640-5647.
152. Pelras, T.; Duong, H. T. T.; Kim, B. J.; Hawkett, B. S.; Müllner, M., A 'grafting from' approach to polymer nanorods for pH-triggered intracellular drug delivery. *Polymer* **2017,** *112*, 244-251.
153. Ma, B.; Zhuang, W.; Wang, Y.; Luo, R.; Wang, Y., pH-sensitive doxorubicin-conjugated prodrug micelles with charge-conversion for cancer therapy. *Acta Biomater.* **2018,** *70*, 186-196.
154. Zhang, Y.; Xiao, C.; Li, M.; Ding, J.; He, C.; Zhuang, X.; Chen, X., Core-cross-linked micellar nanoparticles from a linear-dendritic prodrug for dual-responsive drug delivery. *Polym. Chem.* **2014,** *5* (8), 2801-2808.
155. Zhang, T.; Wang, Y.; Ma, X.; Hou, C.; Lv, S.; Jia, D.; Lu, Y.; Xue, P.; Kang, Y.; Xu, Z., A bottlebrush-architectured dextran polyprodrug as an acidity-responsive vector for enhanced chemotherapy efficiency. *Biomater. Sci.* **2020,** *8* (1), 473-484.
156. Braunova, A.; Kostka, L.; Sivak, L.; Cuchalova, L.; Hvezdova, Z.; Laga, R.; Filippov, S.; Cernoch, P.; Pechar, M.; Janouskova, O.; Sirova, M.; Etrych, T., Tumor-targeted micelle-forming block copolymers for overcoming of multidrug resistance. *J. Control. Release* **2017,** *245*, 41-51.
157. Wei, X.; Luo, Q.; Sun, L.; Li, X.; Zhu, H.; Guan, P.; Wu, M.; Luo, K.; Gong, Q., Enzyme- and pH-Sensitive Branched Polymer-Doxorubicin Conjugate-Based Nanoscale Drug Delivery System for Cancer Therapy. *ACS Appl. Mater. Interfaces* **2016,** *8* (18), 11765-11778.
158. Filippov, S. K.; Franklin, J. M.; Konarev, P. V.; Chytil, P.; Etrych, T.; Bogomolova, A.; Dyakonova, M.; Papadakis, C. M.; Radulescu, A.; Ulbrich, K.; Stepanek, P.; Svergun, D. I., Hydrolytically degradable polymer micelles for drug delivery: a SAXS/SANS kinetic study. *Biomacromolecules* **2013,** *14* (11), 4061-4070.
159. Duan, X.; Xiao, J.; Yin, Q.; Zhang, Z.; Yu, H.; Mao, S.; Li, Y., Smart pH-sensitive and temporal-controlled polymeric micelles for effective combination therapy of doxorubicin and disulfiram. *ACS Nano* **2013,** *7* (7), 5858-5869.
160. Li, L.; Sun, W.; Zhong, J.; Yang, Q.; Zhu, X.; Zhou, Z.; Zhang, Z.; Huang, Y., Multistage nanovehicle delivery system based on stepwise size reduction and charge reversal for programmed nuclear targeting of systemically administered anticancer drugs. *Adv. Funct. Mater.* **2015,** *25* (26), 4101-4113.
161. Kamra, M.; Moitra, P.; Ponnalagu, D.; Karande, A. A.; Bhattacharya, S., New Water-Soluble Oxyamino Chitosans as Biocompatible Vectors for Efficacious Anticancer Therapy via Co-Delivery of Gene and Drug. *ACS Appl. Mater. Interfaces* **2019,** *11* (41), 37442-37460.
162. Bae, Y.; Nishiyama, N.; Fukushima, S.; Koyama, H.; Yasuhiro, M.; Kataoka, K., Preparation and biological characterization of polymeric micelle drug carriers with intracellular pH-triggered drug release property: tumor permeability, controlled subcellular drug distribution, and enhanced in vivo antitumor efficacy. *Bioconjug. Chem.* **2005,** *16* (1), 122-130.

163. Cao, D.; He, J.; Xu, J.; Zhang, M.; Zhao, L.; Duan, G.; Cao, Y.; Zhou, R.; Ni, P., Polymeric prodrugs conjugated with reduction-sensitive dextran–camptothecin and pH-responsive dextran–doxorubicin: an effective combinatorial drug delivery platform for cancer therapy. *Polym. Chem.* **2016,** *7* (25), 4198-4212.
164. Zhang, Y.; Ding, J.; Li, M.; Chen, X.; Xiao, C.; Zhuang, X.; Huang, Y.; Chen, X., One-Step "Click Chemistry"-Synthesized Cross-Linked Prodrug Nanogel for Highly Selective Intracellular Drug Delivery and Upregulated Antitumor Efficacy. *ACS Appl. Mater. Interfaces* **2016,** *8* (17), 10673-10682.
165. Ganivada, M. N.; Kumar, P.; Kanjilal, P.; Dinda, H.; Sarma, J. D.; Shunmugam, R., Polycarbonate-based biodegradable copolymers for stimuli responsive targeted drug delivery. *Polym. Chem.* **2016,** *7* (25), 4237-4245.
166. Li, F.; He, J.; Zhang, M.; Ni, P., A pH-sensitive and biodegradable supramolecular hydrogel constructed from a PEGylated polyphosphoester-doxorubicin prodrug and α-cyclodextrin. *Polym. Chem.* **2015,** *6* (28), 5009-5014.
167. Du, J. Z.; Du, X. J.; Mao, C. Q.; Wang, J., Tailor-made dual pH-sensitive polymer-doxorubicin nanoparticles for efficient anticancer drug delivery. *J. Am. Chem. Soc.* **2011,** *133* (44), 17560-17563.
168. Wang, H.; Wang, Y.; Chen, Y.; Jin, Q.; Ji, J., A biomimic pH-sensitive polymeric prodrug based on polycarbonate for intracellular drug delivery. *Polym. Chem.* **2014,** *5* (3), 854-861.
169. Wang, Y.; Luo, Q.; Zhu, W.; Li, X.; Shen, Z., Reduction/pH dual-responsive nano-prodrug micelles for controlled drug delivery. *Polym. Chem.* **2016,** *7* (15), 2665-2673.
170. Russo, A.; DeGraff, W.; Friedman, N.; Mitchell, J. B., Selective modulation of glutathione levels in human normal versus tumor cells and subsequent differential response to chemotherapy drugs. *Cancer Res.* **1986,** *46* (6), 2845-2848.
171. Zan, M.; Li, J.; Luo, S.; Ge, Z., Dual pH-triggered multistage drug delivery systems based on host-guest interaction-associated polymeric nanogels. *Chem. Commun.* **2014,** *50* (58), 7824-7827.
172. Guo, Z.; Sui, J.; Ma, M.; Hu, J.; Sun, Y.; Yang, L.; Fan, Y.; Zhang, X., pH-Responsive charge switchable PEGylated epsilon-poly-l-lysine polymeric nanoparticles-assisted combination therapy for improving breast cancer treatment. *J. Control. Release* **2020,** *326*, 350-364.
173. Wang, C.; Chen, X.; Yao, X.; Chen, L.; Chen, X., Dual acid-responsive supramolecular nanoparticles as new anticancer drug delivery systems. *Biomater. Sci.* **2016,** *4* (1), 104-114.
174. Sun, L.; Wei, H.; Zhang, X.; Meng, C.; Kang, G.; Ma, W.; Ma, L.; Wang, B.; Yu, C., Synthesis of polymeric micelles with dual-functional sheddable PEG stealth for enhanced tumor-targeted drug delivery. *Polym. Chem.* **2020,** *11* (27), 4469-4476.
175. Li, J.; Liu, P., pH/Reduction Dual-Triggered Degradable Poly(doxorubicin) Prodrug Nanoparticles for Leakage-Free Tumor-Specific Self-Delivery. *Macromol. Rapid Commun.* **2018,** *39* (18), 1800381.
176. Hu, X.; Li, H.; Luo, S.; Liu, T.; Jiang, Y.; Liu, S., Thiol and pH dual-responsive dynamic covalent shell cross-linked micelles for triggered release of chemotherapeutic drugs. *Polym. Chem.* **2013,** *4* (3), 695-706.
177. Xiong, D.; Yao, N.; Gu, H.; Wang, J.; Zhang, L., Stimuli-responsive shell cross-linked micelles from amphiphilic four-arm star copolymers as potential nanocarriers for "pH/redox-triggered" anticancer drug release. *Polymer* **2017,** *114*, 161-172.

178. Su, Z.; Xu, Y.; Wang, Y.; Shi, W.; Han, S.; Shuai, X., A pH and reduction dual-sensitive polymeric nanomicelle for tumor microenvironment triggered cellular uptake and controlled intracellular drug release. *Biomater. Sci.* **2019,** *7* (9), 3821-3831.
179. Zhang, J.; Tang, H.; Shen, Y.; Yu, Q.; Gan, Z., Shell-Sheddable Poly(N-2-hydroxypropyl methacrylamide) Polymeric Micelles for Dual-Sensitive Release of Doxorubicin. *Macromol. Rapid Commun.* **2018,** *39* (20), 1800139.
180. Dong, S.; Sun, Y.; Liu, J.; Li, L.; He, J.; Zhang, M.; Ni, P., Multifunctional Polymeric Prodrug with Simultaneous Conjugating Camptothecin and Doxorubicin for pH/Reduction Dual-Responsive Drug Delivery. *ACS Appl. Mater. Interfaces* **2019,** *11* (9), 8740-8748.
181. Wang, L.; Tian, B.; Zhang, J.; Li, K.; Liang, Y.; Sun, Y.; Ding, Y.; Han, J., Coordinated pH/redox dual-sensitive and hepatoma-targeted multifunctional polymeric micelle system for stimuli-triggered doxorubicin release: Synthesis, characterization and in vitro evaluation. *Int. J. Pharm.* **2016,** *501* (1-2), 221-235.
182. Hu, J.; Zhang, G.; Liu, S., Enzyme-responsive polymeric assemblies, nanoparticles and hydrogels. *Chem. Soc. Rev.* **2012,** *41* (18), 5933-5949.
183. Slor, G.; Amir, R. J., Using High Molecular Precision to Study Enzymatically Induced Disassembly of Polymeric Nanocarriers: Direct Enzymatic Activation or Equilibrium-Based Degradation? *Macromolecules* **2021,** *54* (4), 1577-1588.
184. Duan, Z.; Cai, H.; Zhang, H.; Chen, K.; Li, N.; Xu, Z.; Gong, Q.; Luo, K., PEGylated Multistimuli-Responsive Dendritic Prodrug-Based Nanoscale System for Enhanced Anticancer Activity. *ACS Appl. Mater. Interfaces* **2018,** *10* (42), 35770-35783.
185. Pramod, P. S.; Shah, R.; Jayakannan, M., Dual stimuli polysaccharide nanovesicles for conjugated and physically loaded doxorubicin delivery in breast cancer cells. *Nanoscale* **2015,** *7* (15), 6636-6652.
186. Oh, J. K.; Tang, C.; Gao, H.; Tsarevsky, N. V.; Matyjaszewski, K., Inverse miniemulsion ATRP: a new method for synthesis and functionalization of well-defined water-soluble/cross-linked polymeric particles. *J. Am. Chem. Soc.* **2006,** *128* (16), 5578-5584.
187. Covington, A. K.; Paabo, M.; Robinson, R. A.; Bates, R. G., Use of the glass electrode in deuterium oxide and the relation between the standardized pD (paD) scale and the operational pH in heavy water. *Anal. Chem.* **1968,** *40* (4), 700-706.
188. Wang, J.; Matyjaszewski, K., Controlled/"living" radical polymerization. atom transfer radical polymerization in the presence of transition-metal complexes. *J. Am. Chem. Soc.* **1995,** *117* (20), 5614-5615.
189. Matyjaszewski, K., Atom transfer radical polymerization (ATRP): current status and future perspectives. *Macromolecules* **2012,** *45* (10), 4015-4039.
190. Jakubowski, W.; Min, K.; Matyjaszewski, K., Activators regenerated by electron transfer for atom transfer radical polymerization of styrene. *Macromolecules* **2006,** *39* (1), 39-45.
191. Ding, Y.; Liu, J.; Zhang, Y.; Li, X.; Ou, H.; Cheng, T.; Ma, L.; An, Y.; Liu, J.; Huang, F.; Liu, Y.; Shi, L., A novel strategy based on a ligand-switchable nanoparticle delivery system for deep tumor penetration. *Nanoscale Horiz.* **2019,** *4* (3), 658-666.
192. Chan, N.; An, S. Y.; Oh, J. K., Dual location disulfide degradable interlayer-crosslinked micelles with extended sheddable coronas exhibiting enhanced colloidal stability and rapid release. *Polym. Chem.* **2014,** *5* (5), 1637-1649.
193. Goodwin, A. P.; Mynar, J. L.; Ma, Y.; Fleming, G. R.; Fréchet, J. M., Synthetic micelle sensitive to IR light via a two-photon process. *J. Am. Chem. Soc.* **2005,** *127* (28), 9952-9953.

194. Jazani, A. M.; Arezi, N.; Shetty, C.; Hong, S. H.; Li, H.; Wang, X.; Oh, J. K., Tumor-targeting intracellular drug delivery based on dual acid/reduction-degradable nanoassemblies with ketal interface and disulfide core locations. *Polym. Chem.* **2019,** *10* (22), 2840-2853.

Appendix

Figure A1. ^{13}C-NMR spectrum of BzImOH in $CDCl_3$.

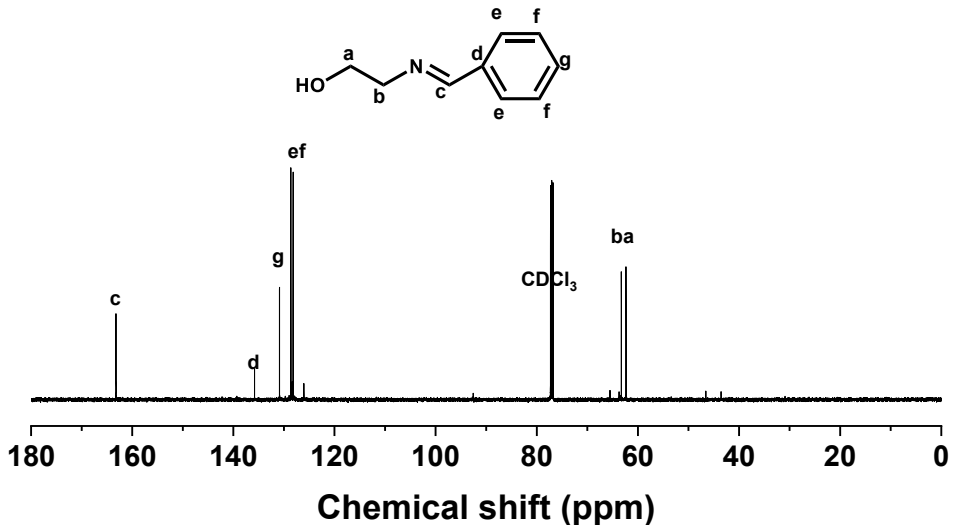

Figure A2. ^{13}C-NMR spectrum of HEMA-CI in $CDCl_3$.

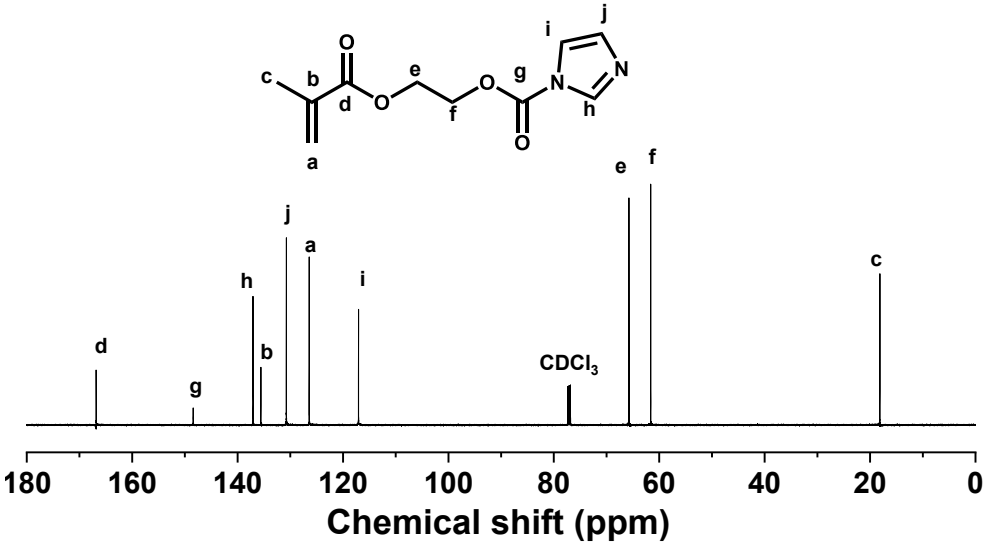

Figure A3. ^{13}C-NMR spectrum of BzImMA in $CDCl_3$.

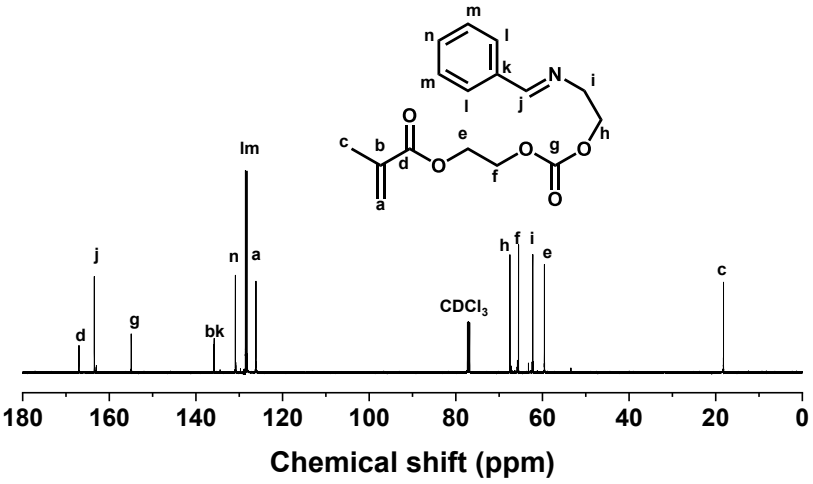

Figure A4. First-order kinetic plot over time (a), evolution of molecular weight and molecular weight distribution (b), and overlaid GPC traces over conversion (c) for ATRP of BzImMA in the presence of PEG-Br at 60 °C in anisole; Conditions: $[BzImMA]_0/[PEG\text{-}Br]_0/[Cu(II)Br_2]_0/[TPMA]_0/[Sn(EH)_2]_0$ = 50 /1/0.05/0.15/0.4; BzImMA/anisole = 0.6 wt/wt.

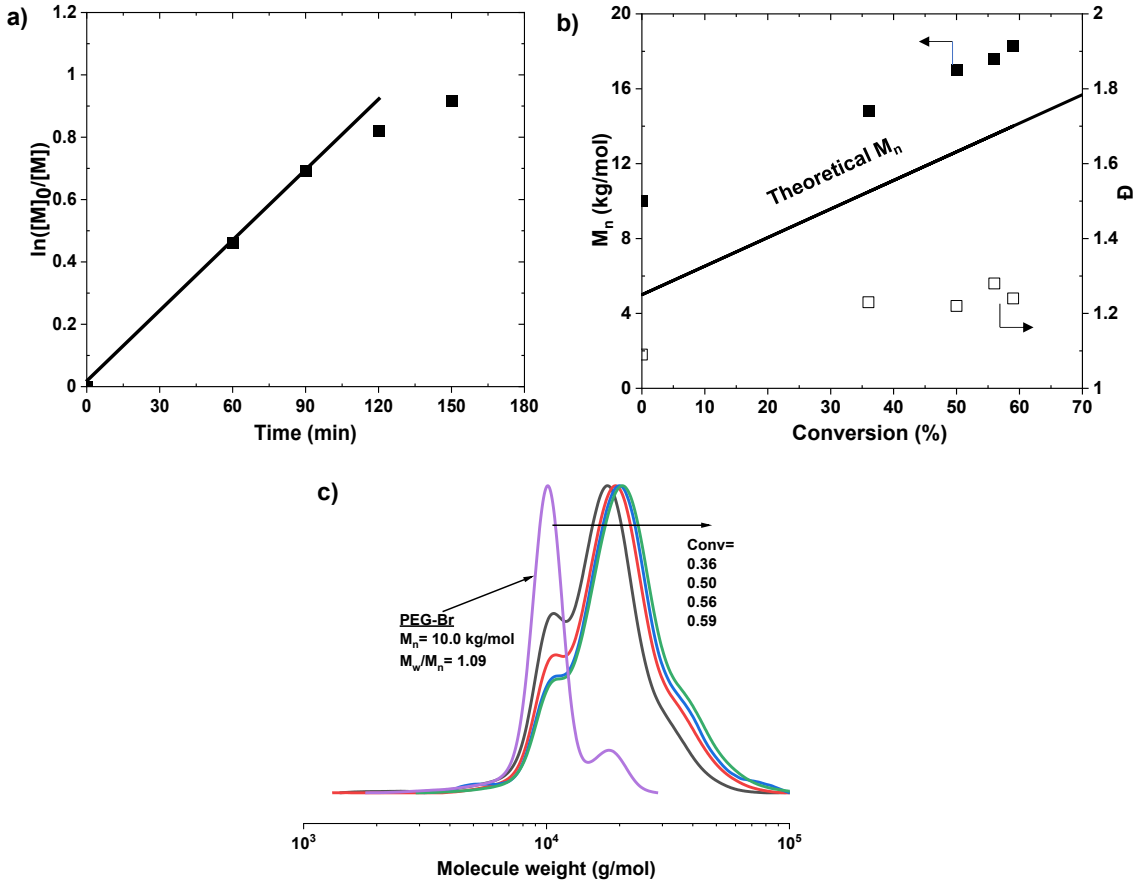

Figure A5. GPC diagrams of PEG-b-PBzImMA synthesized by ATRP after precipitation from hexane, compared with PEG-Br macro-initiator.

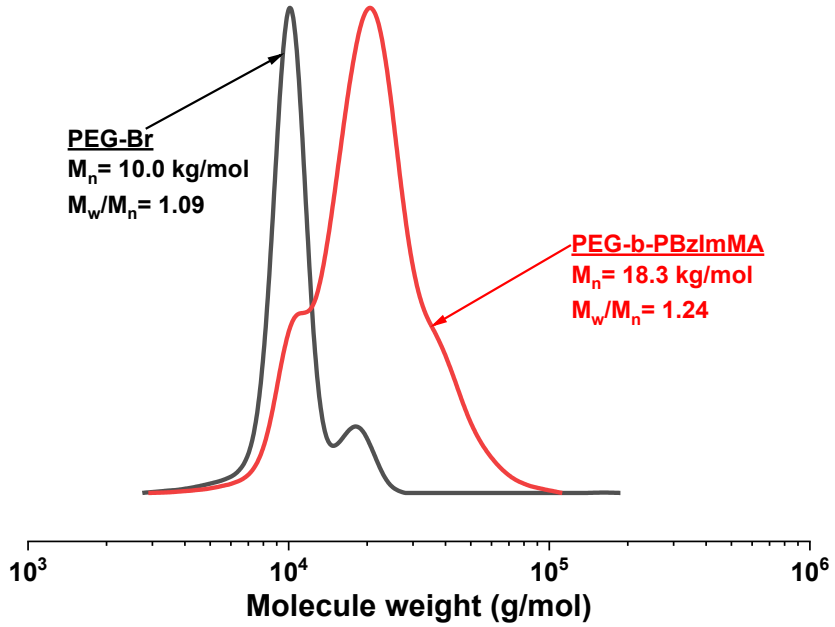

Figure A6. ^{1}H-NMR spectra in $CDCl_3$ of PEG-b-PBzImMA precipitated from hexane before (a) and after (b) treatment with basic aluminum oxide.

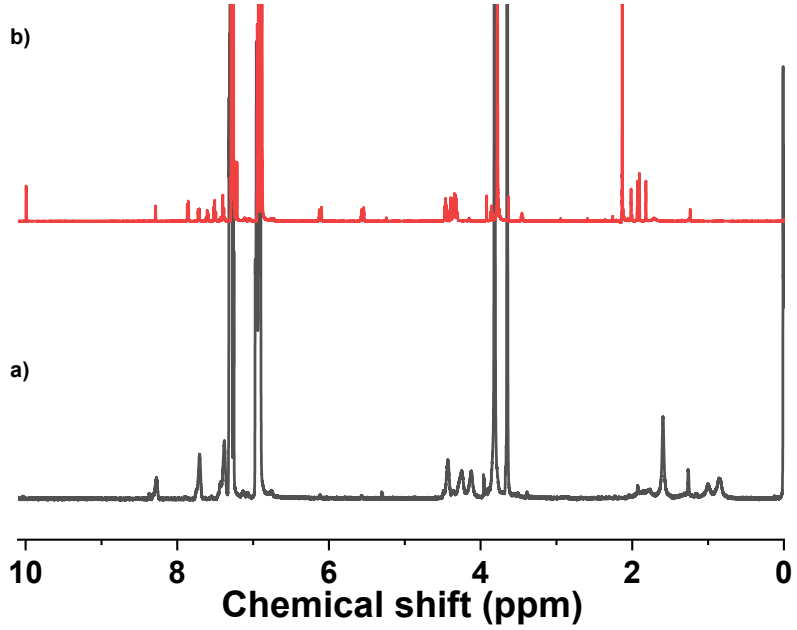

Figure A7. ^{1}H-NMR spectrum of PEG-CTA in $CDCl_3$. x denotes residual solvents.

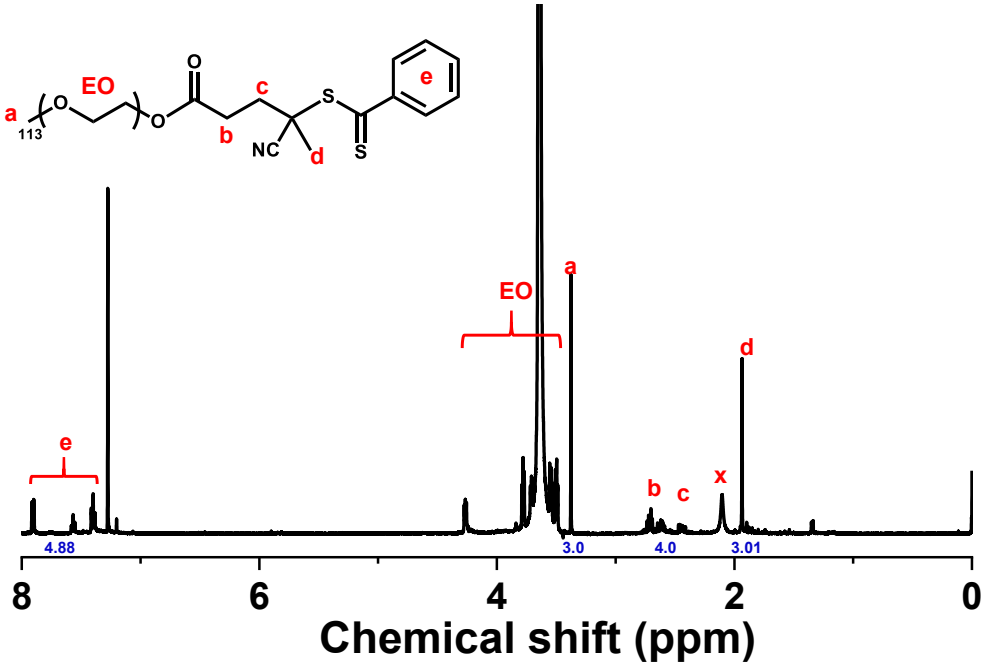

Figure A8. GPC diagrams of ImP diblock copolymers compared with PEG-CTA macro-RAFT mediator.

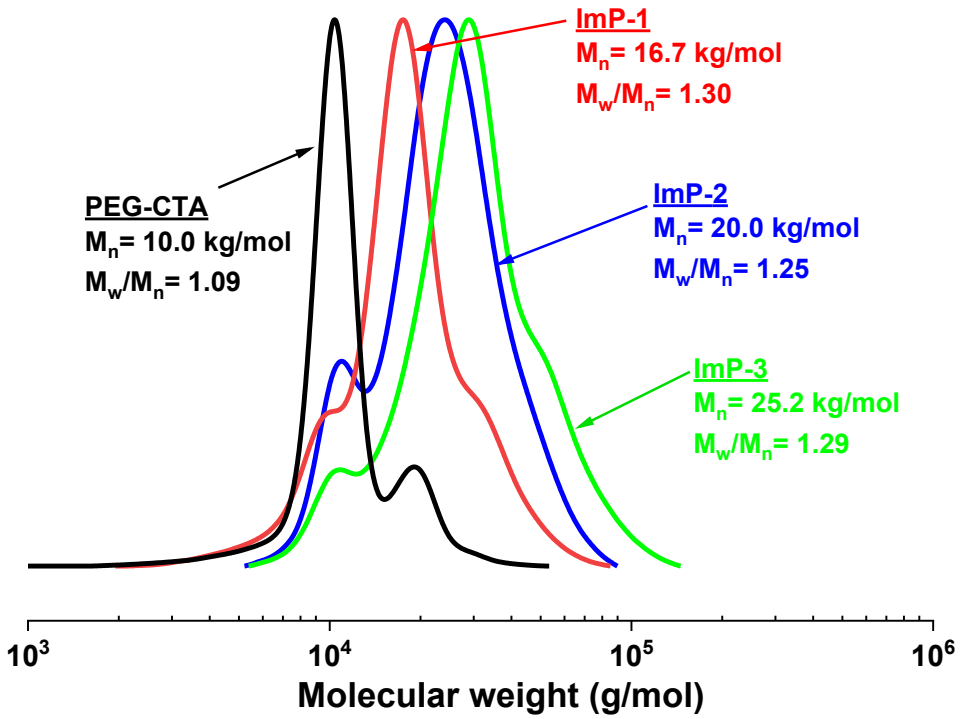

Figure A9. First-order kinetic plot over time (a), evolution of molecular weight and molecular weight distribution (b), and overlaid GPC traces over conversion (c) for RAFT polymerizatioin of BzImMA in the presence of with PEG-CTA. Conditions: [BzImMA]o/[PEG-CTA]o/[AMBN]o = 50/1/0.3 in anisole at 70 °C, BzImMA /anisole = 0.6 wt/wt.

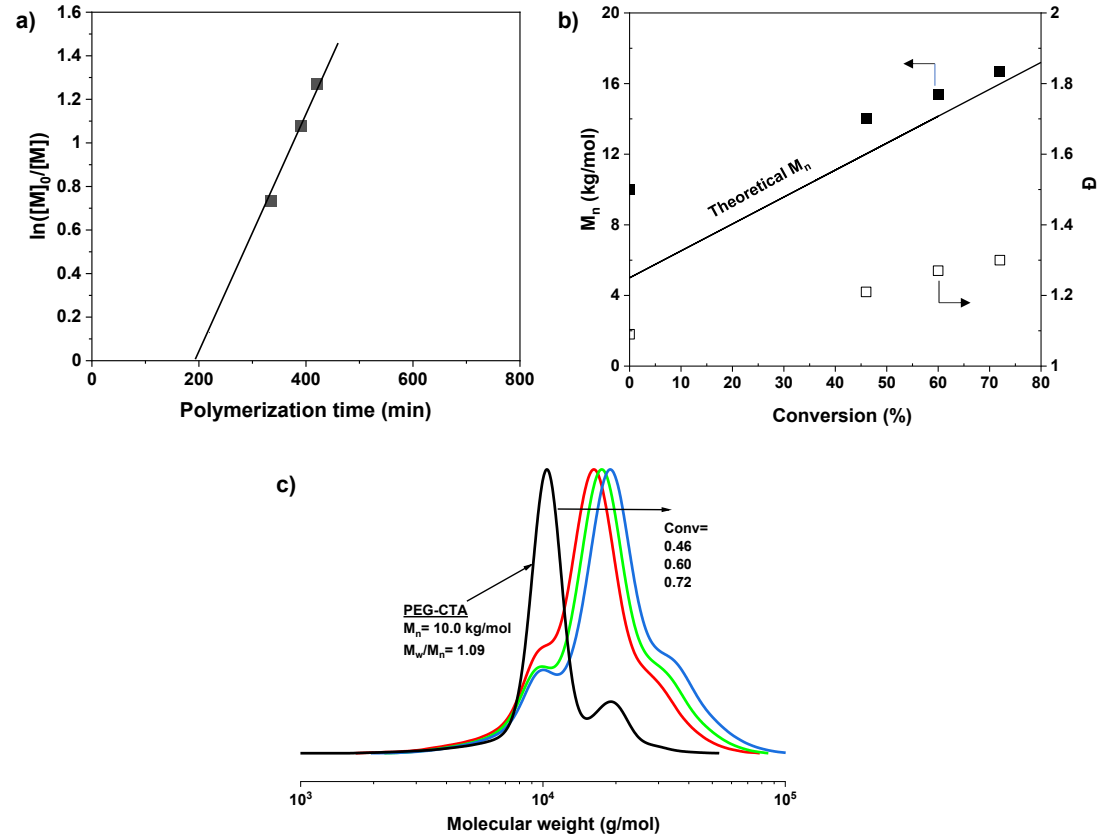

Figure A10. Evolution of count rate of ImP micelles at 1 mg/mL, incubated at physiological pH = 7.4 and acidic pH = 5.0.

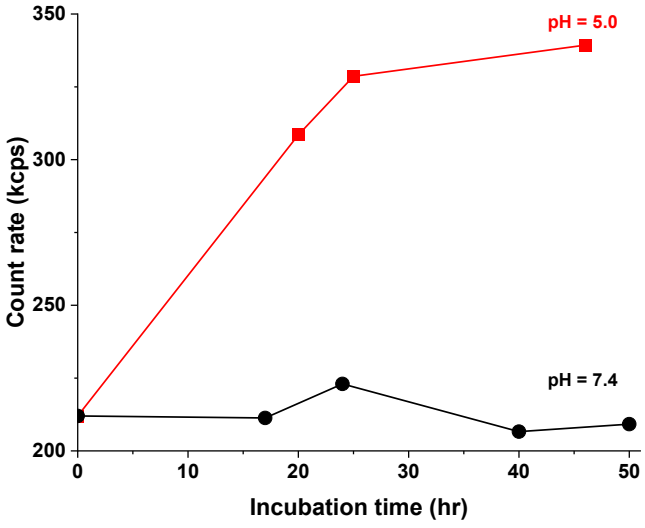

Figure A11. Evolution of z-average diameter in PBS at pH = 7.4 for shelf stability.